GA-A16258
UC-77

POSTIRRADIATION EXAMINATION AND EVALUATION OF FORT ST. VRAIN FUEL ELEMENT 1-0743

by
J. J. SAURWEIN, C. M. MILLER, and C. A. YOUNG

Prepared under
Contract DE-AT03-76ET35301
for the San Francisco Operations Office
Department of Energy

DATE PUBLISHED: MAY 1981

GENERAL ATOMIC COMPANY

Printed in the United States of America
Available from
National Technical Information Service
U.S. Department of Commerce
5285 Port Royal Road
Springfield, Virginia 22161
NTIS Price Code: Printed Copy A07; Microfiche A01

GA-A16258
UC-77

POSTIRRADIATION EXAMINATION AND EVALUATION OF FORT ST. VRAIN FUEL ELEMENT 1-0743

by
J. J. SAURWEIN, C. M. MILLER, and C. A. YOUNG

Prepared under
Contract DE-AT03-76ET35301
for the San Francisco Operations Office
Department of Energy

GENERAL ATOMIC PROJECT 7400
DATE PUBLISHED: MAY 1981

GENERAL ATOMIC COMPANY

ABSTRACT

Fort St. Vrain (FSV) fuel element 1-0743 was irradiated in core location 17.04.F.06 from July 3, 1976 until February 1, 1979. The element experienced an average fast neutron exposure of about 0.95×10^{25} n/m^2 ($E > 29$ fJ)$_{HTGR}$, a time-and-volume-averaged fuel temperature in the vicinity of 680°C, fissile and fertile particle burnups of approximately 6.2% and 0.3%, respectively, and a total burnup of 12,210 MWd/tonne. The postirradiation examination of the fuel element was performed as part of the Department of Energy (DOE) sponsored surveillance program for the FSV high-temperature gas-cooled reactor (HTGR). The purpose of the examination was to verify the acceptable performance of the element and to acquire in-pile data for verification of HTGR core design data and methods.

The postirradiation examination revealed that the element was in excellent condition. No cracks were observed on any of the element surfaces. The structural integrity of the fuel rods was good. No evidence of mechanical interaction between the fuel rods and fuel body was observed. The performance of the TRISO fuel particles was excellent. No kernel migration or fission product attack on the SiC coating was detected. As a result of the fabrication process, there was some fuel dispersion in the buffer coating, but it apparently did not detrimentally affect the irradiation performance of the particles. Metallography and fission gas release measurements revealed that there was no in-pile fuel failure.

Calculated irradiation parameters obtained with HTGR design codes were compared with measured data. Radial and axial power distributions, irradiation temperatures, neutron fluences, and fuel burnups were in good agreement with measurements. Calculated fuel rod strains were about a factor of three greater than were observed. In-pile failure of 0.3% for the $(Th,U)C_2$ fissile particles and 0.1% for the ThC_2 fertile particles, primarily due

to failure of as-manufactured defective particles, was calculated, but no in-pile failure was observed. This suggests that the model for failure of particles with as-manufactured defects is conservative. However, more comparisons of calculations and in-pile data over a wider range of irradiation conditions are required before conclusions concerning the accuracy of HTGR design data and methods can be made.

An additional result of the postirradiation examination of FSV fuel element 1-0743 was verification of the techniques developed for performing nondestructive examinations of irradiated core components in the hot service facility at FSV using automated surveillance equipment.

CONTENTS

FIGURES

FIGURES (Continued)

FIGURES (Continued)

TABLES

TABLES (Continued)

1. INTRODUCTION

Fort St. Vrain (FSV) fuel element 1-0743 (serial number) was irradiated for 174 effective full-power days (EFPD) in core location 17.04.F.06;* it experienced an average fast neutron exposure of about 0.95 x 10^{25} n/m^2 (E > 29fJ)$_{HTGR}$, a time-and-volume-averaged fuel temperature in the vicinity of 680°C, fissile and fertile fuel particle burnups of approximately 6.2% and 0.3% fissions per initial heavy metal atom (FIMA), respectively, and a total burnup of 12,210 MWd/tonne. The element was removed from the reactor during the first refueling in February 1979. After undergoing nondestructive examination in the hot service facility at FSV in July 1979, the element was shipped to General Atomic Company (GA) for extensive postirradiation examination (PIE).

The first part of the PIE involved visual and metrological examinations of the fuel block to verify the results obtained with the metrology robot system at FSV (Ref. 1). Next, extensive gamma scanning of the intact fuel element was performed to determine the distributions of measurable radioisotopes in the fuel. This exercise also served as a demonstration of the validity of gamma scanning as a method for determining fuel burnup and of the capabilities of the gamma scan robot. This device is currently being developed at GA for performing gamma spectroscopic examinations of FSV fuel elements at FSV.

Upon completion of the nondestructive portion of the PIE, the fuel hole plugs at the top of the element and the graphite containment at the bottom were cored and broken out, and the fuel rods were removed from the element. Examination of the fuel rods included visual examination, dimensional

---

*Core region 17, column 4, axial layer 6 (axial layer 3 of active core).

characterization, fission gas release measurements, metallography, and compressive strength testing. Individual stacks of fuel rods were also gamma scanned to verify the results obtained from the earlier in situ scanning of the fuel. Four monitor packages containing SiC pellets, dosimetry wires, and UC_2 particles for monitoring temperatures, neutron fluence, and fuel burnup were recovered from the element and subjected to analysis. The results of these analyses were compared with design code predictions.

The postirradiation examinations of FSV fuel element 1-0743 at FSV and at GA were performed as part of the surveillance program for the FSV high-temperature gas-cooled reactor (HTGR) sponsored by the Department of Energy (DOE). The FSV surveillance program includes nondestructive and destructive examinations of core components from the initial core reload segments. The purpose of these examinations is to verify the acceptable performance of the components and to acquire in-pile data over a wide range of irradiation conditions for verification of HTGR design data and methods. The benefit of these examinations will be early identification of performance defects and design margins. Specific objectives of the surveillance program are given in Table 1-1.

TABLE 1-1
OBJECTIVES OF FSV SURVEILLANCE PROGRAM

Required Data	Objective	Postirradiation Examination Techniques
General mechanical integrity and dimensional changes of fuel rods at reactor temperatures and fast neutron exposures	To judge irradiation limit for mechanical integrity of fuel rods and fuel blocks, and to permit the extrapolation necessary for predicting fuel performance and confirming existing design data based on irradiation capsule experiments.	Comparison of preirradiation and postirradiation dimensional measurements, visual examination, comparison with preirradiation photographs
Fuel block mechanical integrity and critical dimensions, including bow at several reactor temperatures and fast neutron exposures	To judge the irradiation limit for mechanical integrity of fuel rods and fuel blocks, and to confirm design data and, in conjunction with fuel rod dimensional change data, permit a confident prediction of fuel performance	Visual examination, comparison of preirradiation and postirradiation dimensional measurements
Fission product release rate from fuel rods	To evaluate the validity of design data and confirm the limit for time-temperature-irradiation with regard to fission product release from the particles	Burn-leach test for SiC integrity, comparison of preirradiation and postirradiation Kr-85m R/B values
Fuel rod microstructure	To judge fuel performance relative to kernel-coating interaction and coating microstructure. These data are needed for correlation with irradiation capsule data and out-of-pile data.	Metallographic examination
Mechanical strength of fuel rods	To obtain knowledge of the change in mechanical strength of fuel rods with increasing neutron exposure. The relative integrity of the rod, and the exposure at which integrity may be lost, could be judged from this work.	Uniaxial compression tests to failure. Includes irradiated fuel rods as well as nonirradiated historical samples
Measured temperature, neutron exposure, and fuel burnup	To confirm calculated temperatures, neutron exposures, and fuel burnup	Samples of SiC placed in fuel holes will provide a temperature monitor. Standard dosimetry wires developed for capsule irradiations placed in fuel holes will provide a measure of neutron exposure. UC_2 particles placed in fuel holes will provide a measure of the fissile burnup. Fertile burnup can be determined through analysis of ThC_2 particles from fuel rods.

2. ELEMENT DESCRIPTION

Fuel element 1-0743 consisted of a standard H-327 graphite fuel body having 210 fuel holes, 6 burnable poison holes, and 108 coolant holes. The element (see Fig. 2-1) contained 3130 fuel rods consisting of $(Th,U)C_2$ TRISO* fissile particles and ThC_2 TRISO fertile particles bonded together by a carbonaceous matrix. The fuel rods were carbonized at 1800°C in a packed bed of Al_2O_3 powder. The nominal dimensions of the rods were 12.5 mm (0.49 in.) in diameter and 29.3 mm (1.94 in.) in length. Fuel rod and fuel particle attributes are given in Tables 2-1, 2-2, and 2-3. The element contained no lumped burnable poison.

Fuel element 1-0743 was one of 32 surveillance fuel elements irradiated in the initial core. Surveillance elements are readily distinguished from nonsurveillance elements by the fiducial holes drilled in each corner of the block. The dimensions of these elements were accurately characterized prior to loading the fuel. The elements contain fuel rods which were dimensionally characterized and measured for fission gas release prior to irradiation. In addition, SiC pellets, dosimetry wires, and UC_2 fuel particles enclosed in 25.4-mm-long crucibles made of H-327 graphite are included in all surveillance elements to monitor temperature, neutron fluence, and fuel burnup. The design of the monitor packages is shown in Fig. 2-2.

---

*In the TRISO particle design, a layer of SiC is sandwiched between two layers of high-density pyrolytic carbon, which provides a composite pressure vessel to retain gaseous fission products. The SiC coating also provides a barrier against the diffusion of metallic fission products and increases the mechanical and dimensional stability of the particle during irradiation. An inner low-density, or buffer, coating adjacent to the fuel kernel provides a void volume to accommodate fission gases and kernel swelling and, in addition, attenuates fission product recoils.

Fuel element 1-0743 contained 87 fuel rods that were dimensionally characterized prior to irradiation. These rods were loaded into fuel holes 12, 47, 157, 189, 278, and 285. The locations of these holes are shown in Fig. 2-3. Preirradiation fission gas release measurements were made on a group of five rods, four of which were loaded into the fuel element. (The fifth rod was placed in permanent storage as a historical sample.) The four rods were situated in fuel stacks 47, 157, 278, and 285. The element included four monitor packages located in fuel stacks 12 and 278. The axial locations of the fuel rods measured for fission gas release prior to irradiation and of the monitor packages are shown in Fig. 2-4. The preirradiation dimensional measurements for the fuel block are shown in Figs. 2-5 and 2-6.

TABLE 2-1
PREIRRADIATION FUEL ROD ATTRIBUTES FOR FSV FUEL ELEMENT 1-0743

Fuel blend type:	CR-18-1-0165-1
Preirradiation fission gas release, Kr-85m at 1100°C:	1.3×10^{-4}
Fraction exposed fuel after burning rod[(a)]	
U:	7.1×10^{-3}
Th:	5.2×10^{-3}
Thorium contamination:[(b)]	5.9×10^{-5}
Heavy metal loadings	
U:	0.148 g/rod
Th:	4.082 g/rod
Impurities (ppm)	
B:	2
Fe:	80
S:	280
Ti:	40
V:	40
Residual hydrogen:	100
Residual ash:	2053
H_2O:	1
Cl:	--[(c)]
Firing temperature:[(d)]	--

(a) Determined by burn leach test; value indicates broken SiC layer.

(b) Determined by hydrolysis test; value indicates exposed Th.

(c) (--)denotes no available data.

(d) Final heat treatment.

TABLE 2-2
FISSILE FUEL PARTICLE ATTRIBUTES FOR FSV FUEL ELEMENT 1-0743

Coated particle batch number:	CU-6A-3036C, -6045C, -6054C
Kernel type:	$(4Th,U)C_2$
Kernel nominal diameter:	100 to 175 μm[a]
Particle type:	TRISO
As-manufactured coating parameters	
Mean thickness:	
Buffer:	56.3 ± 12.0 μm
IPyC:	25.4 ± 4.5 μm
SiC:	24.4 ± 3.1 μm
OPyC:	33.2 ± 6.5 μm
Total:	139.3 μm
OPyC density:	1.83 ± 0.050 g/cm^3
OPyC BAF:[b]	1.114 ± 0.013
SiC density	3.20 ± 0.006 g/cm^3
Total particle properties:	
Diameter:	379 to 454 μm
Density:	2.37 g/cm^3
% U:	4.072
% Th:	16.711

[a] Nominal ranges are reference values and are not an inspection requirement.

[b] Bacon anisotropy factor, relative units.

TABLE 2-3
FERTILE FUEL PARTICLE ATTRIBUTES FOR FSV FUEL ELEMENT 1-0743

	Fertile A	Fertile B
Coated particle batch number	CT-6A-1101C	CT-6B-0127C
Kernel type	ThC_2	ThC_2
Kernel nominal diameter	300 to 410 µm[a]	410 to 500 µm[a]
Particle type	TRISO	TRISO
As-manufactured coating parameters		
Mean thickness		
Buffer	52.5 ± 13.1 µm	56.7 ± 14.9 µm
IPyC	29.6 ± 7.8 µm	33.[illegible] ± 8.0 µm
SiC	25.6 ± 3.8 µm	26.4 ± 4.5 µm
OPyC	42.7 ± 10.3 µm	44.0 ± 8.3 µm
Total	150.4 µm	160.9 µm
OPyC density	1.773 ± 0.086 g/cm^3	1.799 ± 0.037 g/cm^3
OPyC BAF[b]	1.14 ± 0.035	1.16 ± 0.039
SiC density	3.19 ± 0.016 g/cm^3	3.19 ± 0.016 g/cm^3
Total particle properties		
Diameter	601 to 711 µm	732 to 822 µm
Density	3.17 g/cm^3	3.45 g/cm^3
% U	0	0
% Th	45.32	51.97

[a] Nominal ranges are reference values and are not an inspection requirement.

[b] Bacon anisotropy factor, relative units.

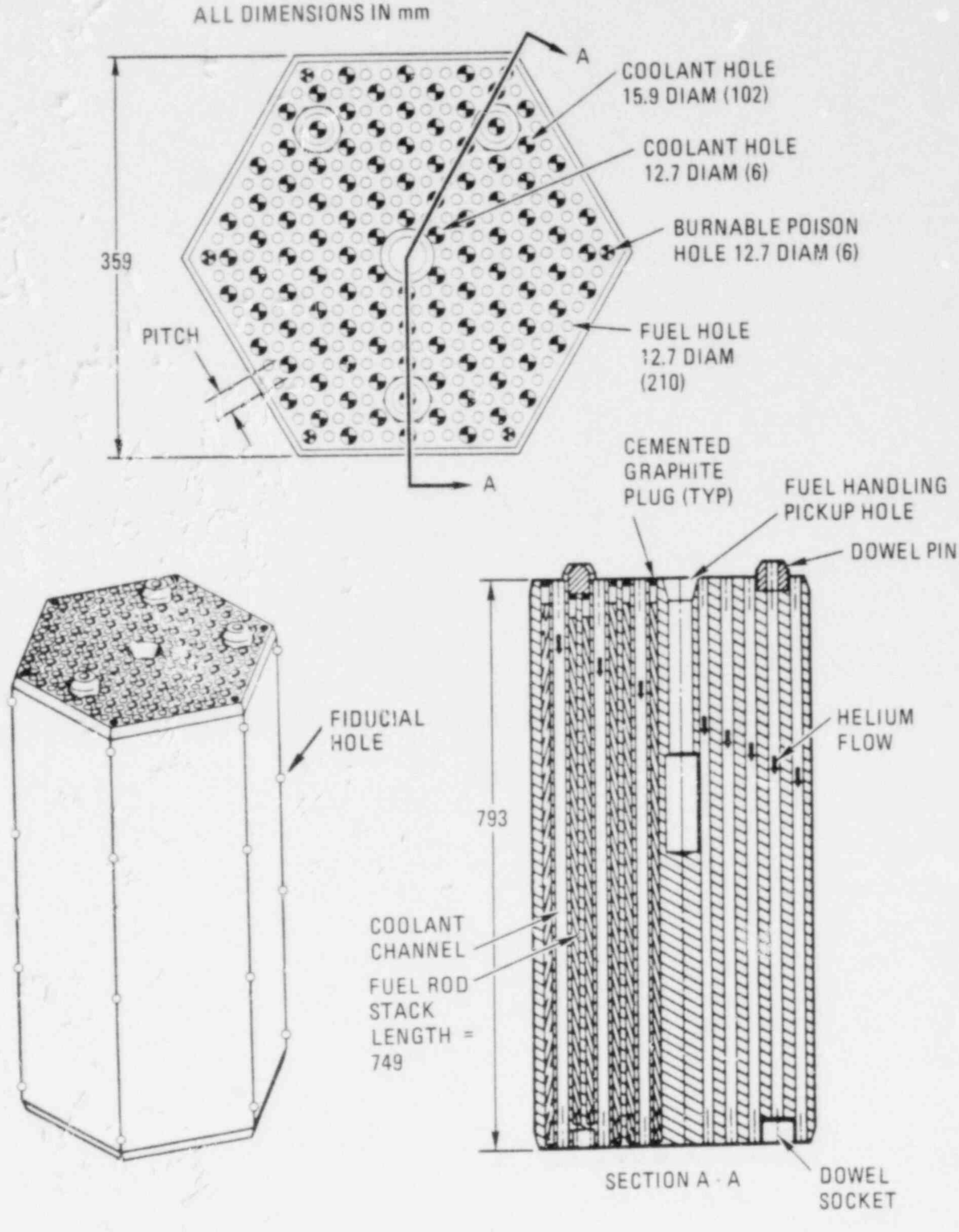

Fig. 2-1. FSV fuel element 1-0743

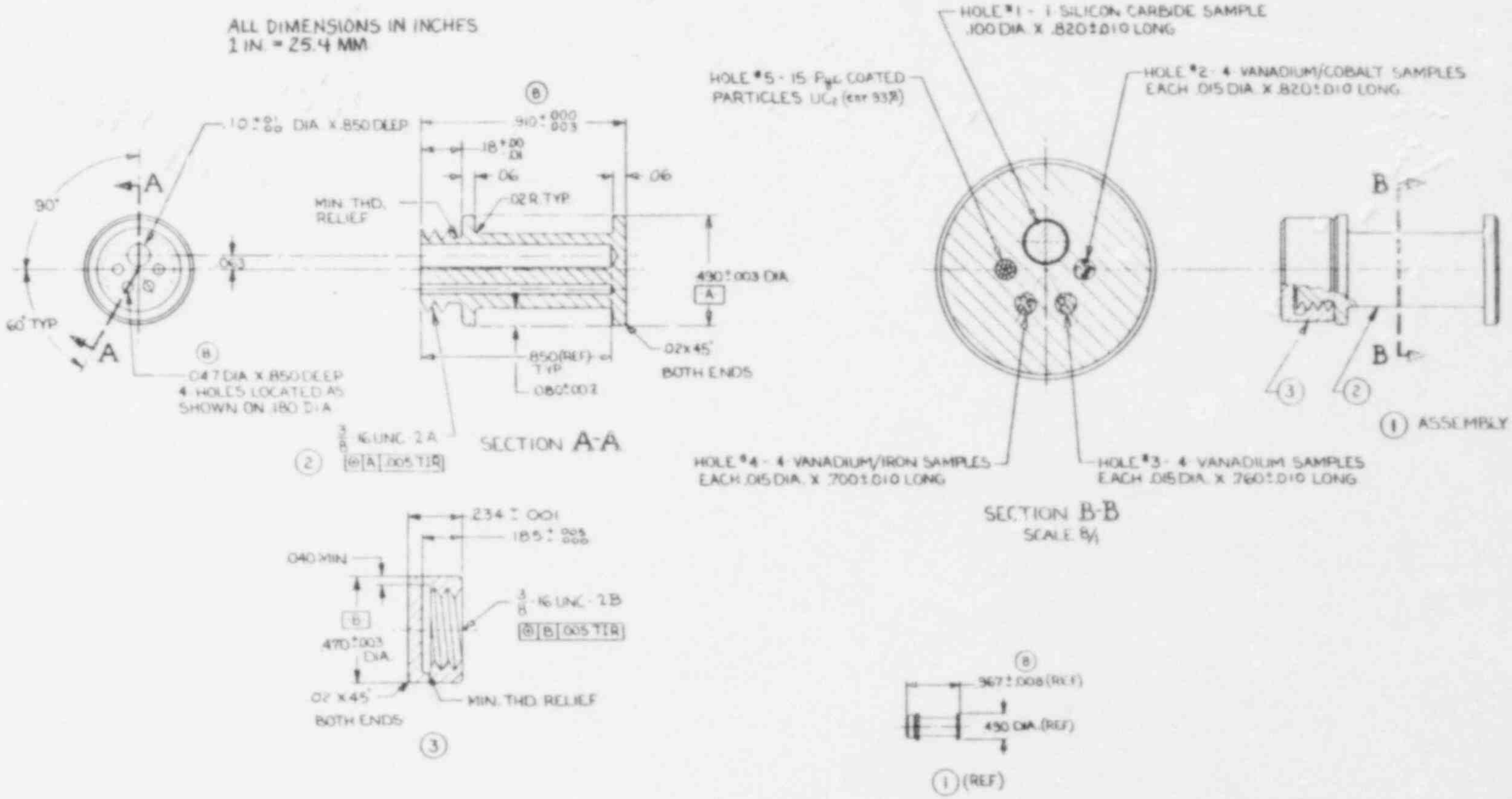

Fig. 2-2. Temperature, fluence, and burnup monitor package

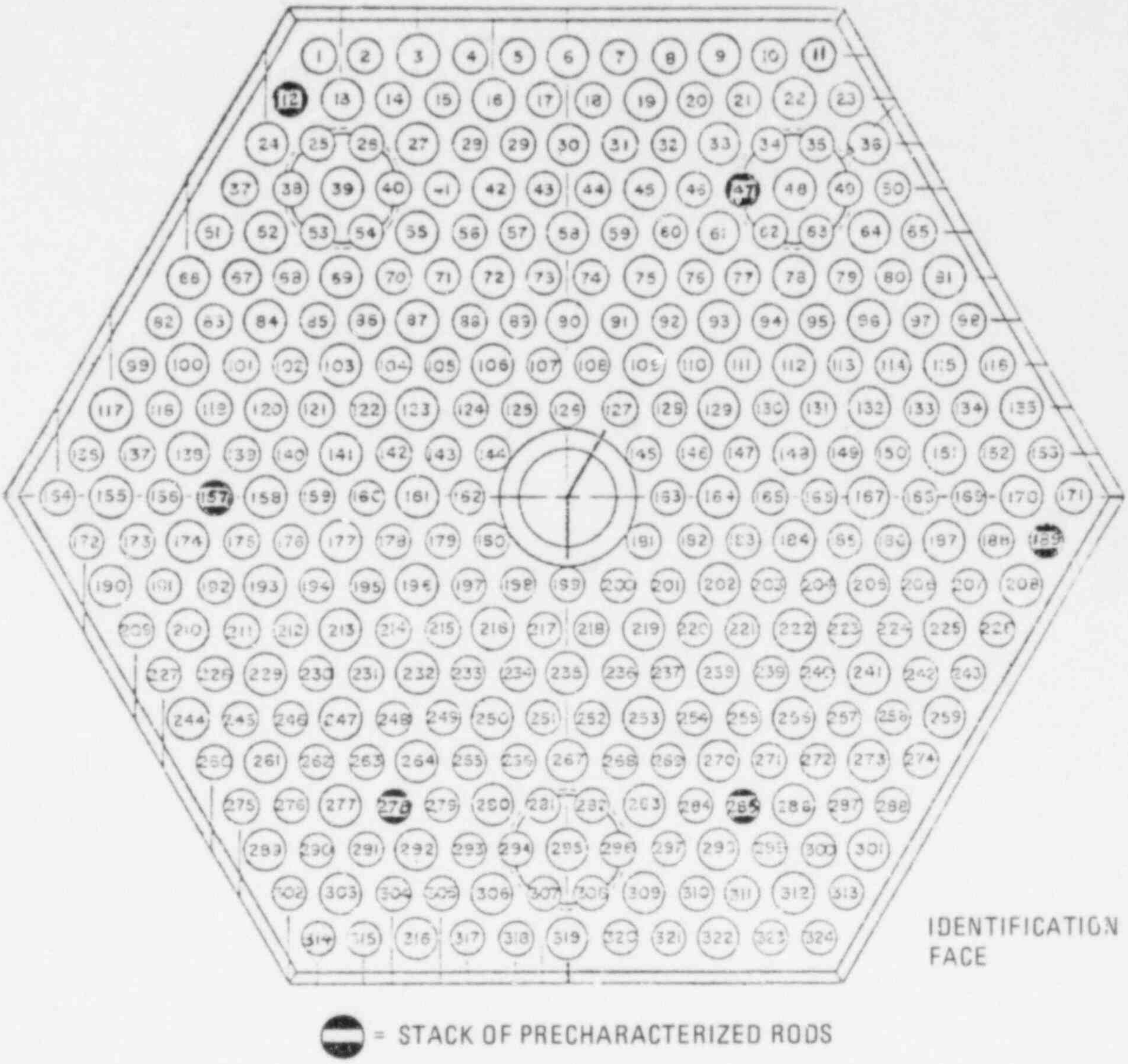

Fig. 2-3. Top view of FSV fuel element 1-0743 showing locations of fuel holes containing precharacterized fuel rods

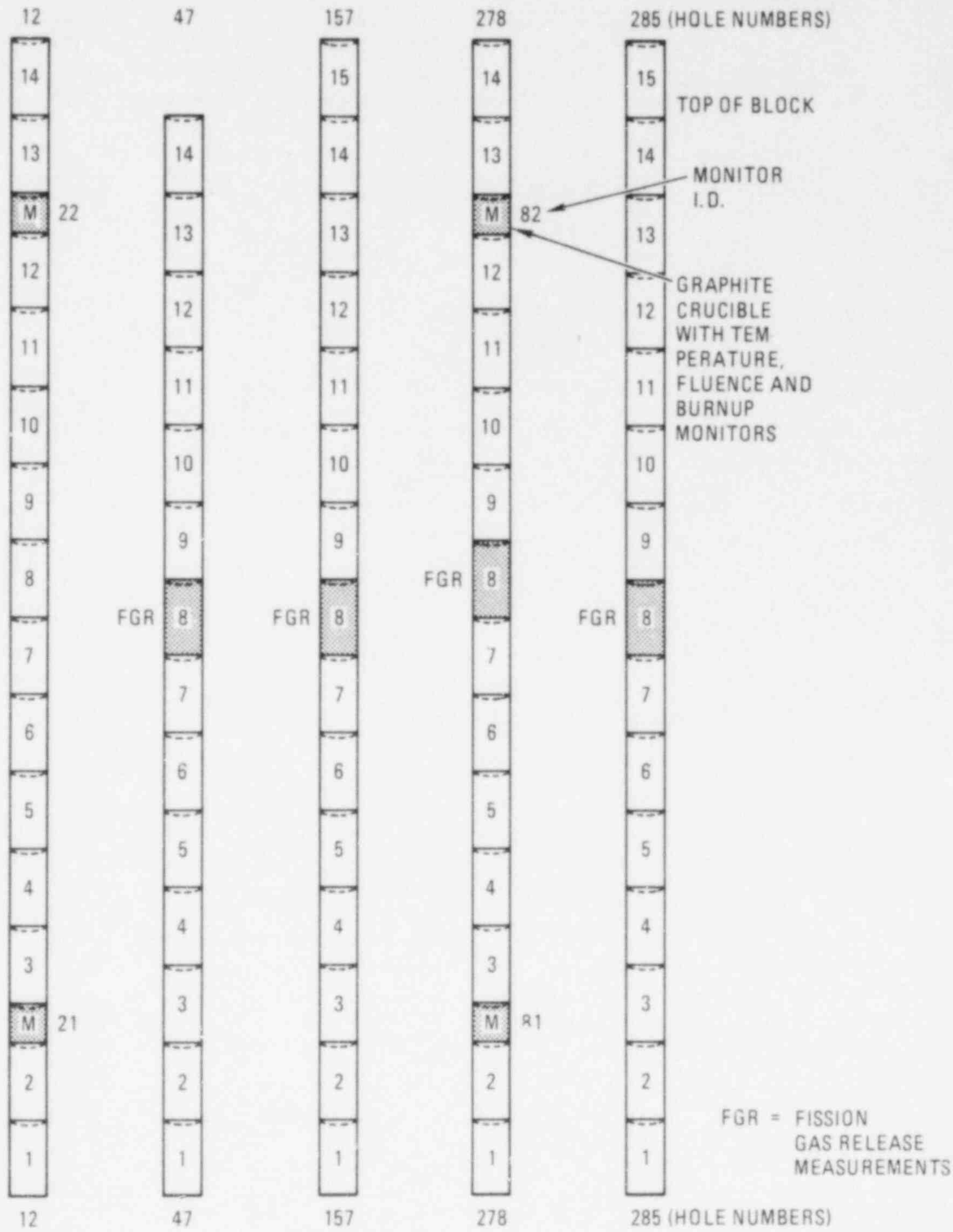

Fig. 2-4. Locations of fuel rods which underwent preirradiation fission gas release measurement and of monitor packages in FSV fuel element 1-0743

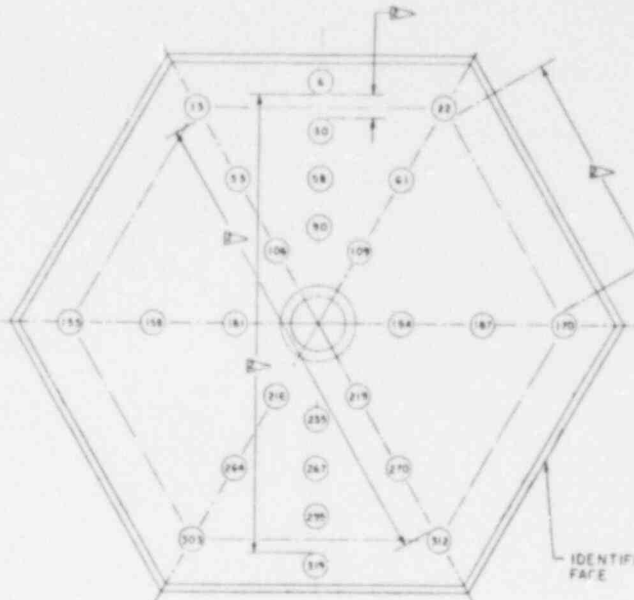

DISTANCE BETWEEN COOLANT HOLES

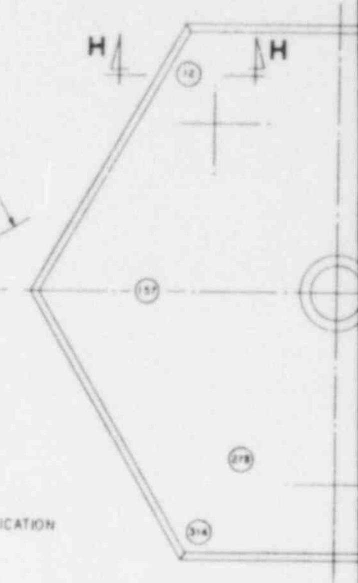

FUEL HOLE DIAMETE
POISON HOLE DIAME

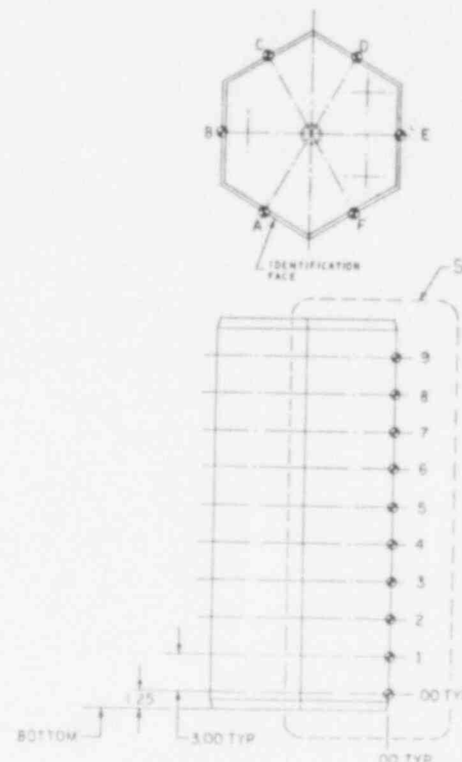

SQUARENESS DATUM PLANES

DETAIL **T** 'KEY' TO
(+) AND (-) DIMENSION
READINGS

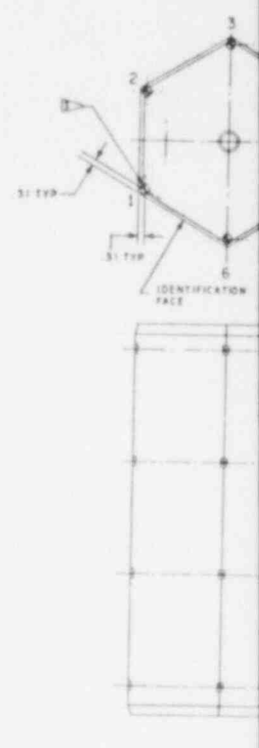

AXIAL DIMEN

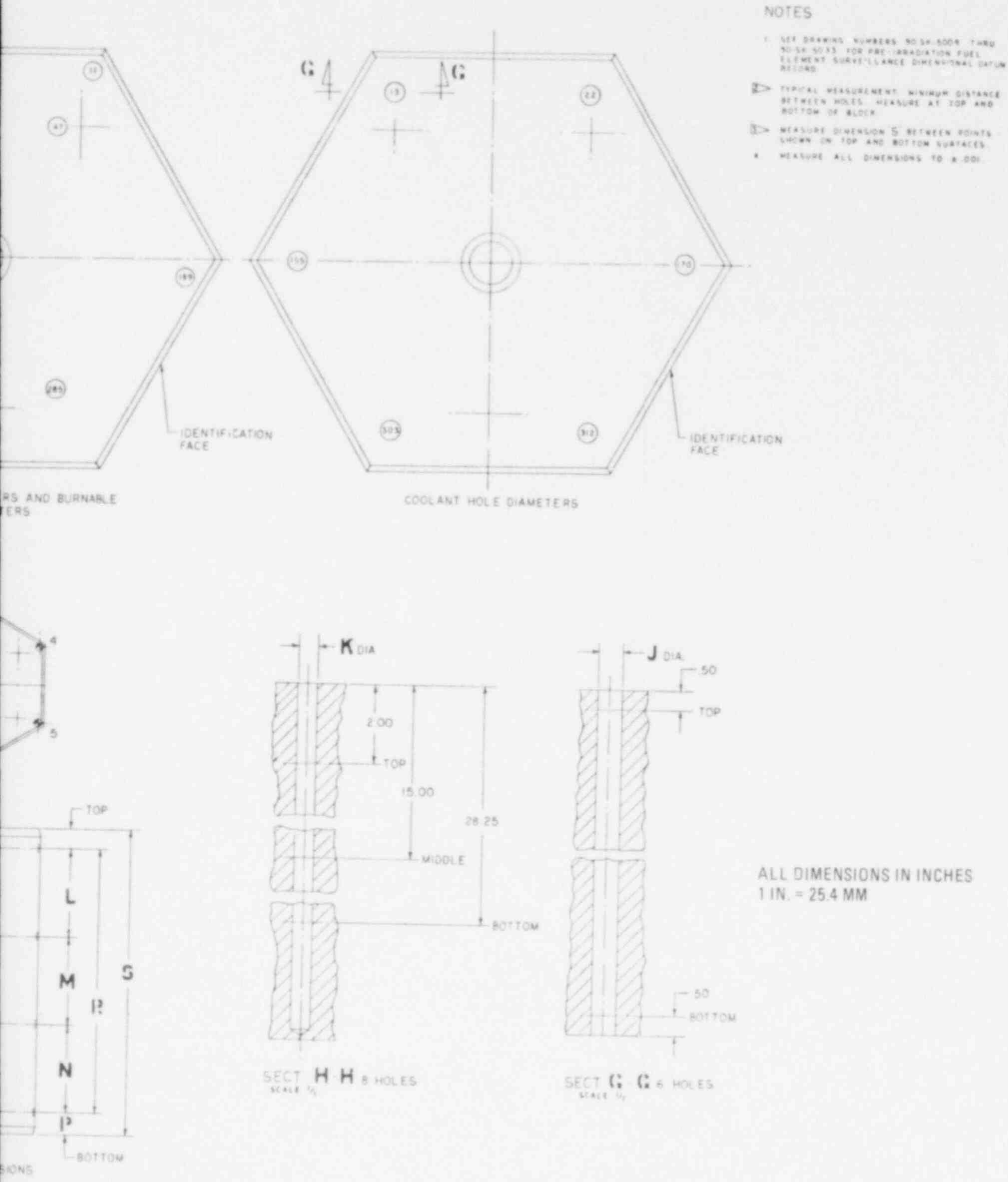

Fig. 2-5. Preirradiation fuel block measurements for FSV fuel element 1-0743

DISTANCE BETWEEN COOLANT HOLES

TABLE

DATUM PLANE	LOCATION AND MINIMUM DISTANCE BETWEEN COOLANT HOLES								
HOLES 312 TO 13		312 TO 270	270 TO 219	219 TO 106	106 TO 55	55 TO 13	312 TO 13		
TOP OF BLOCK	PRE IRRADIATION	1.594	1.597	3.818	1.595	1.601	12.495		
	POST IRRADIATION								
	DIFFERENCE								
BOTTOM OF BLOCK	PRE IRRADIATION	1.598	1.594	3.816	1.601	1.598	12.500		
	POST IRRADIATION								
	DIFFERENCE								
HOLES 319 TO 6		319 TO 295	295 TO 267	267 TO 235	235 TO 90	90 TO 58	58 TO 30	30 TO 6	319 TO 6
TOP OF BLOCK	PRE IRRADIATION	.655	.655	.657	4.535	.658	.660	.658	12.191
	POST IRRADIATION								
	DIFFERENCE								
BOTTOM OF BLOCK	PRE IRRADIATION	.655	.654	.655	4.508	.656	.657	.662	12.196
	POST IRRADIATION								
	DIFFERENCE								
HOLES 303 TO 22		303 TO 264	264 TO 216	216 TO 109	109 TO 51	51 TO 22	303 TO 22		
TOP OF BLOCK	PRE IRRADIATION	1.596	1.597	3.825	1.598	1.596	12.496		
	POST IRRADIATION								
	DIFFERENCE								
BOTTOM OF BLOCK	PRE IRRADIATION	1.598	1.598	3.825	1.596	1.601	12.395		
	POST IRRADIATION								
	DIFFERENCE								
HOLES 170 TO 155		170 TO 167	167 TO 164	164 TO 161	161 TO 158	158 TO 155	170 TO 155		
TOP OF BLOCK	PRE IRRADIATION	1.598	1.596	3.819	1.595	1.594	12.490		
	POST IRRADIATION								
	DIFFERENCE								
BOTTOM OF BLOCK	PRE IRRADIATION	1.594	1.596	3.817	1.597	1.596	12.492		
	POST IRRADIATION								
	DIFFERENCE								
HOLES		13 TO 22	22 TO 170	170 TO 312	312 TO 303	303 TO 155	155 TO 13		
TOP OF BLOCK	PRE IRRADIATION	6.037	6.036	6.034	6.036	6.035	6.038		
	POST IRRADIATION								
	DIFFERENCE								
BOTTOM OF BLOCK	PRE IRRADIATION	6.036	6.037	6.035	6.035	6.038	6.037		
	POST IRRADIATION								
	DIFFERENCE								

ALL DIMENSIONS IN INCHES. 1 IN. = 25.4 MM

FUEL HOLE DIAMETERS AND BURNABLE POISON HOLE DIAMETERS

TABLE

HOLE NO.		HOLE DIAMETER TOP K DIA.	MIDDLE K DIA.	BOTTOM K DIA.
11	PRE IRRADIATION	.498	.4975	.4975
	POST IRRADIATION			
	DIFFERENCE			
12	PRE IRRADIATION	.498	.498	.4975
	POST IRRADIATION			
	DIFFERENCE			
47	PRE IRRADIATION	.498	.498	.4975
	POST IRRADIATION			
	DIFFERENCE			
157	PRE IRRADIATION	.4975	.497	.497
	POST IRRADIATION			
	DIFFERENCE			
189	PRE IRRADIATION	.4985	.4985	.498
	POST IRRADIATION			
	DIFFERENCE			
278	PRE IRRADIATION	.498	.498	.4975
	POST IRRADIATION			
	DIFFERENCE			
285	PRE IRRADIATION	.498	.498	.4975
	POST IRRADIATION			
	DIFFERENCE			
514	PRE IRRADIATION	.498	.498	.4975
	POST IRRADIATION			
	DIFFERENCE			

AXIAL DIMENSIONS

TABLE

CORNER NO.		L DIM.	M DIM.	N DIM.	P DIM.	R DIM.	S DIM.
1	PRE IRRADIATION	9.0015	9.003	9.002	2.251	27.002	31.2545
	POST IRRADIATION						
	DIFFERENCE						
2	PRE IRRADIATION	9.0015	9.002	9.003	2.2515	27.0045	31.233
	POST IRRADIATION						
	DIFFERENCE						
3	PRE IRRADIATION	9.001	9.002	9.0015	2.2485	27.0045	31.233
	POST IRRADIATION						
	DIFFERENCE						
4	PRE IRRADIATION	9.0025	9.0005	9.0025	2.2515	27.0035	31.232
	POST IRRADIATION						
	DIFFERENCE						
5	PRE IRRADIATION	9.002	9.001	9.0015	2.253	27.0055	31.2315
	POST IRRADIATION						
	DIFFERENCE						
6	PRE IRRADIATION	9.0015	9.0025	9.0025	2.2505	27.0045	31.233
	POST IRRADIATION						
	DIFFERENCE						

SQUARENESS DATUM PLANES

TABLE

MAXIMUM DISPLACEMENT FROM SQUARENESS AT VERTICAL INCREMENTAL DISTANCE UP LENGTH OF BLOCK. SEE DETAIL T FOR INTERPRETATION OF (+) AND (−) VALUES

SIDE ON ℄		1	2	3	4	5	6	7	8	9
A	PRE IRRADIATION	−.0005	−.001	−.002	−.002	−.001	.000	−.004	−.0015	−.0001
	POST IRRADIATION									
	DIFFERENCE									
B	PRE IRRADIATION	+.001	+.0005	.000	+.001	−.0005	.000	−.001	−.001	−.001
	POST IRRADIATION									
	DIFFERENCE									
C	PRE IRRADIATION	+.0005	+.001	+.001	+.001	+.001	+.0015	+.001	+.0005	+.0015
	POST IRRADIATION									
	DIFFERENCE									
D	PRE IRRADIATION	+.0005	+.0005	+.001	+.001	+.001	+.0001	+.0015	+.002	+.0015
	POST IRRADIATION									
	DIFFERENCE									
E	PRE IRRADIATION	.000	+.0005	.000	+.0005	+.001	+.001	+.001	+.0015	+.002
	POST IRRADIATION									
	DIFFERENCE									
F	PRE IRRADIATION	.000	+.001	+.0005	.000	.000	.000	+.0005	+.0005	+.0005
	POST IRRADIATION									
	DIFFERENCE									

COOLANT HOLE DIAMETERS

TABLE

HOLE NO		HOLE DIAMETER TOP J DIA	BOTTOM J DIA
13	PRE IRRADIATION	.625	.625
	POST IRRADIATION		
	DIFFERENCE		
22	PRE IRRADIATION	.625	.625
	POST IRRADIATION		
	DIFFERENCE		
155	PRE IRRADIATION	.625	.624
	POST IRRADIATION		
	DIFFERENCE		
170	PRE IRRADIATION	.625	.624
	POST IRRADIATION		
	DIFFERENCE		
303	PRE IRRADIATION	.625	.624
	POST IRRADIATION		
	DIFFERENCE		
312	PRE IRRADIATION	.625	.624
	POST IRRADIATION		
	DIFFERENCE		

Fig. 2-6. Preirradiation fuel block dimensions for FSV fuel element 1-0743

3. IRRADIATION CONDITIONS

3.1. IRRADIATION HISTORY

Fort St. Vrain fuel element 1-0743 was irradiated in core location 17.04.F.06 from July 3, 1976 until February 1, 1979. During this time, the cumulative core power was 146,500 MWd. The reactor was at significant power (>10 MW) for aproximately 500 days, and the average reactor power was about 293 MW (35% power). In terms of EFPD,* the irradiation time was 174 days.

The irradiation history of the element has been simulated using the following HTGR design codes:

GAUGE (Ref. 2): a two-dimensional, four-group neutron diffusion and core depletion code. GAUGE treats the core as a single layer and calculates nuclide densities as a function of time and radial core location.

GATT (Ref. 3): a three-dimensional, four-group neutron diffusion and core depletion code. GATT calculates nuclide densities as a function of time and axial and radial core location.

FEVER (Ref. 4): a one-dimensional, multigroup neutron diffusion and depletion program for calculating nuclide densities as a function of axial core location.

---

*An EFPD is the equivalent of 1 day of operation at full power (842 MW).

BUG-2 (Ref. 5): a two-dimensional, multigroup neutron diffusion and depletion program for calculating nuclide densities as a function of axial core location for fuel assemblies influenced by partially inserted control rods.

SURVEY (Ref. 6): a computer program for the thermal and fuel performance analysis of HTGR fuel elements. The code is used to perform coarse mesh survey analyses for large numbers of spatial positions, calculating a time history of the irradiation conditions and fuel performance for each space point. SURVEY calculations are based on radial power distributions obtained from GAUGE and axial power distributions obtained from FEVER and BUG-2.

SURVEY/STRESS (Ref. 7): a computer program for calculating stresses, strains, and deformations in a large HTGR fuel block using viscoelastic beam theory. The code employs a relatively simple model and is used to survey an entire core to identify elements with high stresses. Once identified, these elements are subjected to more rigorous analyses using codes which employ more complex models. The irradiation conditions used in the stress calculations are obtained from SURVEY.

The reactor operating power is logged on an hourly basis. However, because of the numerous changes in power during cycle 1, an analysis of the actual power history would be prohibitively expensive. Consequently, the power history for cycle 1 was reduced to 335 time intervals of approximately uniform power. Cycle 1 operation was simulated with the GAUGE code using this "detailed" power history. A SURVEY analysis of selected elements, including fuel element 1-0743, was then performed based on the GAUGE results. The number of time intervals was further reduced from 335 to 36 representative time intervals for this analysis. The power history for the SURVEY analysis is shown in Fig. 3-1. Finally, a SURVEY/STRESS analysis was performed based on the SURVEY results. In GAUCE, SURVEY, and SURVEY/ STRESS analyses, calculations are performed at seven radial locations per element, as shown in Fig. 3-2.

In addition to the detailed GAUGE analysis, a three-dimensional burnup analysis of cycle 1 was performed using GATT. The primary objective was to obtain the fuel accountability for the segment 1 fuel elements. Power distributions, neutron fluences, and fuel burnup were also obtained. Because of the great expense of running GATT, the power history had to be reduced to a relatively few time intervals. For the GATT analysis, described in Ref. 8, cycle 1 was represented by 11 time intervals.

A second GAUGE analysis of cycle 1, based on the 11-time-interval power history, and a FEVER code analysis, specifically for fuel element 1-0743, were also performed (Ref. 9). SURVEY code analyses based on the results of these analyses and the results from GATT were not performed.

Envelope and time-averaged temperatures calculated for fuel element 1-0743 are given in Tables 3-1 through 3-8. Fast neutron fluences are shown in Table 3-9. The time- and volume-averaged graphite and fuel temperatures for the element were 646°C and 680°C, respectively. The maximum fuel temperature experienced by the element was 935°C. The element average fast neutron fluence was 0.95×10^{25} n/m^2 (E > 29 fJ)$_{HTGR}$, and the maximum fast fluence was 1.1×10^{25} n/m^2 (E > 29 fJ)$_{HTGR}$. Temperatures and fluences were lowest on the side of the element adjacent to the central column of region 17 and highest on the opposite side. The differences between the highest and lowest time-averaged graphite and fuel temperatures in the element are 68° and 70°C, respectively. The difference between the highest and lowest fast fluence is 0.28×10^{25} n/m^2 (E > 29 fJ)$_{HTGR}$. The fissile and fertile burnups remained approximately constant over the length of the element and were 6.2% and 0.3% FIMA. Fuel burnups were not computed as a function of radial location.

The above results were obtained from the SURVEY-detailed GAUGE analysis. The fuel accountability for element 1-0743 (obtained from GATT) is given in Table 3-10.

3.2. POWER DISTRIBUTION MEASUREMENTS

As part of the PIE of FSV surveillance element 01-0743, extensive gamma scanning was performed to determine the relative distributions of measurable radioisotopes in the fuel. These data provide information on the power distribution in the element during irradiation and can be used to verify nuclear design calculations and to better define the nuclear and thermal parameters corresponding to observed materials performance.

Of particular value are the measured Cs-137 and Zr-95 distributions. Since Cs-137 is a direct-yield isotope from the fission of U-235 and U-233 and has a half-life (30 yr) far greater than the irradiation period for the element, the Cs-137 distribution is representative of the time-averaged power distribution, providing that significant quantities of Cs-137 did not escape from the fuel. This can reasonably be assumed to be the case, since the element contained all-TRISO fuel and experienced relatively low temperature (<1000°C) and neutron exposure [$\sim 1.0 \times 10^{25}$ n/m^2 (E > 29 fJ)$_{HTGR}$]. Zr-95 is also a direct-yield isotope from the fission of U-235 and U-233 but has a half-life of only 65.5 days. The Zr-95 distribution is therefore representative of the power distribution at end of life (EOL).

A brief discussion of how the gamma scanning was performed is presented below. The measured Cs-137 and Zr-95 distributions are then presented and compared with predicted power distributions. Homogeneity data obtained for segment 1 fuel rods are also discussed.

3.2.1. Description of Gamma Scanning System

The gamma scanning system consists of a robotic device that accurately positions the fuel element in front of a collimator aligned with an out-of-cell high-resolution Ge(Li) detector. The signal from the detector is sent to a Nuclear Data (ND) 6620 data acquisition system and to a single-channel analyzer (SCA)-ratemeter-recorder system. The ND 6620 system collects the spectra and stores them on a disk, where they are later accessed and analyzed by various spectral analysis programs. The SCA-ratemeter-recorder system monitors and traces the Cs-137 distribution. A collimator constructed of aluminum and having a length of 1759 mm and a 15.9 x 12.7 mm cross-sectional opening is used for all gamma scanning. An overview of the system is shown in Fig. 3-3.

The _in situ_ gamma spectroscopic examination of FSV surveillance element 01-0743 was performed using three basic scanning geometries. These geometries, which are referred to as the axial corner, axial side-face, and end-on scanning geometries, are shown in Figs. 3-4, 3-5, and 3-6, respectively.

Axial scanning was performed as the fuel block was moved slowly past the collimator. Spectra were acquired at intervals approximately equal to the length of a fuel rod. The acquisition times for an axial corner scan and for a side-face scan (one rod length per scan) were approximately 8 and 5 min, respectively. The length of the block was scanned a total of 15 times, 9 times via the side-face scaning geometry and 6 times via the corner scanning geometry. Each end-on scan was obtained by summing a series of static scans that traversed the cross section of the fuel stack under observation. The acquisition time for an end-on scan was approximately 6 min. End-on scans of 70 fuel stacks were acquired. The end-on scans were performed with the bottom of the block facing the detector. All in situ gamma scanning was performed in an automated mode under the direction of the ND 6620 computer.

3.2.2. Radial Power Distributions

The normalized radial distributions of Cs-137 and Zr-95 in FSV surveillance element 01-0743 are shown in Figs. 3-7 and 3-8. The Cs-137 distribution is compared with calculated time-averaged power distributions in Table 3-11 and the Zr-95 distribution with calculated radial power distributions at EOL in Table 3-12. Little intrablock tilting in the radial power distribution was calculated and little was observed. For time-averaged power the maximum observed tilt (difference between the highest and lowest relative power factor) was 9%, and the maximum calculated tilts were 13% for the SURVEY-detailed GAUGE analysis and 4% for the 11-time-interval GAUGE analysis. The reason for the relatively large difference in the calculated tilts has not been determined. At EOL, the maximum observed tilt was 8% and the calculated tilts were 4% for the SURVEY-detailed GAUGE analysis, 3% for the GATT analysis, and 4% for the 11-time-interval GAUGE analysis. The agreement between calculated and measured local-to-block average power factors was within 7.5% for all local points This is well within the ±10% uncertainty (1σ) generally quoted for GAUGE calculations and confirmed in Ref. 10.

3.2.3. Axial Power Distributions

Measured and calculated axial power distributions for fuel element 1-0743 are shown in Figs. 3-9 (time averaged) and 3-10 (EOL). The measured profiles are normalized Cs-137 and Zr-95 profiles obtained by averaging the results of six axial side-face scans. A cross-sectional view of the portion of the element observed by these scans is shown in Fig. 3-11. The calculated profiles were otained with the FEVER code.

The agreement between the measured and calculated profiles at EOL is excellent. The time-averaged profiles are also in good agreement except near the bottom of the element, where the disagreement approaches 10%. The reason for the discrepancy near the bottom of the element is that the FEVER model cannot account for the control rod in region 34, which was partially inserted during much of cycle 1. The effect of this partially inserted control rod was to tilt the axial power distribution toward the bottom of the element. At EOL the rod was nearly withdrawn, so its influence on the axial power distribution was minimal. This explains the improved agreement between the measured and calculated power profiles at EOL.

3.2.4. Fuel Rod Homogeneity

The distribution of Cs-137 and other measured radioisotopes along the length of individual fuel rods was observed to be markedly U-shaped, with the activity near the ends being almost twice the activity in the middle for many of the rods. A portion of a typical Cs-137 trace for an axial scan is shown in Fig. 3-12. Nearly all rods were observed to have this U-shaped profile, suggesting a manufacturing process that tended to segregate the fissile particles toward the ends of the rods. This has been confirmed via gamma scanning of unirradiated fuel (Ref. 11), which showed the U-235 distribution in segment 1 fuel rods to have the same shape as the Cs-137 distribution.

3.3. FLUENCE MEASUREMENTS

Three types of dosimeters were included in the monitor packages irradiated in fuel element 1-0743: V-Co and pure V wires for measuring the thermal neutron fluence and V-Fe wires for measuring the fast neutron fluence. The reactions of interest for the dosimeters are listed in Table 3-13. All dosimeters were recovered from the four monitor packages and submitted for gamma ray analysis. The measured activities for the radionuclides of interest were back-decayed to EOL and used to compute the fast and thermal fluences for each monitor location. The cross sections used in the calculations were obtained from Ref. 12 and are listed in Table 3-14.

Measured fluences are compared with predictions in Table 3-15. The predicted fluences were obtained from the SURVEY-detailed GAUGE, GATT, and 11-time-interval GAUGE analyses of cycle 1. The agreement between measured and calculated fast fluences is excellent (within 6% for all comparisons). The agreement between measured and calculated thermal fluences is not as good. The predicted thermal fluence is 11.9% smaller than the thermal fluence determined from the V-Co dosimeters and 39.9% greater than the fluence determined from the pure V dosimeters. The fluence established from the V dosimeters is believed to be in error, but it is not certain at this time whether the error is due to using the wrong cross section for the $^{51}V(n,\gamma)^{52}V$ reaction or to a defect in the technique for measuring the ^{52}Cr resulting from the β decay of ^{52}V.

3.4. TEMPERATURE MEASUREMENTS

Irradiation of SiC produces a small increase in macrodimensions which is related to the irradiation temperature. Postirradiation annealing at progressively higher temperatures causes no change to occur in the SiC until a critical temperature is reached, after which the length decreases as the irradiation damaged is annealed out. This decrease in length is approximately linear with increasing temperature. The critical temperature, which is determined from the intersection of the regression lines for the two essentially linear portions of the annealing curve, is related to the irradiation temperature.

Irradiation temperatures for the four SiC pellets recovered from the monitor packages were determined via isochronal annealing. The pellets were annealed for a period of about 1 hr at temperatures from 200° to 1100°C in 50°C increments. The annealing curves for the SiC pellets are shown in Fig. 3-13. Irradiation temperatures were determined from the annealing curve intersection temperatures using the calibration curve for SiC temperature monitors presented in Ref. 13.

A comparison of measured and calculated temperatures for the monitors is made in Table 3-16. The measured temperatures are assumed to be approximately representative of temperatures during periods of higher reactor power operation shortly before shutdown. This is thought to be the case since irradiation damage accumulated at low temperatures would have been annealed out at the relatively high temperatures experienced by the samples during these periods, and since the period of lower power (and temperature) operation just prior to shutdown was too short for a significant accumulation of low-temperature-related irradiation damage. The core power over the last ~2×10^{20} n/cm^2 $(E > 29fJ)_{HTGR}$ is shown in Fig. 3-14.* Calculated temperatures were obtained from SURVEY-calculated peak fuel and coolant temperatures at the axial locations of neighboring fuel rods using a factor obtained with the TAC-2D (Ref. 14) code.**

The calculated temperature for each temperature monitor was approximately 25°C greater than the measured temperature. In all cases, the calculated temperature was within the 95% confidence limits for the measured temperature.

3.5. BURNUP MEASUREMENTS

UC_2 fissile particles from three of the four monitor packages and ThC_2 fertile particles obtained from neighboring fuel rods were submitted for burnup analysis. The fissile particles were analyzed using (1) a radiochemistry method employing Cs-137 as a burnup monitor and (2) a mass spectrometric method in which burnup was determined from changes in uranium isotopic composition. The fertile particles were analyzed using a method in which the thorium content in the particles was deduced from the Pa-233 activity following a short irradiation in the TRIGA test reactor. The details of the analyses are provided in Appendix A. The results of the analyses are summarized in Table 3-17. The composite burnups for the $(Th,U)C_2$ fissile particle and for the total fuel have been calculated from the fissile and fertile burnups using the equation

$$F_c = F_5 \cdot X + F_3 (1 - X) \quad ,$$

where F_c = composite burnup,

F_5 = fissile burnup from analyses of UC_2 particles,

F_3 = fertile burnup from analyses of ThC_2 particles,

---

*The power history shown is from the 335 time interval history used for the "detailed" GAUGE analysis of FSV cycle 1. The hour-by-hour power history exhibited far more variations in power.

**$T_c = T_{coolant} + f\ (T_{fuel} - T_{coolant})$; $f = 0.62$.

and

$$X = \frac{U_o}{U_o + Th_o} ,$$

where U_o = appropriate initial uranium loading (atoms),

Th_o = appropriate initial thorium loading (atoms).

Initial heavy metal loadings were obtained from the fuel accountability (Table 3-10).

In addition to the above burnup analyses, fuel burnup was also measured via gamma spectrometry. As part of the gamma spectroscopic examination of the intact fuel element (see Section 3.2), all six pairs of fuel stacks occupying the corner fuel holes were scanned. Later, upon removal of the fuel from the element, each of these 12 fuel stacks was scanned individually. The stacks were placed in thin-walled plexiglass tubes and scanned rod-by-rod as they were moved slowly past the collimator. Absolute calibration of the gamma scanning system using a Cs-137 standard permitted fuel burnup to be determined for the fuel stacks. Burnup data obtained from gamma spectrometry are presented in Table 3-18. Since gamma spectrometry cannot distinguish between the components of an aggregate sample, only the composite burnup for the aggregate (in this case, fuel rods) was determined. However, the composite burnup could be divided into fissile and fertile particle burnup if the fraction of fissions occurring in each type of particle were accurately known from some other source.

Examination of the burnups determined by gamma spectroscopy and by destructive techniques yields the following conclusions:

1. The relative difference between the burnups determined from the gamma scanning of single fuel stacks after removal from the

element and the burnups determined from scanning of the fuel while still in the element is ±5.6% (1σ) with a bias of 1.9%. The bias is not statistically significant.

2. The relative difference between the element average composite burnup determined from gamma spectrometry (1.38%) and from destructive measurements (1.42% ± 0.03%) is 2.8% ± 2.1% (1σ).

These results are important because they verify the calibration of the gamma scanning system and demonstrate the validity of gamma scanning as a means of inexpensively acquiring data for fuel burnup (and therefore power generation) in an HTGR fuel element. As part of the FSV surveillance program, gamma spectrometric examinations of irradiated fuel elements in the hot service facility at FSV are planned after each reload, starting with reload 3. These examinations will be performed using a gamma scan robot system currently being developed at GA. This system was successfully employed, in a preliminary state of development, to examine fuel element 1-0743 in the hot cell at GA.

Measured and calculated element average burnups for fuel element 1-0743 are compared in Table 3-19. The relative differences between calculated and measured composite burnups (indicative of total power generation) are -3.5% ± 2.0%* (1σ) for the SURVEY-detailed GAUGE analysis, -9.9% ± 1.9% (1σ) for the GATT analysis, and -17.6% ± 1.7% (1σ) for burnups calculated using fluxes from the FEVER analysis. In each case, the fissile particle burnup is somewhat better predicted than the fertile particle burnup.

A comparison of measured and calculated uranium isotopic concentrations in the UC_2 fissile particles irradiated in the burnup monitors is given in Table 3-20. The U-234 and U-235 concentrations are slightly overpredicted

---

*The uncertainties in the relative differences are based on the measurement uncertainties only. The relative difference is given by (Calc - Meas)/Meas, so a negative value means that the calculated burnup is less than the measured burnup.

and the U-236 and U-238 concentrations are underpredicted. This result is as expected, since it has already been observed that the burnup was underpredicted.

TABLE 3-1
ENVELOPE AND TIME-AVERAGED TEMPERATURES FOR FSV FUEL ELEMENT 1-0743
ELEMENT AVERAGE

TEMPERATURE ENVELOPE

	DISTANCE FROM BOTTOM OF ELEMENT (MM)	MAXIMUM FUEL(C)	MINIMUM FUEL(C)	MAXIMUM GRAPHITE(C)	MINIMUM GRAPHITE(C)
	793.	749.	515.	691.	495.
	595.	778.	540.	719.	523.
	396.	803.	558.	744.	539.
	198.	827.	573.	769.	552.
	0.	855.	591.	796.	567.
MEAN	396.	803.	555.	744.	535.
RMS		37.	26.	37.	25.

TIME WEIGHTED IRRADIATION TEMPERATURES

	DISTANCE FROM BOTTOM OF ELEMENT (MM)	MAX FUEL (C)	RMS (C)	AVG FUEL (C)	RMS (C)	MIN FUEL (C)	RMS (C)	MAX (a) GRAP (C)	RMS (C)	AVG (a) GRAP (C)	RMS (C)	MIN (a) GRAP (C)	RMS (C)	COOL(b) (C)	RMS (C)
	793.	644.	73.	633.	68.	621.	62.	603.	55.	598.	52.	593.	49.	471.	27.
	595.	669.	74.	658.	69.	646.	64.	628.	56.	623.	53.	618.	50.	493.	29.
	396.	692.	75.	680.	70.	669.	65.	651.	57.	646.	54.	641.	52.	515.	31.
	198.	714.	76.	702.	71.	690.	66.	673.	58.	668.	56.	663.	53.	537.	33.
	0.	738.	77.	726.	72.	714.	67.	697.	60.	692.	57.	688.	55.	560.	34.
MEAN,RMS(T)	396.	691.	75.	680.	70.	668.	65.	650.	57.	646.	54.	641.	52.	515.	31.
RMS(X),CRMS		33.	82.	33.	77.	33.	72.	33.	66.	33.	64.	33.	61.	32.	44.

(a) GRAP = GRAPHITE
(b) COOL = COOLANT

TABLE 3-2

ENVELOPE AND TIME-AVERAGED TEMPERATURES FOR FSV FUEL ELEMENT 1-0743

SURVEY LOCAL POINT 1[(a)]

TEMPERATURE ENVELOPE

	DISTANCE FROM BOTTOM OF ELEMENT (MM)	MAXIMUM FUEL (C)	MINIMUM FUEL (C)	MAXIMUM GRAPHITE (C)	MINIMUM GRAPHITE (C)
	793.	749.	517.	691.	498.
	595.	778.	544.	719.	525.
	396.	803.	560.	744.	539.
	198.	828.	575.	769.	552.
	0.	856.	593.	797.	567.
MEAN	396.	803.	558.	744.	536.
RMS		37.	26.	37.	24.

TIME WEIGHTED IRRADIATION TEMPERATURES

	DISTANCE FROM BOTTOM OF ELEMENT (MM)	MAX FUEL (C)	RMS (C)	AVG FUEL (C)	RMS (C)	MIN FUEL (C)	RMS (C)	MAX (b) GRAP (C)	RMS (C)	AVG (b) GRAP (C)	RMS (C)	MIN (b) GRAP (C)	RMS (C)	COOL (c) (C)	RMS (C)
	793.	646.	71.	635.	66.	623.	61.	606.	53.	601.	50.	596.	47.	472.	27.
	595.	672.	73.	660.	67.	649.	62.	631.	55.	626.	52.	621.	49.	494.	29.
	396.	695.	73.	683.	68.	671.	63.	653.	56.	649.	53.	644.	50.	517.	30.
	198.	716.	74.	705.	69.	693.	64.	675.	57.	671.	54.	666.	51.	539.	32.
	0.	741.	75.	729.	70.	717.	65.	700.	58.	695.	56.	691.	53.	562.	34.
MEAN,RMS(T)	396.	694.	73.	682.	68.	671.	63.	653.	56.	648.	53.	643.	50.	517.	30.
RMS(X),CRMS		33.	80.	33.	76.	33.	71.	33.	65.	33.	62.	33.	60.	32.	44.

(a) SEE FIG. 3-2
(b) GRAP = GRAPHITE
(c) COOL = COOLANT

TABLE 3-3
ENVELOPE AND TIME-AVERAGED TEMPERATURES FOR FSV FUEL ELEMENT 1-0743
SURVEY LOCAL POINT 2[(a)]

TEMPERATURE ENVELOPE

	DISTANCE FROM BOTTOM OF ELEMENT (MM)	MAXIMUM FUEL (C)	MINIMUM FUEL (C)	MAXIMUM GRAPHITE (C)	MIMIMUM GRAPHITE (C)
	793.	741.	439.	683.	437.
	595.	769.	455.	711.	452.
	396.	794.	469.	736.	466.
	198.	818.	482.	760.	479.
	0.	846.	497.	788.	495.
MEAN	396.	796.	468.	736.	466.
RMS		37.	20.	37.	20.

TIME WEIGHTED IRRADIATION TEMPERATURES

	DISTANCE FROM BOTTOM OF ELEMENT (MM)	MAX FUEL (C)	RMS (C)	AVG FUEL (C)	RMS (C)	MIN FUEL (C)	RMS (C)	MAX(b) GRAP (C)	RMS (C)	AVG(b) GRAP (C)	RMS (C)	MIN(b) GRAP (C)	RMS (C)	COOL(c) (C)	RMS (C)
	793.	616.	96.	605.	90.	594.	85.	577.	76.	573.	73.	568.	70.	456.	39.
	595.	639.	100.	628.	94.	617.	88.	600.	80.	595.	77.	591.	74.	476.	42.
	396.	660.	103.	648.	97.	637.	91.	620.	83.	616.	80.	611.	77.	496.	46.
	198.	679.	106.	668.	100.	657.	94.	640.	86.	635.	83.	631.	80.	516.	49.
	0.	701.	109.	690.	103.	678.	97.	662.	89.	657.	87.	653.	84.	536.	52.
MEAN,RMS(T)	396.	659.	103.	648.	97.	637.	91.	620.	83.	615.	80.	611.	77.	496.	46.
RMS(X),CRMS		30.	107.	30.	101.	29.	96.	30.	88.	30.	85.	30.	83.	28.	54.

(a) SEE FIG. 3-2
(b) GRAP = GRAPHITE
(c) COOL = COOLANT

TABLE 3-4
ENVELOPE AND TIME-AVERAGED TEMPERATURES FOR FSV FUEL ELEMENT 1-0743
SURVEY LOCAL POINT 3[(a)]

TEMPERATURE ENVELOPE

	DISTANCE FROM BOTTOM OF ELEMENT (MM)	MAXIMUM FUEL (C)	MINIMUM FUEL (C)	MAXIMUM GRAPHITE (C)	MIMIMUM GRAPHITE (C)
	793.	745.	515.	687.	496.
	595.	773.	537.	721.	519.
	396.	798.	553.	757.	535.
	198.	822.	568.	792.	550.
	0.	849.	585.	830.	565.
MEAN	396.	797.	552.	757.	533.
RMS		36.	24.	50.	24.

TIME WEIGHTED IRRADIATION TEMPERATURES

	DISTANCE FROM BOTTOM OF ELEMENT (MM)	MAX FUEL (C)	RMS (C)	AVG FUEL (C)	RMS (C)	MIN FUEL (C)	RMS (C)	MAX (b) GRAP (C)	RMS (C)	AVG (b) GRAP (C)	RMS (C)	MIN (b) GRAP (C)	RMS (C)	COOL (c) (C)	RMS (C)
	793.	647.	64.	635.	59.	624.	55.	606.	48.	601.	45.	596.	42.	473.	25.
	595.	672.	65.	661.	60.	650.	56.	632.	49.	627.	46.	622.	44.	495.	27.
	396.	695.	65.	684.	61.	672.	56.	655.	50.	650.	47.	645.	45.	518.	29.
	198.	717.	66.	706.	61.	694.	57.	677.	51.	672.	48.	667.	46.	540.	31.
	0.	742.	67.	731.	62.	719.	58.	701.	52.	697.	50.	692.	48.	563.	33.
MEAN,RMS(T)	396.	695.	65.	683.	61.	672.	56.	654.	50.	649.	47.	644.	45.	518.	29.
RMS(X),CRMS		33.	73.	33.	69.	33.	65.	33.	60.	33.	58.	33.	56.	32.	43.

(a) SEE FIG. 3-2
(b) GRAP = GRAPHITE
(c) COOL = COOLANT

TABLE 3-5

ENVELOPE AND TIME-AVERAGED TEMPERATURES FOR FSV FUEL ELEMENT 1-0743

SURVEY LOCAL POINT 4[(a)]

TEMPERATURE ENVELOPE

	DISTANCE FROM BOTTOM OF ELEMENT (MM)	MAXIMUM FUEL(C)	MINIMUM FUEL(C)	MAXIMUM GRAPHITE(C)	MIMIMUM GRAPHITE(C)
	793.	765.	526.	756.	508.
	595.	804.	544.	801.	525.
	396.	847.	560.	844.	541.
	198.	889.	576.	886.	557.
	0.	935.	594.	932.	575.
MEAN	396.	848.	560.	844.	541.
RMS		60.	24.	62.	24.

TIME WEIGHTED IRRADIATION TEMPERATURES

	DISTANCE FROM BOTTOM OF ELEMENT (MM)	MAX FUEL (C)	RMS (C)	AVG FUEL (C)	RMS (C)	MIN FUEL (C)	RMS (C)	MAX(b) GRAP (C)	RMS (C)	AVG(b) GRAP (C)	RMS (C)	MIN(b) GRAP (C)	RMS (C)	COOL(c) (C)	RMS (C)
	793.	670.	61.	658.	57.	646.	53.	628.	48.	623.	46.	617.	44.	485.	28.
	595.	697.	62.	685.	58.	673.	55.	655.	50.	650.	48.	644.	46.	509.	31.
	396.	722.	63.	710.	59.	698.	56.	680.	52.	674.	50.	669.	49.	533.	34.
	198.	746.	64.	734.	61.	721.	57.	703.	54.	698.	52.	693.	51.	558.	37.
	0.	773.	66.	760.	62.	748.	60.	730.	57.	725.	55.	720.	54.	583.	41.
MEAN,RMS(T)	396.	721.	63.	709.	60.	697.	56.	679.	52.	674.	51.	669.	49.	533.	34.
RMS(X),CRMS		36.	73.	36.	69.	36.	67.	36.	63.	36.	62.	36.	61.	35.	49.

(a) SEE FIG. 3-2

(b) GRAP = GRAPHITE

(c) = COOLANT

TABLE 3-6
ENVELOPE AND TIME-AVERAGED TEMPERATURES FOR FSV FUEL ELEMENT 1-0743
SURVEY LOCAL POINT 5[(a)]

TEMPERATURE ENVELOPE

	DISTANCE FROM BOTTOM OF ELEMENT (MM)	MAXIMUM FUEL (C)	MINIMUM FUEL (C)	MAXIMUM GRAPHITE (C)	MINIMUM GRAPHITE (C)
	793.	759.	525.	724.	506.
	595.	793.	543.	764.	524.
	396.	825.	559.	803.	540.
	198.	856.	574.	842.	556.
	0.	893.	592.	884.	573.
MEAN	396.	825.	559.	804.	540.
RMS		47.	23.	56.	23.

TIME WEIGHTED IRRADIATION TEMPERATURES

	DISTANCE FROM BOTTOM OF ELEMENT (MM)	MAX FUEL (C)	RMS (C)	AVG FUEL (C)	RMS (C)	MIN FUEL (C)	RMS (C)	MAX (b) GRAP (C)	RMS (C)	AVG (b) GRAP (C)	RMS (C)	MIN (b) GRAP (C)	RMS (C)	COOL (c) (C)	RMS (C)
	793.	665.	65.	654.	60.	642.	56.	624.	50.	618.	48.	613.	45.	482.	28.
	595.	693.	66.	681.	62.	669.	58.	651.	52.	645.	50.	640.	47.	506.	30.
	396.	717.	67.	705.	63.	693.	59.	675.	54.	670.	51.	664.	49.	530.	33.
	198.	740.	68.	728.	64.	716.	60.	698.	55.	693.	53.	688.	51.	554.	36.
	0.	767.	69.	755.	65.	742.	62.	724.	58.	719.	56.	714.	54.	578.	39.
MEAN,RMS(T)	396.	716.	67.	704.	63.	692.	59.	674.	54.	669.	52.	664.	50.	530.	33.
RMS(X),CRMS		35.	76.	35.	72.	35.	68.	35.	64.	35.	63.	36.	61.	34.	48.

(a) SEE FIG. 3-2
(b) GRAP = GRAPHITE
(c) COOL = COOLANT

TABLE 3-7

ENVELOPE AND TIME-AVERAGED TEMPERATURES FOR FSV FUEL ELEMENT 1-0743

SURVEY LOCAL POINT 6[a]

TEMPERATURE ENVELOPE

	DISTANCE FROM BOTTOM OF ELEMENT (MM)	MAXIMUM FUEL(C)	MINIMUM FUEL(C)	MAXIMUM GRAPHITE(C)	MINIMUM GRAPHITE(C)
	793.	745.	506.	687.	493.
	595.	774.	527.	715.	517.
	396.	798.	547.	740.	532.
	198.	822.	566.	764.	547.
	0.	850.	583.	791.	563.
MEAN	396.	798.	546.	739.	530.
RMS		36.	27.	36.	24.

TIME WEIGHTED IRRADIATION TEMPERATURES

	DISTANCE FROM BOTTOM OF ELEMENT (MM)	MAX FUEL (C)	RMS (C)	AVG FUEL (C)	RMS (C)	MIN FUEL (C)	RMS (C)	MAX(b) GRAP (C)	RMS (C)	AVG(b) GRAP (C)	RMS (C)	MIN(b) GRAP (C)	RMS (C)	COOL(c) (C)	RMS (C)
	793.	639.	75.	628.	70.	617.	65.	599.	57.	594.	54.	589.	51.	468.	29.
	595.	664.	77.	653.	72.	641.	67.	624.	59.	618.	56.	613.	53.	490.	31.
	396.	686.	78.	675.	73.	663.	68.	646.	60.	641.	58.	636.	55.	512.	33.
	198.	708.	79.	696.	74.	685.	69.	667.	62.	662.	59.	657.	56.	534.	35.
	0.	732.	81.	720.	76.	708.	71.	691.	64.	686.	61.	682.	58.	556.	37.
MEAN,RMS(T)	396.	686.	78.	674.	73.	663.	68.	645.	61.	640.	58.	635.	55.	512.	33.
RMS(X),CRMS		32.	85.	32.	80.	32.	75.	32.	69.	32.	66.	32.	64.	31.	45.

(a) SEE FIG. 3-2
(b) GRAP = GRAPHITE
(c) COOL = COOLANT

TABLE 3-8
ENVELOPE AND TIME-AVERAGED TEMPERATURES FOR FSV FUEL ELEMENT 1-0743
SURVEY LOCAL POINT 7[a]

TEMPERATURE ENVELOPE

	DISTANCE FROM BOTTOM OF ELEMENT (MM)	MAXIMUM FUEL(C)	MINIMUM FUEL(C)	MAXIMUM GRAPHITE(C)	MIMIMUM GRAPHITE(C)
	793.	744.	426.	687.	424.
	595.	773.	440.	715.	438.
	396.	798.	453.	740.	450.
	198.	823.	465.	764.	463.
	0.	850.	479.	792.	477.
MEAN	396.	798.	453.	740.	450.
RMS		37.	18.	37.	18.

TIME WEIGHTED IRRADIATION TEMPERATURES

	DISTANCE FROM BOTTOM OF ELEMENT (MM)	MAX FUEL (C)	RMS (C)	AVG FUEL (C)	RMS (C)	MIN FUEL (C)	RMS (C)	MAX[b] GRAP (C)	RMS (C)	AVG[b] GRAP (C)	RMS (C)	MIN[b] GRAP (C)	RMS (C)	COOL[c] (C)	RMS (C)
	793.	616.	102.	605.	96.	594.	90.	577.	81.	572.	78.	568.	75.	455.	42.
	595.	639.	106.	628.	100.	617.	94.	599.	86.	595.	83.	590.	80.	475.	46.
	396.	659.	110.	648.	104.	637.	98.	620.	89.	615.	86.	611.	83.	495.	49.
	198.	679.	113.	667.	107.	656.	101.	639.	93.	635.	90.	630.	87.	515.	53.
	0.	701.	117.	690.	111.	678.	105.	661.	97.	657.	94.	652.	91.	535.	57.
MEAN,RMS(T)	396.	659.	110.	648.	104.	636.	98.	619.	89.	615.	86.	610.	83.	495.	50.
RMS(X),CRMS		30.	114.	30.	109.	29.	102.	29.	94.	30.	91.	30.	89.	28.	57.

(a) See Fig. 3-2
(b) GRAP = GRAPHITE
(c) COOL = COOLANT

TABLE 3-9
FAST NEUTRON FLUENCES FOR FSV FUEL ELEMENT 1-0743

Radial Location		Fast Neutron Fluence (10^{25} n/m^2) (E > 29 fJ)$_{HTGR}$[a]				
FSV	SURVEY Local Point	z = 793 mm[b]	z = 594.7 mm	z = 396.5 mm	z = 198.2 mm	z = 0 mm
Center	1	0.95	0.96	0.96	0.96	0.91
Corner 1	4	1.09	1.10	1.10	1.10	1.04
Corner 2	5	1.08	1.09	1.10	1.09	1.03
Corner 3	6	0.99	1.00	1.00	0.99	0.94
Corner 4	7	0.83	0.83	0.84	0.83	0.79
Corner 5	2	0.82	0.82	0.83	0.82	0.78
Corner 6	3	0.98	0.99	0.99	0.99	0.93
Element average	Element average	0.96	0.97	0.97	0.96	0.91

[a] From SURVEY-detailed GAUGE analyses.

[b] Axial location relative to bottom of element.

TABLE 3-10
FUEL ACCOUNTABILITY FOR FSV FUEL ELEMENT 1-0743

Particle	Nuclide	Heavy Metal Weight	
		Initial	Current
Fertile	Th-232	10827.37	10680.89
Fertile	Pa-231	0.00	0.03
Fertile	U-232	0.00	0.01
Fertile	U-233[a]	0.00	114.24
Fertile	U-234	0.00	5.02
Fertile	U-235	0.00	0.28
Fertile	U-236	0.00	0.01
Fissile	Th-232	1949.63	1923.25
Fissile	Pa-231	0.00	0.01
Fissile	U-232	0.00	0.00
Fissile	U-233[a]	0.00	20.57
Fissile	U-234	3.45	3.81
Fissile	U-235	433.15	263.76
Fissile	U-236	1.32	31.94
Fissile	U-238	27.09	25.70
Fissile	Np-237	0.00	1.01
Fissile	Pu-232	0.00	0.09
Fissile	Pu-239[b]	0.00	0.56
Fissile	Pu-240	0.00	0.17
Fissile	Pu-241	0.00	0.10
Fissile	Pu-242	0.00	0.02
Total		13242.00	13071.44
Total fissile uranium		433.15	398.85
Total uranium		465.00	465.33
Total fissile plutonium		0.00	0.66
Total plutonium		0.00	0.93
Effective U-233 enrichment (%)		0.00	28.97
Effective U-235 enrichment (%)		93.15	56.74
U-232 (ppm)		0.00	26.26
Fertile particle FIMA (%)		0.00	0.25
Fissile particle FIMA (%)		0.00	5.90
Burnup (MWd/tonne)		0.00	12208.26
Cumulative EFPD		0.00	174.00

[a] Includes full decay of Pa-233.

[b] Includes full decay of Np-239.

TABLE 3-11
COMPARISON OF MEASURED (Cs-137) AND CALCULATED TIME-AVERAGED RADIAL POWER DISTRIBUTIONS FOR FSV FUEL ELEMENT 1-0743

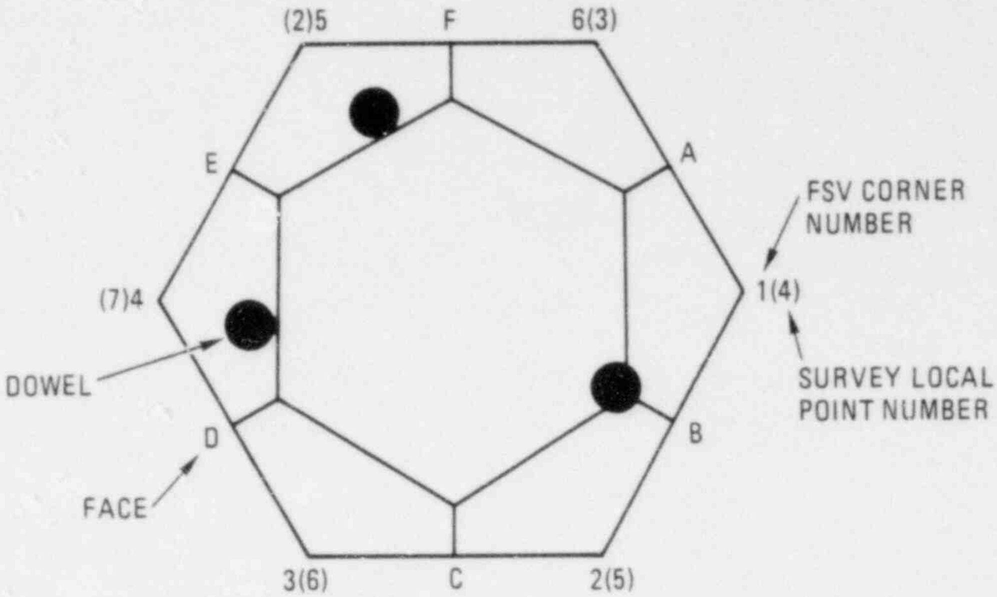

Portion of Element	Normalized Radial Power						
	Measured			Calculated			
				Case I(b)		Case III(c)	
	Number of Fuel Stacks	Relative Power	±1σ(a)	Relative Power	$\frac{\text{Calc}}{\text{Meas}} - 1$ (%)	Relative Power	$\frac{\text{Calc}}{\text{Meas}} - 1$ (%)
Center	30	0.98	0.01	1.01	+3.1	1.00	+2.0
Corner 1	7	1.04	0.02	1.06	+1.9	0.99	-4.8
Corner 2	7	1.06	0.02	1.05	-0.9	1.00	-5.7
Corner 3	5	0.98	0.02	0.98	0	1.00	+2.0
Corner 4	5	0.97	0.02	0.93	-4.1	1.02	+5.2
Corner 5	5	1.00	0.02	0.93	-7.0	1.01	+1.0
Corner 6	7	1.05	0.02	1.01	-3.8	0.98	-6.7

(a) ±1σ error on mean; $\varepsilon = s/\sqrt{n}$, where s = standard deviation and n = number of fuel stacks.

(b) SURVEY-detailed GAUGE analysis.

(c) GAUGE analysis with 11-time-interval power history.

TABLE 3-12
COMPARISON OF MEASURED (Zr-95) AND CALCULATED RADIAL POWER DISTRIBUTIONS AT EOL FOR FSV FUEL ELEMENT 1-0743

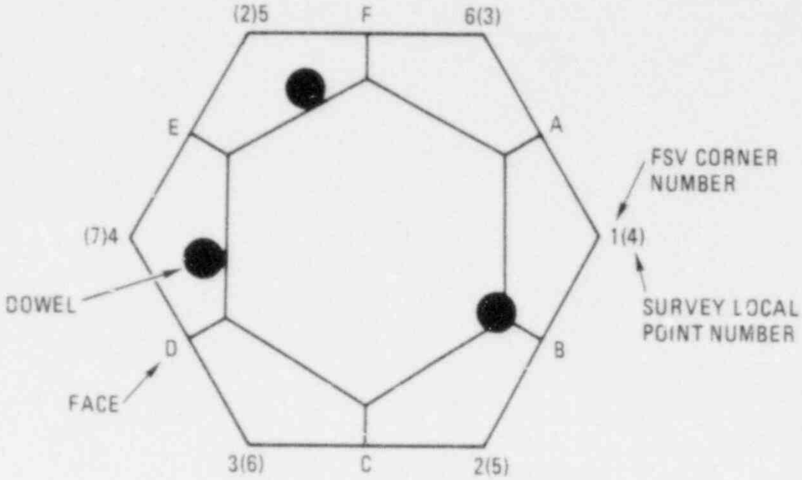

Portion of Element	Normalized Radial Power								
	Measured			Calculated					
				Case I(b)		Case II(c)		Case III(d)	
	Number of Fuel Stacks	Relative Power	±1σ(a)	Relative Power	Calc/Meas - 1 (%)	Relative Power	Calc/Meas - 1 (%)	Relative Power	Calc/Meas - 1 (%)
Center	30	0.98	0.01	1.00	+2.0	1.00	+2.0	1.00	+2.0
Corner 1	7	1.03	0.02	1.02	-1.0	1.01	-1.9	1.00	-2.9
Corner 2	7	1.04	0.01	1.02	-1.9	1.01	-2.9	1.02	-1.9
Corner 3	5	0.98	0.02	0.99	+1.0	0.99	+1.0	1.00	+2.0
Corner 4	5	0.98	0.02	0.99	+1.0	1.01	+3.1	1.01	+3.1
Corner 5	5	1.02	0.01	0.98	-3.9	1.00	-2.0	0.99	-2.9
Corner 6	7	1.06	0.01	0.99	-6.6	0.98	-7.5	0.98	-7.5

(a) ±1σ error on mean; $\varepsilon = s/\sqrt{n}$, where s = standard deviation and n = number of fuel stacks.

(b) SURVEY-detailed GAUGE analysis.

(c) GATT analysis with 11-time-interval power history.

(d) GAUGE analysis with 11-time-interval power history.

TABLE 3-13
DOSIMETER WIRE REACTIONS

Monitor Type	Reaction of Interest	Product Half-Life	Neutron Energy Group
V-Co, 0.216% Co	$^{59}Co(n,\gamma)^{60}Co$	5.26 yr	Thermal (0-0.38 aJ)
V-Fe, 0.522% Fe (88.24% Fe-54)	$^{54}Fe(n,p)^{54}Mn$	312.1 days	Fast (>29 fJ)
V	$^{51}V(n,\gamma)^{32}V \xrightarrow{\beta-} {}^{52}Cr$	Stable	Thermal (0-0.38 aJ)

TABLE 3-14
CROSS SECTIONS USED FOR DOSIMETRY CALCULATIONS

Reaction	Cross Section[a] (barns)
$^{59}Co(n,\gamma)^{60}Co$	18.9
$^{51}V(n,\gamma)^{52}V$	2.04
$^{54}Fe(n,\gamma)^{54}Mn$	0.0275
$^{60}Co(n,\gamma)^{61}Co$	1.0
$^{54}Mn(n,\gamma)^{55}Mn$	5.8
$^{54}Fe(n,\gamma)^{55}Fe$	1.13

(a) Cross section obtained from Ref. 12.

TABLE 3-15

COMPARISON OF CALCULATED AND MEASURED NEUTRON FLUENCE FOR FSV FUEL ELEMENT 1-0743

Dosimeter	Monitor Number	Location in Element: Stack Number	Location in Element: Distance from Bottom of Block (in.)[a]	Neutron Group	Calculated Fluence (10^{25} n/m^2) (E > 29 fJ)$_{HTGR}$: Case I[b]	Case II[c]	Case III[d]	Measured Fluence (x 10^{25} n/m^2)	Relative Difference $\frac{Calc}{Meas} - 1$ (%): Case I[b]	Case II[c]	Case III[d]
V	21	12	4.8	Thermal				1.40			
	22	12	25.2					1.38			
	81	278	4.8					1.33			
	82	278	25.2					1.41			
	Av	--	--		ND[e]	ND	1.93[f]	1.38			+39.9
V-Co	21	12	4.8	Thermal				2.09			
	22	12	25.2					2.19			
	81	278	4.8					2.24			
	82	278	25.2					2.26			
	Av	--	--		ND	ND	1.93[f]	2.19			-11.9
V-Fe	21	12	4.8	Fast	0.81			0.84	-3.6		
	22	12	25.2		0.83			0.88	-5.7		
	81	278	4.8		1.07			1.03	+3.9		
	82	278	25.2		1.09			1.06	+2.8		
	Av	--	--		0.95[g]	0.91[f]	0.94[f]	0.95	-0.7 ± 4.7[h]	-4.2	-1.1

(a) 1 in. = 25.4 mm.

(b) SURVEY-detailed GAUGE analysis.

(c) GATT analysis with 11-time-interval power history.

(d) GAUGE analysis with 11-time-intervals (column average fluxes) and GATT analysis (axial flux factors). Values are taken from Ref. 3-9.

(e) ND = not determined.

(f) Element average fluence.

(g) Shown for comparison only. Not used to calculate average relative difference.

(h) Mean difference and standard deviation.

TABLE 3-16

COMPARISON OF MEASURED AND CALCULATED TEMPERATURES FOR SiC PELLETS IRRADIATED IN FSV FUEL ELEMENT 1-0743

Monitor ID	Fuel Stack	Axial Position (cm from bottom)	Annealing Curve Intersection Temperature (°C)	Measured(a) Irradiation Temperature (°C)	95% Confidence Limits(a) for Measured Irradiation Temperature (°C)	Calculated(b) Temperature (°C)	Difference $T_c - T_M$ (°C)
21	12	12	755	704	674 < T < 737	728	+24
22	12	64	720	648	615 < T < 683	668	+20
81	278	12	758	707	677 < T < 740	737	+30
82	278	64	723	651	618 < T < 686	675	+24
Average	--	--	--	--	--	--	+24 ± 4

(a) Irradiation temperatures determined from annealing curve intersection temperatures using the calibration curve for SiC temperature monitors presented in Ref. 13.

(b) Temperatures obtained from SURVEY-calculated peak fuel and coolant temperatures at the axial locations of the neighboring fuel rods using a factor obtained using the TAC-2D (Ref. 19) code [$T_c = T_{coolant} + f\ (T_{fuel} - T_{coolant})$; f = 0.62]. The temperatures are for the second to the last SURVEY time interval. The core power during this interval was 546 MW, and the temperatures are representative of the highest temperatures over the last ~1 x 10^{20} n/cm^2 (E > 29 fJ)$_{HTGR}$.

TABLE 3-17
BURNUP MEASUREMENTS FOR FSV FUEL ELEMENT 1-0743 USING DESTRUCTIVE TECHNIQUES

	Fissile Burnup						Fertile Burnup						$(Th,U)C_2$[c] Burnup		Composite[c] Burnup	
			FIMA (%)							FIMA (%)						
					All Measurements						All Measurements					
Burnup[a] Monitor	Sample No.	Axial Location (cm)[b]	Radio-chemistry Method	Mass Spectometric Method	Avg.	Std. Dev.	Fuel Rod (Stack-Rod)	Sample No.	Axial Location (cm)[b]	Individual Particles	Avg.	Std. Dev.	FIMA (%)	$\pm 1\sigma$[d] (%)	FIMA (%)	$\pm 1\sigma$[d] (%)
21	4	12.2	32.1	30.2			12-4	1	20.7	0.3[illegible]						
	5		32.2	30.8	31.3	±1.0		2		0.31	0.30	±0.01	6.27	0.19	1.38	0.04
								8		0.30						
22	3	64.0	31.7	30.3			12-11	3	55.5	0.31						
	4		31.6	30.1	30.9	±0.8		4		0.32	0.32	±0.01	6.21	0.15	1.38	0.03
								5		0.33						
81	4	12.2	33.7	32.8			279-3	2	12.2	0.35						
	5		31.6	31.1	32.3	±1.2		6		0.33	0.34	±0.01	6.49	0.23	1.45	0.04
								8		0.35						
Element average[e]											0.32	±0.01	6.38	0.15	1.42	0.03

[a] Monitors 21 and 22 were in fuel stack 12 and monitor 81 was in fuel stack 278.

[b] Centimeters from bottom of element.

[c] $(Th,U)C_2$ burnup = $F_c = (F_5)(X) + (F_3)(1 - X)$, where F_5 = fissile burnup, F_3 = fertile burnup, and $X = U_o/(U_o + Th_o)$. U_o and Th_o are the initial heavy metal loadings.

[d] $dF_c = [(\partial F_c/\partial F_5)^2 (dF_5)^2 + (\partial F_c/\partial F_3)^2 (dF_3)^2]^{1/2} = [(X)^2 (dF5)^2 + (1 - X)^2 (dF_3)^2]$. Uncertainty in heavy metal loadings was omitted because results are to be compared with calculations that assumed the same loadings.

[e] Element average burnups obtained by averaging the results at the locations of monitors 21 and 81. The average neutron flux for these two locations was approximately equivalent to the element average flux.

TABLE 3-18

BURNUP MEASUREMENTS FOR FSV FUEL ELEMENT 1-0743 USING GAMMA SCANNING

Fuel Stack	Fuel Stack Average Burnup				
	Corner Scans,[a] Composite FIMA (%)	Single Stack Scans,[b] Composite FIMA (%)		Average	
				Composite FIMA (%)	Relative Diff, $\frac{\text{Corner}}{\text{Single}} - 1$ (%)
2, 12	1.38	1.39, 1.44	1.42	1.40	-2.82
10, 23	1.27	1.31, 1.47	1.39	1.33	-8.63
153, 189	1.45	1.36, 1.37	1.36	1.40	+6.62
313, [illegible]	1.49	1.51, 1.53	1.52	1.50	-1.97
302, 315	1.38	1.48, 1.47	1.48	1.43	-6.76
136, 172	1.48	1.45, 1.45	1.45	1.46	+2.07
Average				1.42	-1.9 ± 5.6
Element average				1.38[c]	– –

[a] Gamma scans of corner fuel stacks while in block (see Fig. 3-4).

[b] Gamma scans of individual fuel stacks after removal from element.

[c] Average radial power (relative to block average) was 1.027 for the 12 fuel stacks. Average burnup divided by this factor to obtain element average burnup.

TABLE 3-19

COMPARISON OF CALCULATED AND MEASURED FUEL BURNUP FOR FSV FUEL ELEMENT 1-0743

Particle Type	Burnup										
	Measured[a]		Case I[b]			Case II[c]			Case IV[d]		
				$Z = \frac{Calc}{Meas} - 1$			$Z = \frac{Calc}{Meas} - 1$			$Z = \frac{Calc}{Meas} - 1$	
	FIMA (%)	±1σ (%)	FIMA (%)	Z (%)	±1σ[e] (%)	FIMA (%)	Z (%)	±1σ[e] (%)	FIMA (%)	Z (%)	±1σ[e] (%)
$(Th,U)C_2$	6.38	0.15	6.2	-2.8	2.3	5.90	-7.5	2.2	5.30	-16.9	2.0
ThC_2	0.32	0.01	0.3	-6.2	2.9	0.25	-21.9	2.4	0.25	-21.9	2.4
Composite	1.42	0.03	1.37	-3.5	2.0	1.28	-9.9	1.9	1.17	-17.6	1.7

[a] Determined by averaging $(Th,U)C_2$ burnups at location of monitors 21 and 81 and ThC_2 burnups for fuel rods 12-4 and 279-3. These averages should be approximately equivalent to element average burnups.

[b] SURVEY-detailed GAUGE analysis.

[c] GATT analysis.

[d] Calculations based on FEVER-calculated fluxes.

[e] Progressed uncertainty due to measurement uncertainty only.

TABLE 3-20
COMPARISON OF CALCULATED AND MEASURED URANIUM ISOTOPIC CONCENTRATIONS FOR UC_2 BURNUP MONITORS IRRADIATED IN FSV FUEL ELEMENT 1-0743

	Isotopic Concentration				
	Measured[a]		Calculated[b]	Relative Difference $Z = \frac{Calc}{Meas} - 1$ (%)	
Isotope	Atom Percent	$\pm\sigma$	Atom Percent	Z	$\pm 1\sigma$[c]
U-234	0.797	0.002	0.8	0.38	0.25
U-235	79.62	0.02	82.6	3.74	0.03
U-236	10.98	0.02	8.9	-18.94	0.15
U-238	8.60	0.01	7.7	-10.46	0.10

(a) Average values for monitors 21 and 81. The average neutron flux for these two monitors is approximately equivalent to the element average flux.

(b) Calculations based on fluxes obtained from the FEVER code.

(c) Progressed uncertainty due to measurement uncertainty only.

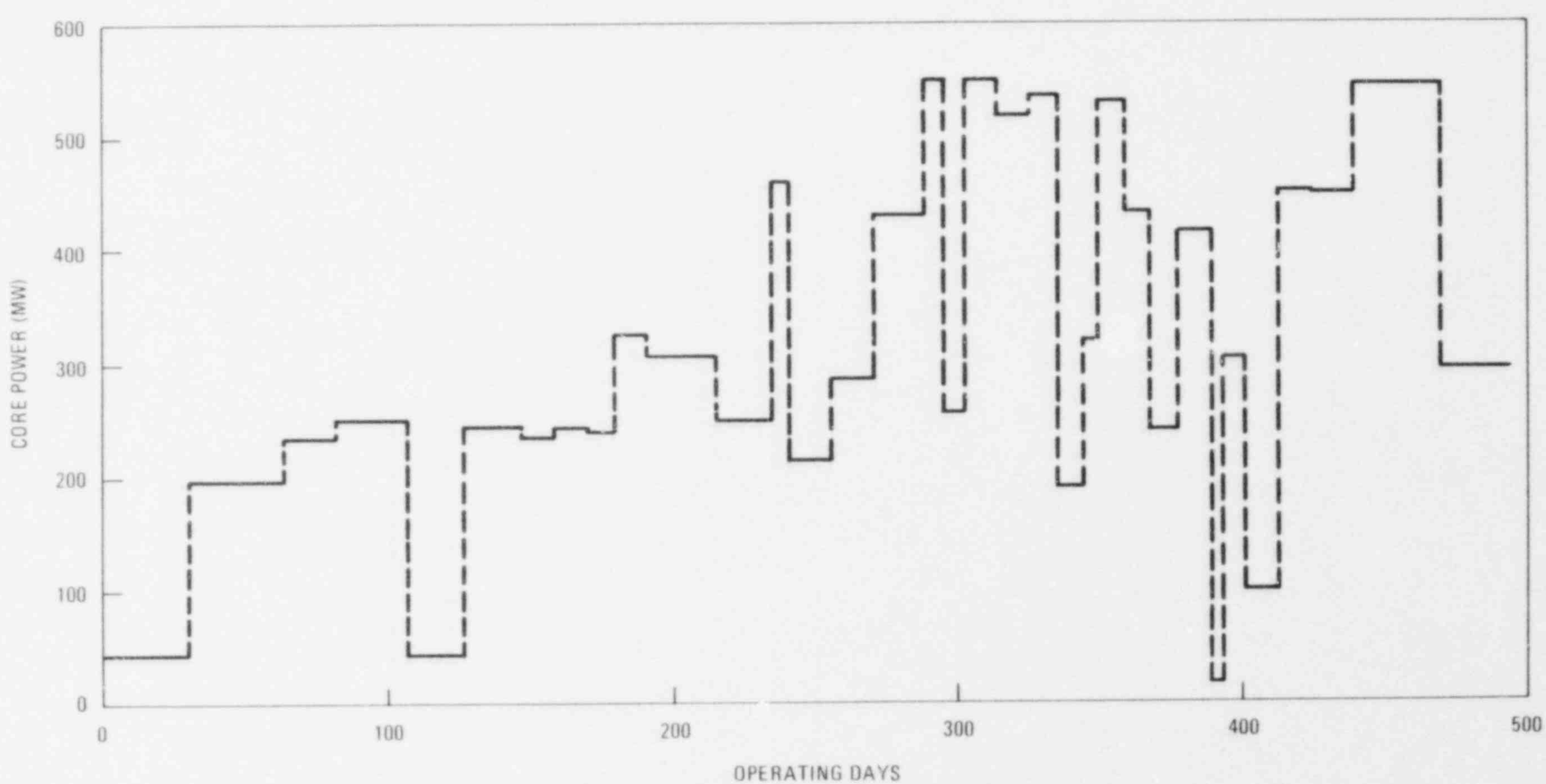

Fig. 3-1. FSV reactor power history: SURVEY analysis of cycle 1

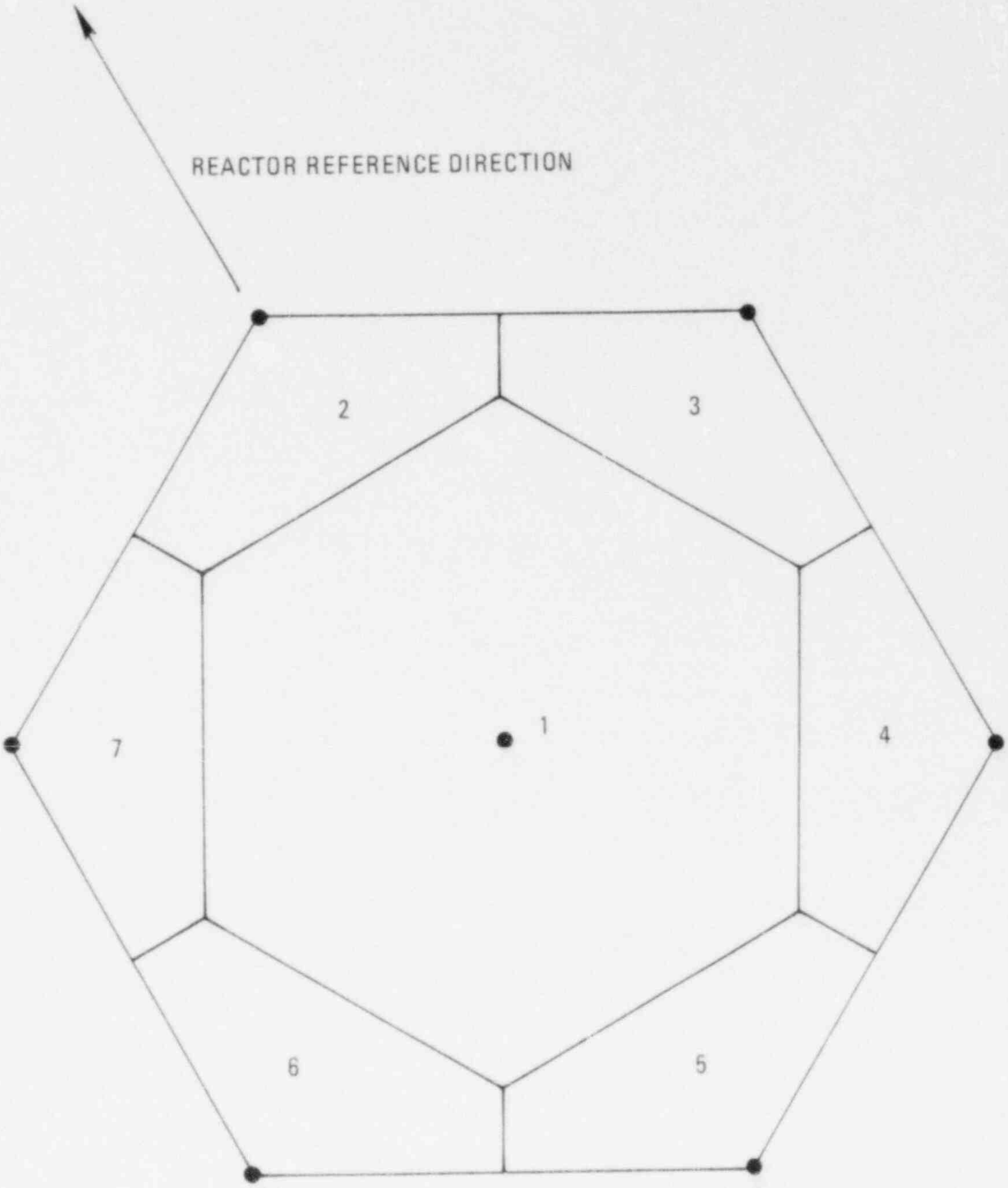

Fig. 3-2. Local point numbering for GAUGE-SURVEY analysis

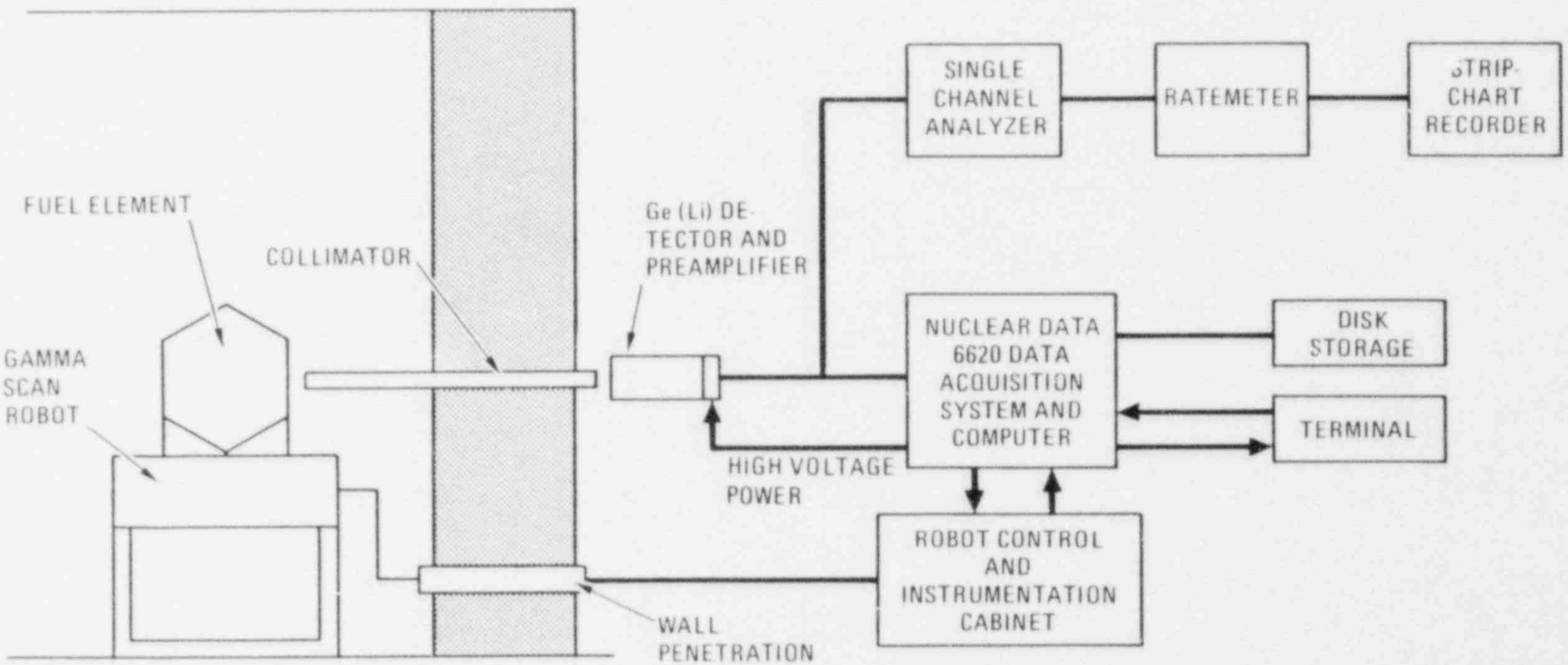

Fig. 3-3. System for scanning FSV core components

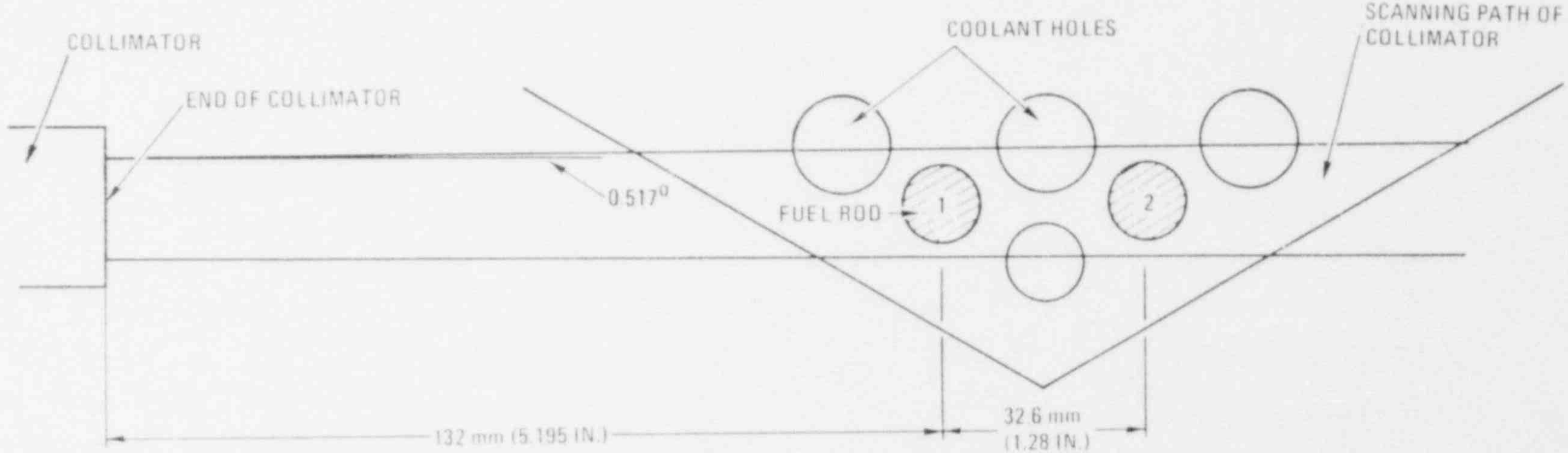

Fig. 3-4. Scanning geometry 1: axial corner scans

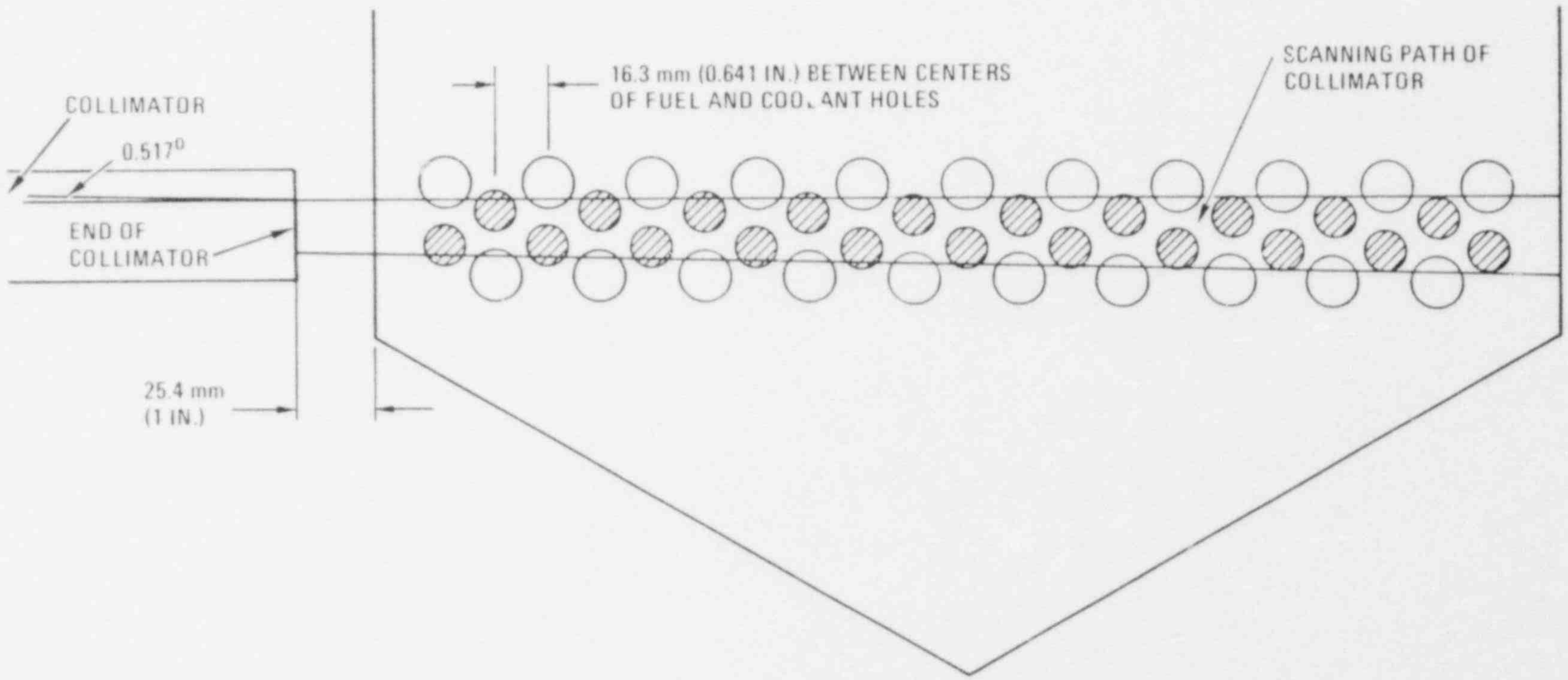

Fig. 3-5. Scanning geometry 2: axial side-face scans

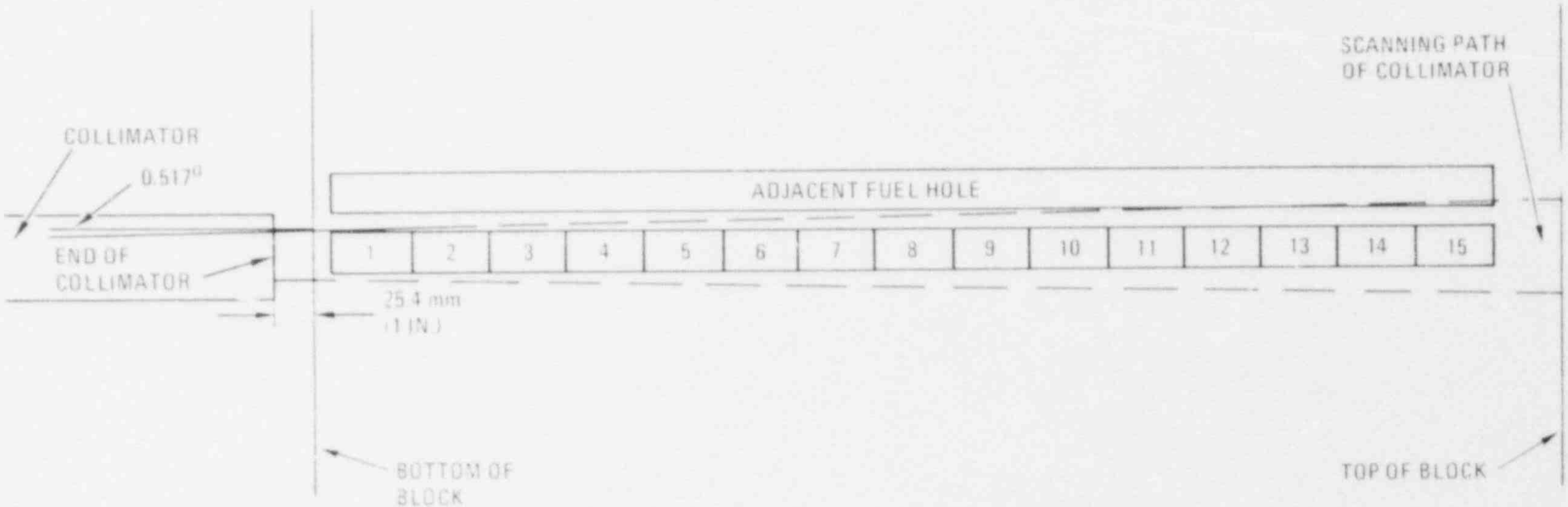

Fig. 3-6. Scanning geometry 3: end-on scans

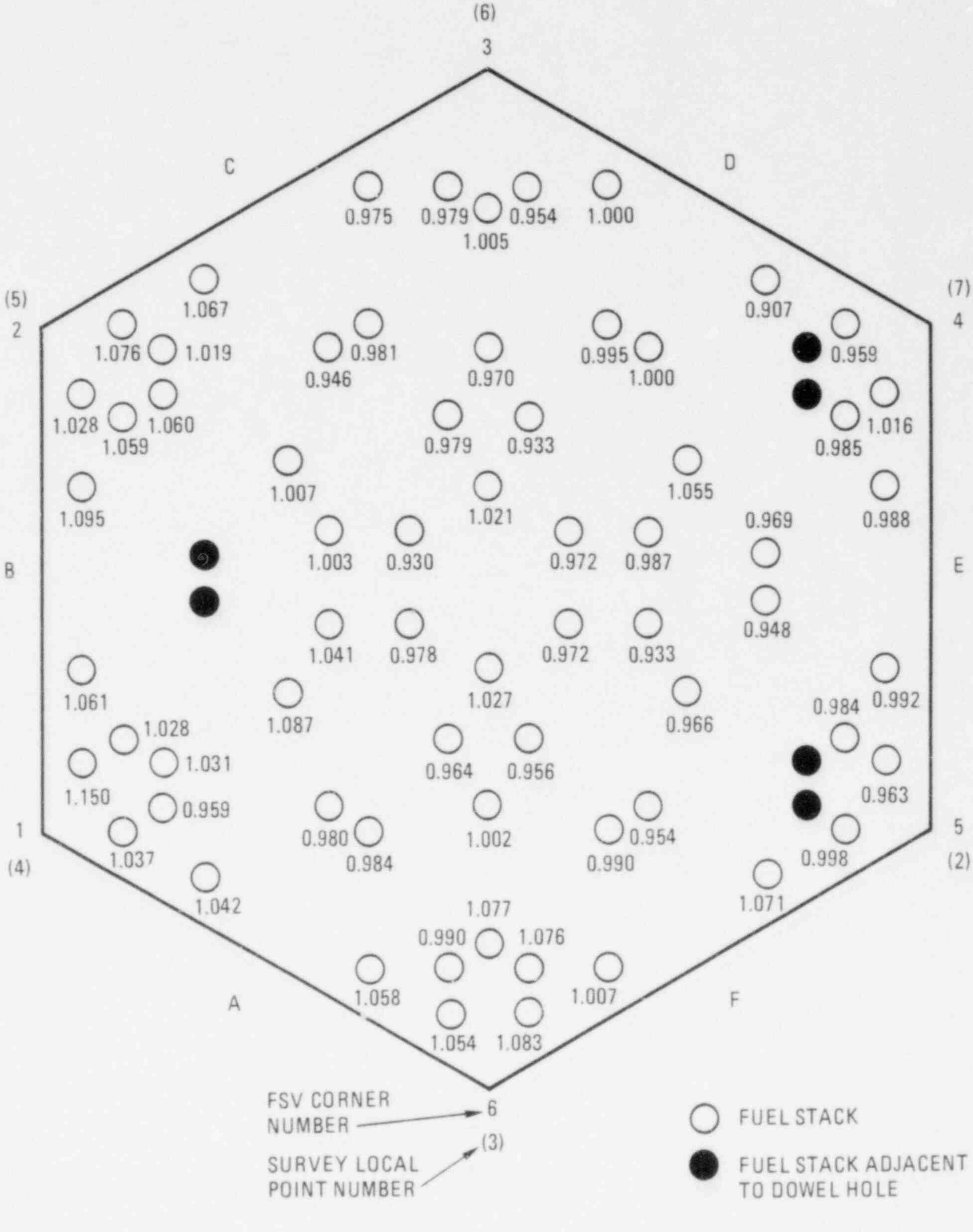

Fig. 3-7. Measured time-averaged radial power distribution for FSV fuel element 1-0743 (normalized Cs-137 distribution from end-on gamma scanning of fuel stacks at bottom of element)

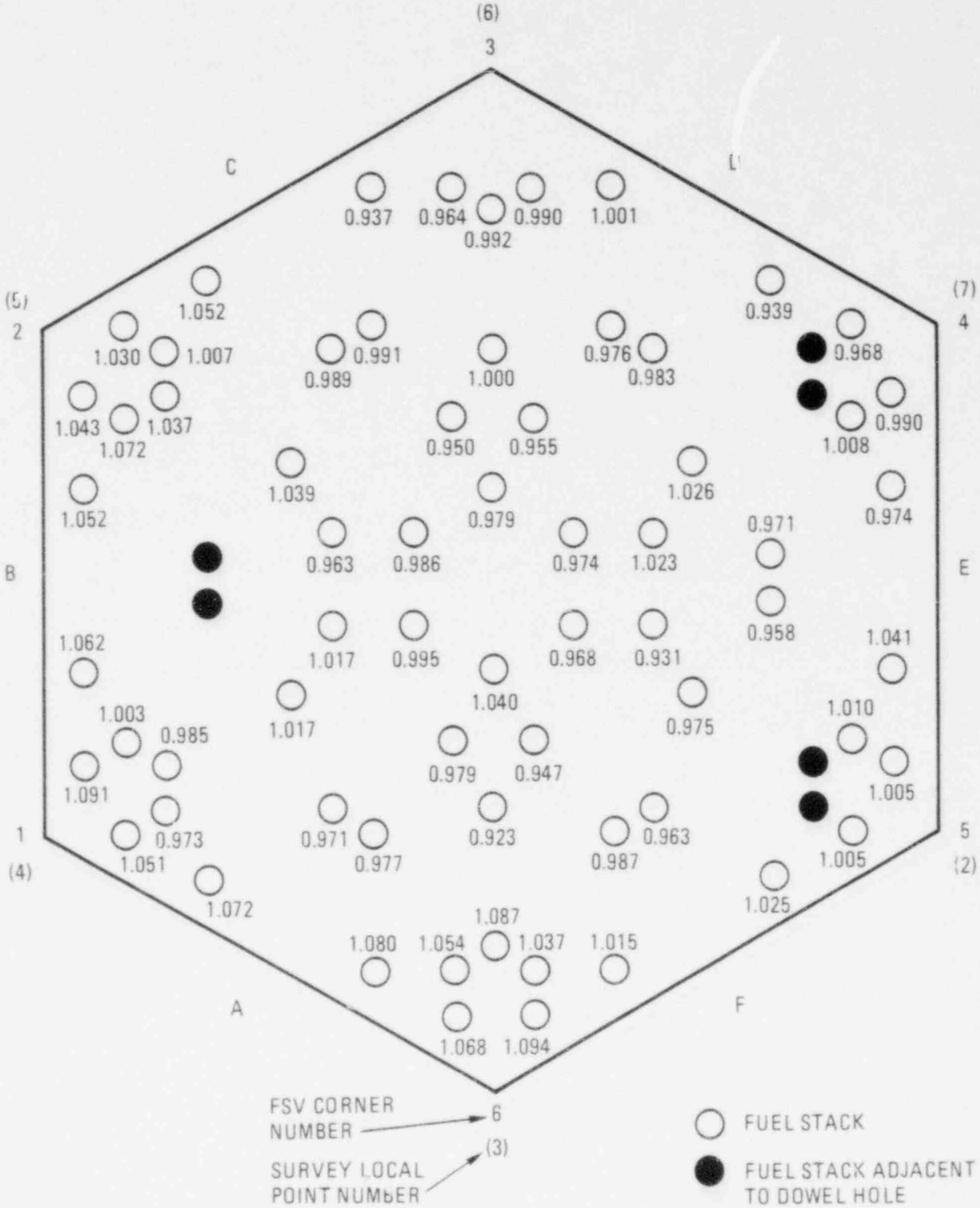

Fig. 3-8. Measured EOL distribution for FSV fuel element 1-0743 (normalized Zr-95 distribution obtained from end-on gamma scanning of fuel stacks at bottom of element)

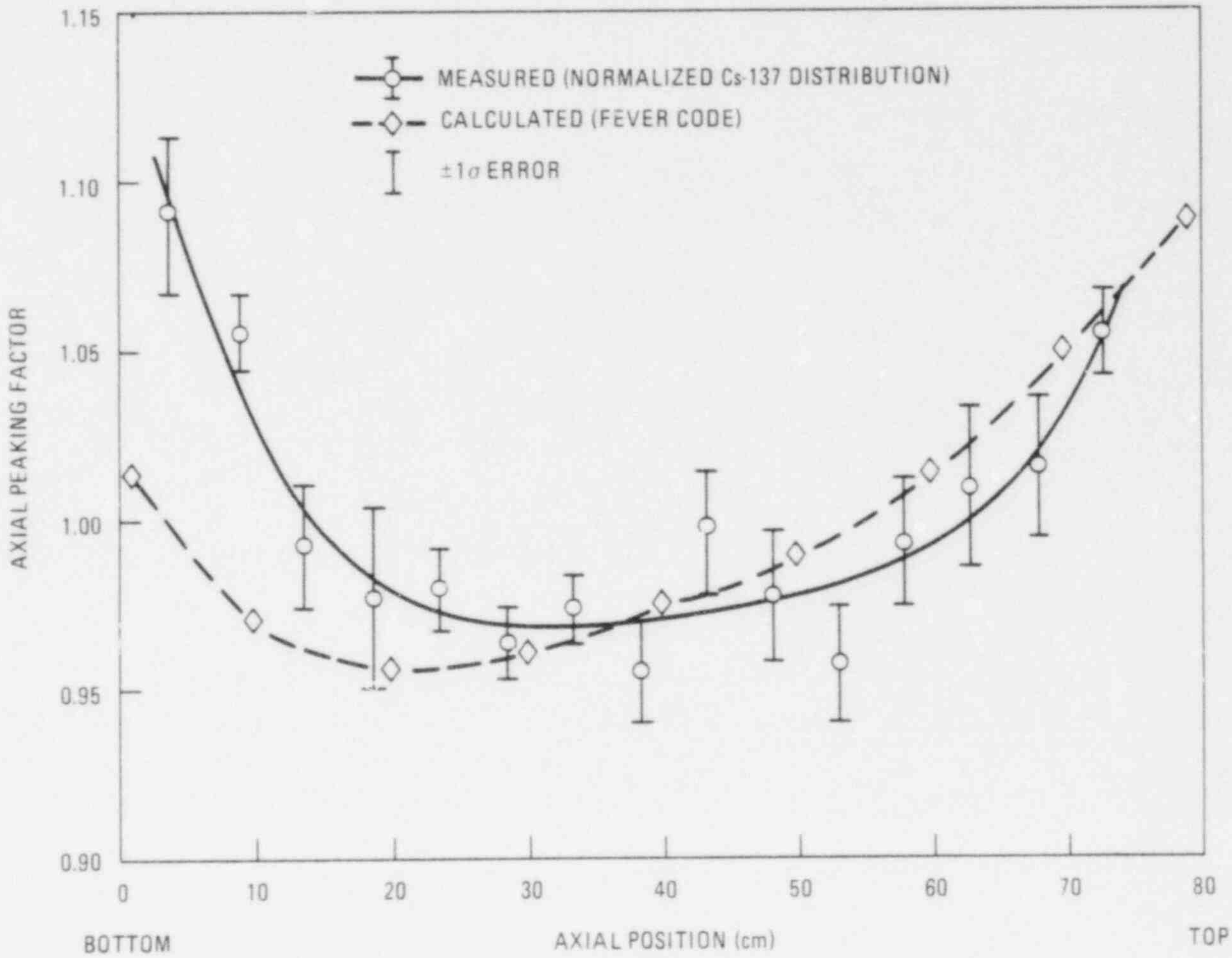

Fig. 3-9. Measured and calculated time-averaged axial power profiles for FSV fuel element 1-0743

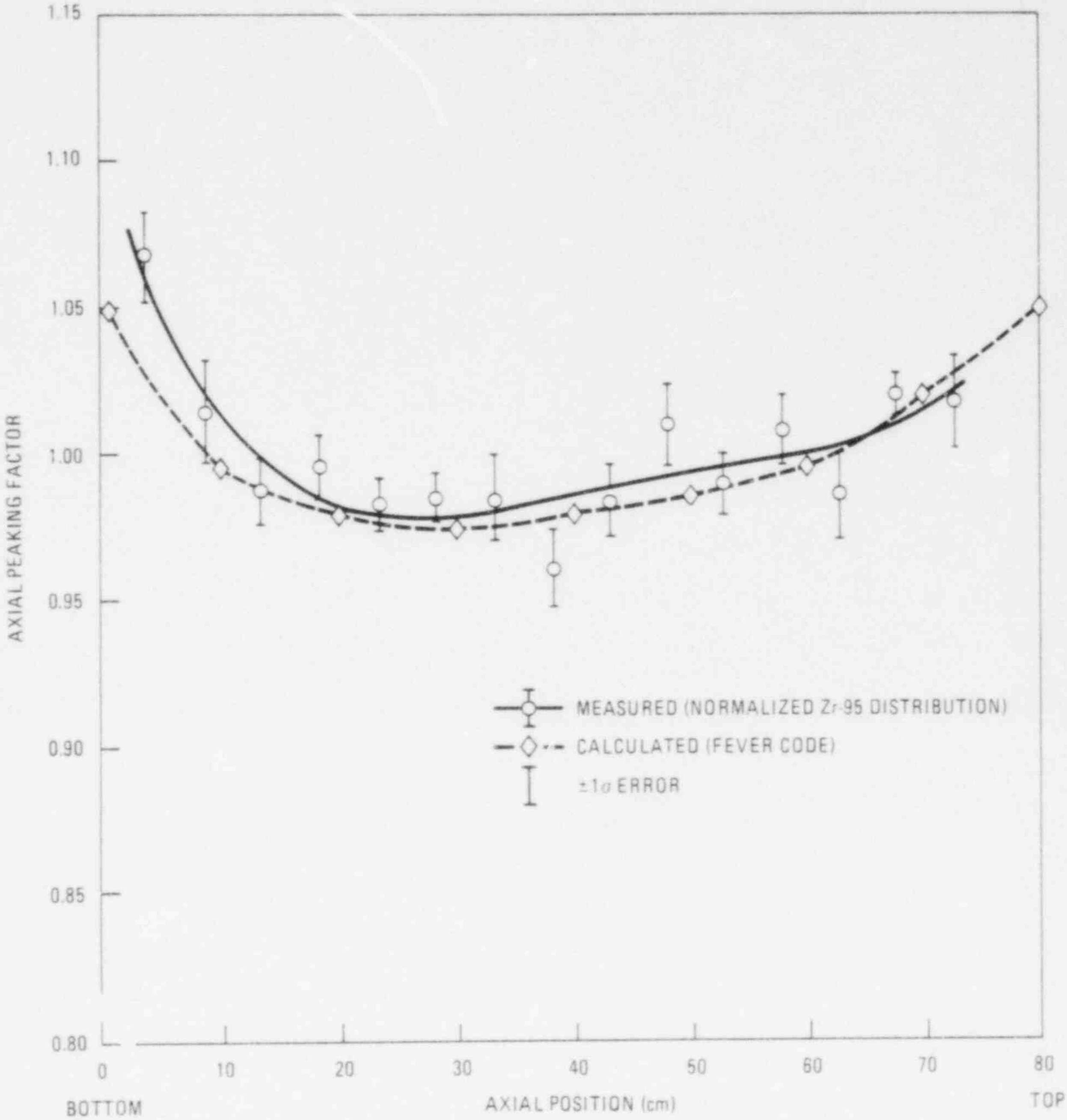

Fig. 3-10. Measured and calculated EOL axial power profiles for FSV fuel element 1-0743

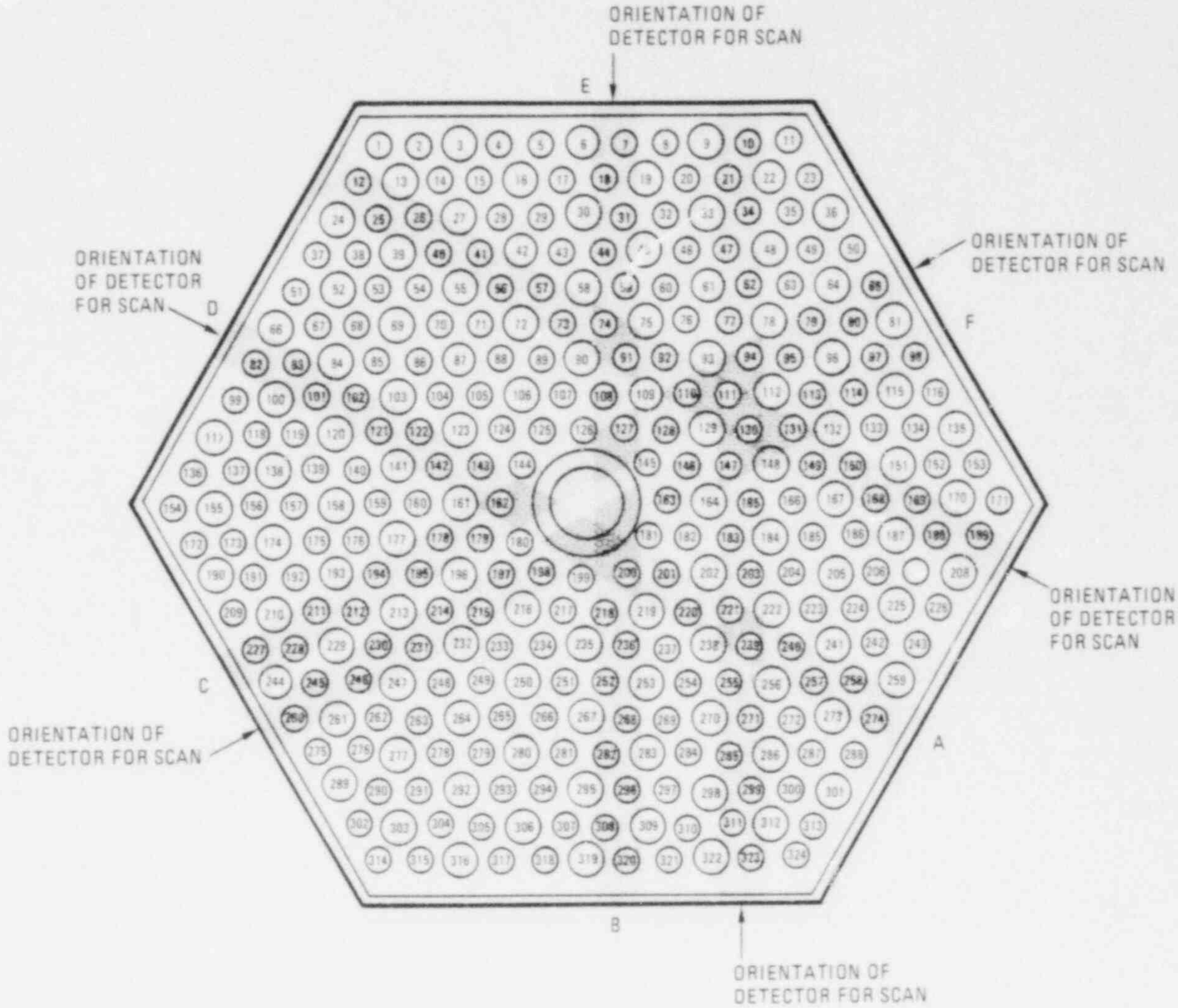

Fig. 3-11. Cross-sectional view showing portion of element observed by detector for six axial scans averaged to give measured power profiles

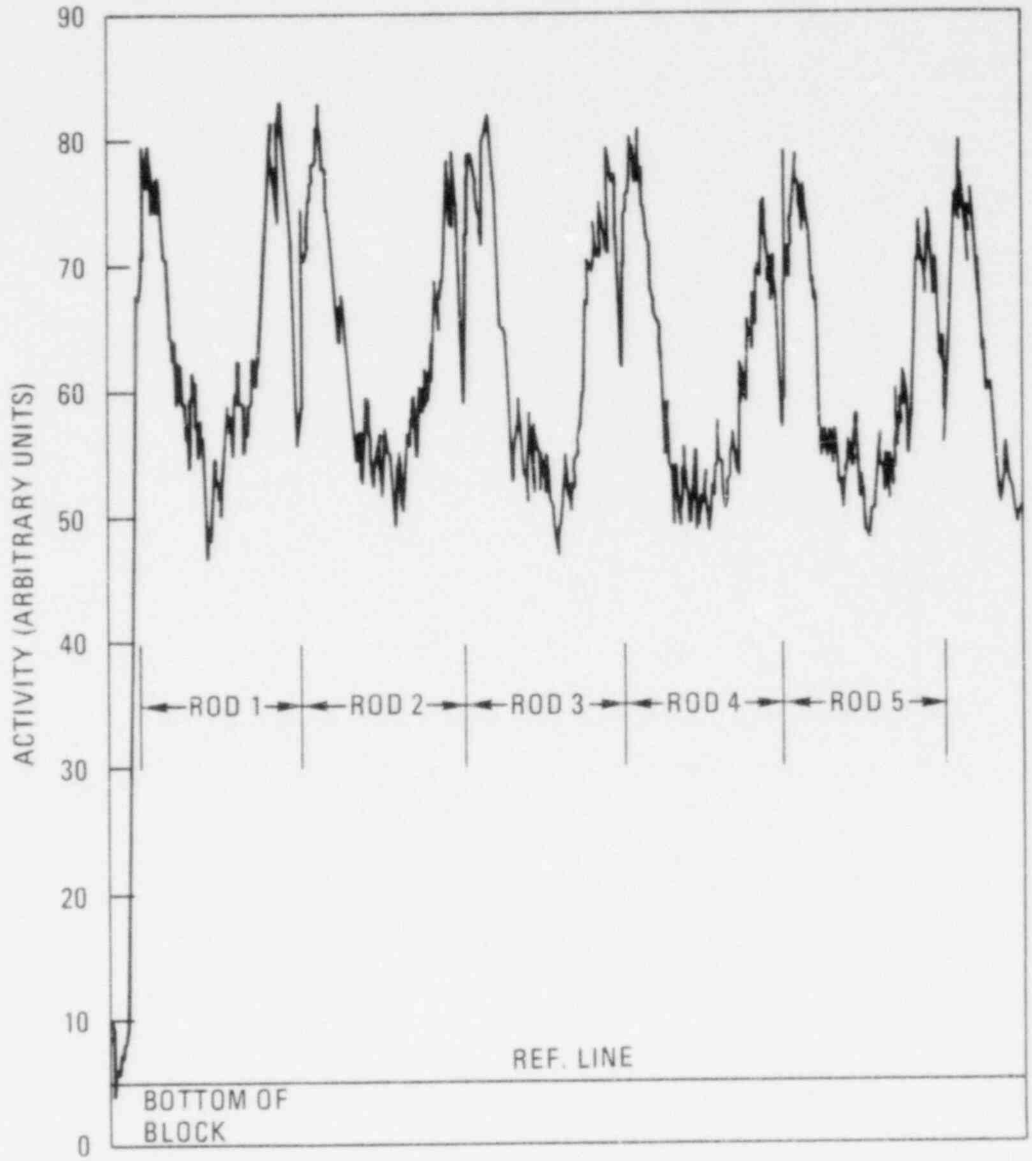

Fig. 3-12. Typical Cs-137 trace (partial) for axial scan of FSV fuel element 1-0743

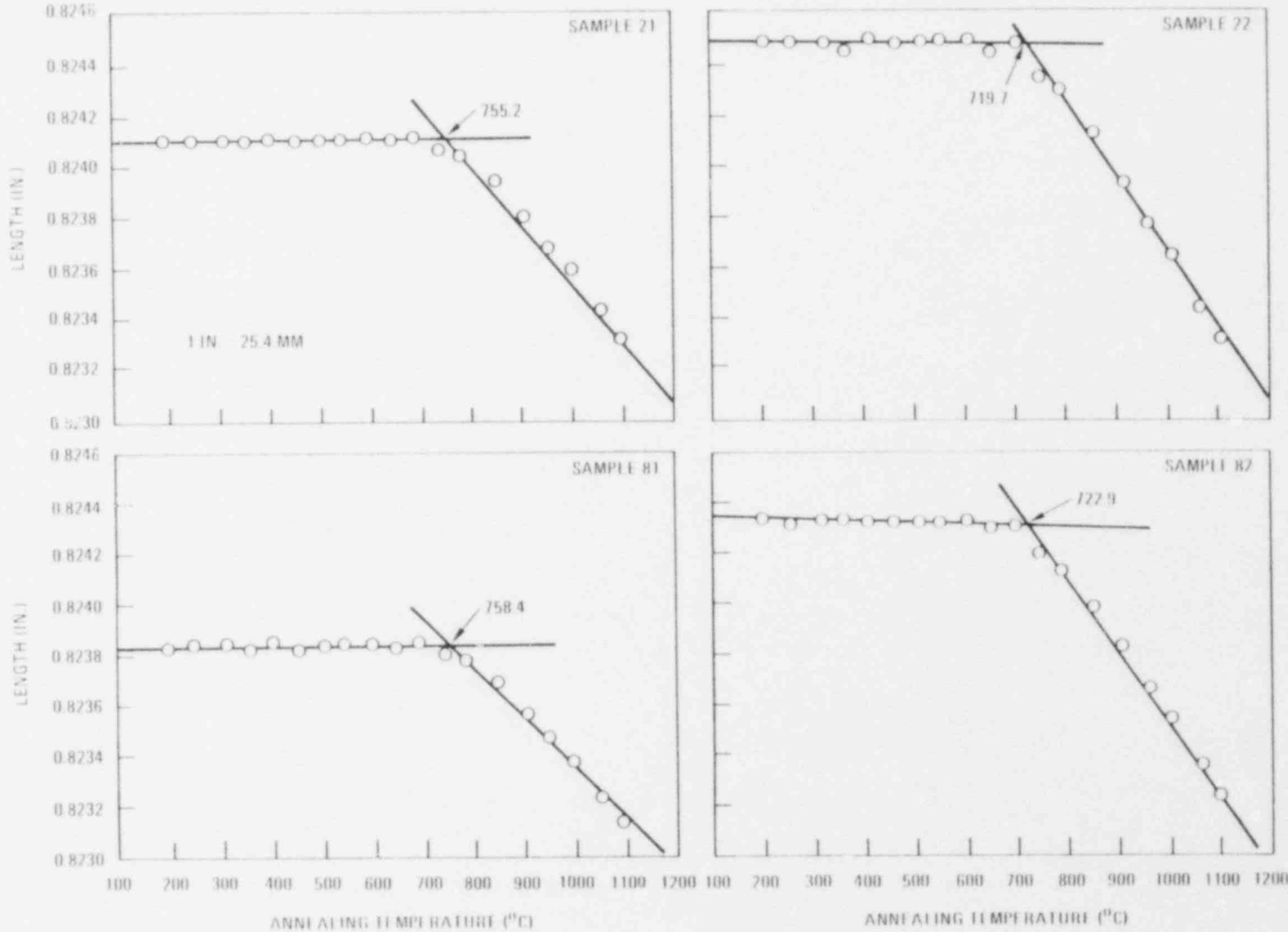

Fig. 3-13. Determination of irradiation temperatures for SiC pellets irradiated in FSV fuel element 1-0743

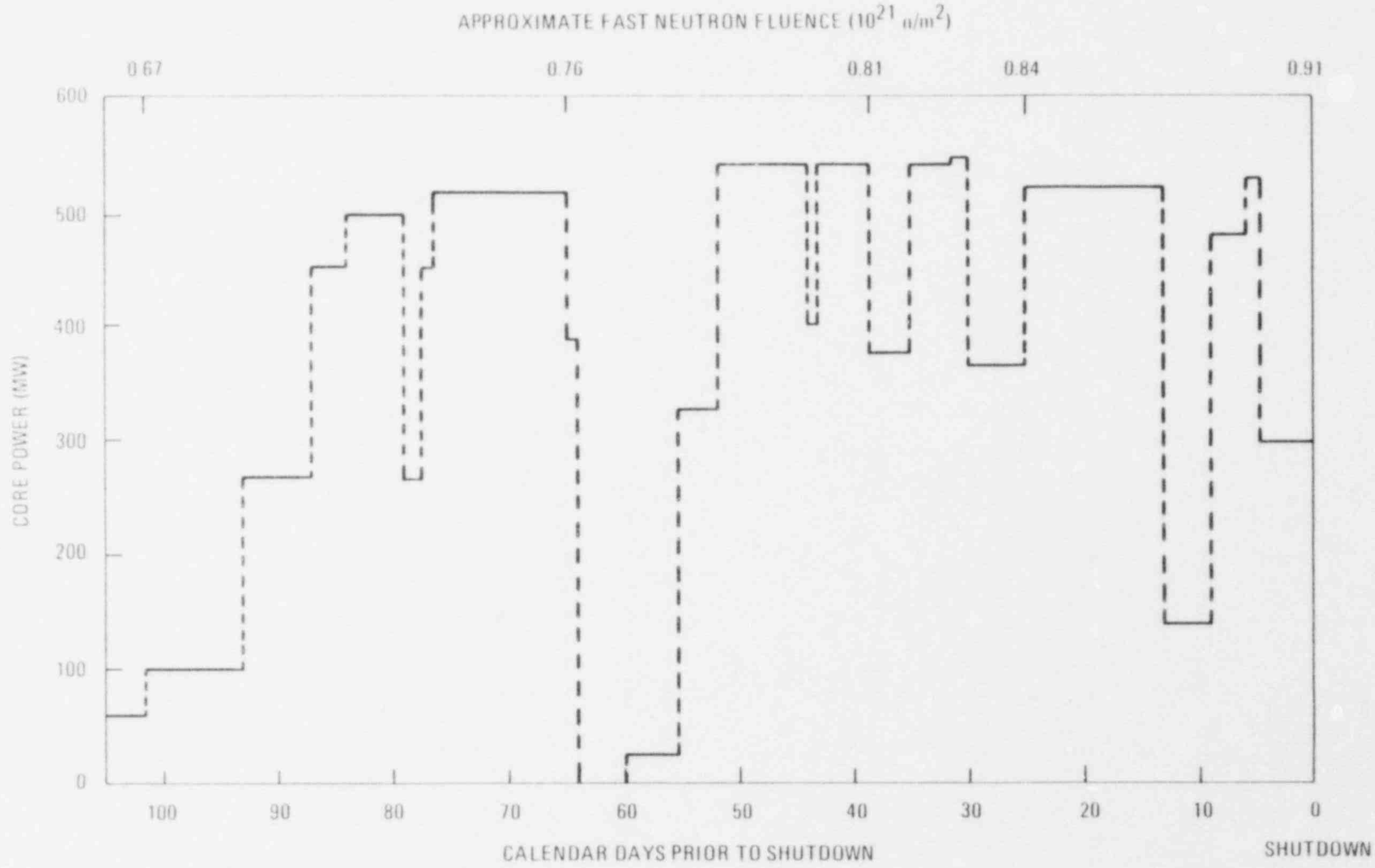

Fig. 3-14. Core power history over the last $\sim 2 \times 10^{24}$ n/m^2 (E > 29 fJ)$_{HTGR}$ exposure for FSV fuel element 1-0743

4. RESULTS OF POSTIRRADIATION EXAMINATION

4.1. EXAMINATION OF GRAPHITE FUEL BLOCK

4.1.1. Visual Examination

Like all of the segment 1 fuel elements examined in the hot service facility at FSV, fuel element 1-0743 was in good condition. No cracks were observed on any of the element surfaces. All observed abnormalities were surface markings only and had not etched the graphite to any harmful extent. Observed abnormalities included rub marks, soot deposits, scrapes, and scratches. Photographs of each side face are presented in Figs. 4-1 through 4-6, and the top surface is shown in Figs. 4-7 and 4-8. The bottom surface of the block was also photographed, but the quality of the pictures is too poor for them to be reproduced in this report. The element was visually examined again in the hot cell at GA, but nothing of significance was observed that had not been observed during the initial examination at FSV. The results of the visual examinations of all 51 segment 1 fuel and reflector blocks inspected at FSV are presented in detail in Ref. 1.

4.1.2. Metrological Examination

To verify the results of the metrological inspections performed by the metrology robot on segment 1 fuel elements at FSV following the first reload (Ref. 1), the dimensional measurements performed on element 1-0743 were repeated at GA using conventional hot cell measuring techniques. These techniques are described in Ref. 15. The results of these measurements are presented below.

4.1.2.1. Irradiation-Induced Dimensional Changes. The metrology robot measurements and hot cell measurements for element 1-0743 are presented and compared with each other and with preirradiation measurements in Tables 4-1 through 4-10. The following results are based on the measurements taken in the GA hot cell:

1. The block average axial strain was -0.17%, corresponding to a length reduction of 1.32 mm. Maximum and minimum length reductions were 1.73 mm and 0.91 mm adjacent to face B and face E, respectively.

2. Block average axial strains determined from preirradiation and postirradiation distances were -0.21%, -0.18%, and -0.19% for dimensions L, M, and N, respectively (see Fig. 2-5). These strains are consistent with each other and with the axial strain determined from element length measurements, indicating the axial strain to be uniform over the length of the block.

3. The block average radial strain was -0.13%, corresponding to a shrinkage of 0.46 mm across flats. The radial strain was nearly uniform for all three pairs of parallel side faces. The radial strain obtained from coolant hole diameter measurements was much higher, -0.38%, but is suspect because of the very small dimensional changes involved. The radial strain deduced from changes in the distances between coolant holes was -0.16%.

4. Face B of the element was observed to have undergone the greatest convex bow and face E the greatest concave bow. The maximum bow for side faces B and E was 0.28 mm.

4.1.2.2. Verification of Metrology Robot Measurements. In addition to the comparison between metrology robot and hot cell measurements for element 1-0743, a comparison between metrology robot measurements and Quality Control (QC) measurements on a spare (calibration) fuel block was performed to quantify and verify the accuracy of the metrology robot. The details of both comparisons have already been presented in Ref. 1 and are therefore omitted in this report. However, a summary of the results is given below.

Accuracy and bias statements developed from these comparisons for the various types of robot measurements are summarized in Table 4-11. The accuracy of the metrology robot was determined to be ±0.18 mm (0.007 in.) 1σ, or better, for each type of robot measurement after corrections were applied for observed measurement biases. Measurement biases were determined to be 0.05 mm (0.002 in.) or less for all robot measurements except length measurements. The bias (Actual -Robot) in the length measurements is 0.18 to 0.28 mm (0.007 to 0.011 in.). The cause of the bias is not currently known but will be identified and corrected prior to inspection of FSV core segment 2. The length measurements for segment 1 fuel elements were corrected to account for this bias.

The comparisons of metrology robot data with the corresponding hot cell and QC measurements also revealed two mechanical defects in the robot which slightly affect the quality of robot measurements. These defects are discussed in Ref. 1. The segment 1 data have been corrected accordingly, and steps have been taken to eliminate the defects.

4.1.2.3. <u>Comparison of Calculated and Measured Strain and Bow</u>. Calculated and measured irradiation-induced strains and bow for fuel element 1-0743 are presented in Table 4-12. Calculated strains and bow were obtained from SURVEY/STRESS and are based on irradiation conditions from SURVEY. The SURVEY analysis is in turn based on the detailed GAUGE analysis of FSV cycle 1. In the sense that both calculated and measured strains and bow are small, the calculations and measurements are in good agreement. However, some discrepancies are observed. In particular, the bow in the element and the variation in the axial strain are greater than expected. The reader is directed to Ref. 1 for a systematic comparison of measured and calculated strains and bow for all 49 fuel elements examined (including element 1-0743) from FSV core segment 1.

4.2. DISASSEMBLY OF ELEMENT

The postirradiation examination of fuel element 1-0743 was unique in that it was the first destructive examination performed at GA on a fuel element having the large HTGR prismatic block design. As such, it required the development of new devices and techniques for handling and disassembling the element. These devices and techniques have been employed, for the most part, with very satisfactory results. The disassembly of the element is described below.

4.2.1. Coring

A coring tool was developed and used to core out the fuel hole plugs at the top of the element and the graphite containment at the bottom. The device is positioned and aligned using the coolant holes and has six stations for the cutter to permit the six fuel holes surrounding a given coolant hole to be cored without relocating the tool. The coring tool is shown in Figs. 4-9 through 4-11. The cutter can be driven either directly by a drill motor or by a conventional ac motor via a flexible shaft. For hole diameters of 12.7 mm, a cutter with an inside diameter of 16.5 mm and an outside diameter of 18.67 mm is used. This allows for some misalignment of the device and prevents damage to the fuel. The cored sections remain in place until forcibly removed. For the element, depths of cut ranged from 7.62 mm at the top surface to 11.4 mm at the bottom. A 40.4-mm depth of cut was required for fuel stacks situated beneath dowels. Once the device was positioned, the coring operation required only about 1 min per fuel stack, except for the stacks beneath dowels.

4.2.2. Plenum Depth Measurements

Once all fuel holes had been cored at both the top and bottom of the element, the cored sections at the top were removed for the six holes containing precharacterized fuel rods. The distance from the top surface to the top fuel rod in each stack was then measured using a depth gauge. These measurements are given in Table 4-13. The measurement technique is illustrated in Fig. 4-12. An approximate 2.5-mm increase in plenum depth was observed for all six fuel holes.

4.2.3. Removal of Fuel Rods

The fuel rods were removed from the element by breaking out the cored sections and pushing the fuel stacks into a dual-tube receiving trough. The fuel stacks were pushed out of the element using either a metal rod or a special device designed to measure the push-out force. The push-out device and receiving trough are shown in Figs. 4-13 and 4-14, respectively. When measuring push-out forces, two forces are generally recorded: (1) the initial force required to start the stack moving and (2) the sustaining force required to continue pushing the rods. The initial force is generally higher, since more fuel rods are resisting.

Since the dimensional changes in the fuel rods and fuel body were quite small, no fuel rod-fuel body interaction, and consequently low push-out forces, were expected. The push-out forces measured for fuel element 1-0743 are given in Table 4-13. As expected, the push-out forces were generally low. However, in a few cases, the push-out forces required were considerable (up to 10 kg). These high push-out forces are believed to be the result of misalignment between the fuel hole and receiving trough and of graphite debris from the breaking-out operation which become wedged between the fuel rods and fuel hole surface. It is concluded that there was no appreciable fuel rod -fuel block interaction in fuel element 1-0743.

4.3. EXAMINATION OF FUEL RODS

4.3.1. Visual Examination

Following fuel stack removal, the six precharacterized stacks were measured for length (Table 4-13), and the fuel rods were individually photographed using the hot cell Kollmorgan periscope system. For the photography, the rods were placed in a trough with mirrors on each side at an angle of 90 deg relative to each other. This arrangement permitted approximately 300 deg of the surface of each fuel rod to be photographed. In addition, stereophotography was performed in the metallography cell for each of the rods selected for fission gas release measurements (Section 4.3.4).

In general, the appearance of the fuel rods was good, although considerable chipping at the ends of the rods (Fig. 4-15) and some surface debonding (Fig. 4-16) were observed. No more than 21 failed particles were observed on the surface of any of the rods (Table 4-14 and Fig. 4-17). Very little particulate debris was found during unloading.

About 3% of the 3130 rods removed from the element were broken. Approximately 2% of these are thought to have been broken when pushed out of the block; the remaining 1% were probably broken prior to assembly of the element. Evidence of breakage prior to assembly was apparent in many instances. The orientation of the pieces in some of the broken rods was reversed so that one or both end caps were toward the middle of the rod rather than at the ends. Some broken fuel rods consisted of nonmatching pieces so that the composite length differed significantly from that of an unbroken rod. Also, some fuel stacks had broken pieces at each end with 14 unbroken rods in between.

4.3.2. Fuel Rod Metrology

A representative sampling of fuel rods, including 70 of the 87 rods dimensionally characterized prior to irradiation (the other 17 were broken during unloading), was measured using an automated fuel rod measuring device. This device consists primarily of a slide with three linear potentiometers that engage the fuel rod and measure the diameter at three axial locations, a slide with one potentiometer for measuring the length, and a motor-driven support roller that holds and rotates the fuel rod. The quick action of the solenoids is dampened by small cylindrical shock absorbers working on the compression and vacuum of air. Several limit switches are attached for remotely signaling the computer that the slides are properly located for each measurement. This device is shown in Fig. 4-18 and an operational description is given in Ref. 16. The device is capable of making eight measurements per fuel rod in a few seconds. The time required to measure a stack of 15 fuel rods averaged about 22 min (including fuel rod handling time), i.e., 1-1/2 min per rod. When compared with the 6 min per rod required by the measuring technique employed for Peach Bottom fuel rods, it is evident that the automated fuel rod metrology device represents a major improvement in fuel rod measuring techniques.

The irradiation-induced strains* in the all-TRISO-particle fuel rods were found to be small and somewhat anisotropic, with the axial strain exceeding the radial. The average radial and axial strains for the 71 precharacterized fuel rods are -0.36% and -0.49%, respectively. The stack-averaged fuel rod strains for each of the five fuel stacks containing

*The strain is calculated using the equation $\varepsilon = X_2/X_1 - 1$, where X_2 is the postirradiation dimension and X_1 the preirradiation dimension. In calculating radial strain, the preirradiation dimensions measured using an air gauge were increased by 0.036 mm (Ref. 17) to make them compatible with the postirradiation micrometer-like measurements.

precharacterized rods (all rods in the sixth stack were broken during unloading) are given in Table 4-15 and compared with predicted fuel rod strain curves in Fig. 4-19. The predicted strain curves were obtained using the model presented in Ref. 18 for irradiation-induced dimensional changes in HTGR fuel rods. It is observed that the predicted strains are about three times the measured strains. In addition, radial strains are predicted to be greater than axial strains, but the opposite occurs. One possible explanation is that the model was developed primarily from design data in the fast fluence range 4 to 10 x 10^{25} n/m2 (E > 29 fJ)$_{HTGR}$ and extrapolated to low fluence. The curve for OPyC densification versus fluence is very steep at low fluence but is unverified, since no low-fluence data are available. This is a potential source of the observed discrepancies.

The detailed strain data for the precharacterized fuel rods are given in Tables 4-16 through 4-20.

4.3.3. Fuel Rod Strength Measurements

Strength testing was performed on 13 irradiated fuel rods from element 1-0743 and 10 unirradiated rods from the same rod lot (CR-18-10165-1). The rods were compressed using an Instron tensile/compression testing machine at a rate of 0.002 mm/s (0.005 in./min). A typical trace showing applied force as a function of time (and fuel rod compression) is shown in Fig. 4-20. Table 4-21 presents the failure load at rupture for each irradiated and unirradiated fuel rod. The mean failure load at rupture was 541.8 ± 16.4 (1σ) N (121.8 ± 3.7 lb) for the irradiated rods and 470.6 ± 13.0 (1σ) N (105.8 ± 2.9 lb) for the unirradiated rods. The mean compressive stresses at rupture for the irradiated and unirradiated rods were 4.3 and 3.7 MPa, respectively. The data indicate a statistically significant increase of approximately 15% in the compressive strength of the fuel rods with irradiation.

Although the mean failure load at rupture for the irradiated rods was 541.8 N, evidence of damage to the rods was observed for applied forces as low as 275 N. This indicates that the maximum force applied in pushing fuel rods out of an element during disassembly should be limited to approximately 220 N (50 lb).

4.3.4. Fission Gas Release

Fission gas release for fuel rods irradiated in fuel element 1-0743 was measured before and after irradiation via neutron activation of the rods in the GA TRIGA reactor facility. Preirradiation measurements yield the uranium contamination and as-manufactured failed fissile particles. Postirradiation measurements yield the heavy metal contamination, as-manufactured failed particles, and in-pile coating failure. The in-pile coating failure can be estimated from the preirradiation and postirradiation fission gas release measurements using the calculation outlined in Ref. 18. This calculation also requires information concerning thorium contamination, as-manufactured defective fertile particles, and the fraction of fissions occurring in the fissile and fertile fuel at EOL.

The results of the fission gas release measurements are given in Table 4-22. Postirradiation measurements on groups of 3 and 10 rods and on 4 individual rods were performed. The Kr-85m R/B value obtained for the 17 rods was 1.0×10^{-4} (weighted average). The preirradiation Kr-85m R/B value was 1.3×10^{-4}. The difference between the preirradiation and postirradiation R/B values is attributed to the uncertainty of the measurement, which is approximately a factor of 1.6 (1σ) for Kr-85m (Ref. 19).

Both the fissile and fertile particles potentially contribute to the postirradiation fission gas release. At EOL, approximately 65% of the fissions were occurring in the fissile particles and 35% in the fertile particles. The fission gas release results indicate that there was no significant fuel failure during irradiation, since there was no increase in the fission gas release. This conclusion is supported by the results of metallography.

4.3.5. Metallography

Four irradiated fuel rods and one unirradiated rod from the same rod lot were subjected to metallographic examination. The four irradiated rods were among the 17 rods for which fission gas release measurements were performed. Each rod was mounted in resin, ground, and polished. Prior to examination, all polished sections were passivated with a 50/50 solution of HNO_3 and H_2O to decrease the rate of hydrolysis of the ThC_2 kernels. The entire polished surface of each rod was examined.

4.3.5.1. Results of Metallographic Examination. The fuel rod matrix appeared to be in good condition. No cracking was observed except for minor cracking in the matrix end cap. The microstructure of the matrix prior to and after irradiation is shown in Fig. 4-21. The irradiated microstructure is similar to the microstructure observed for FSV fuel rods irradiated in capsule F-30 (Ref. 20). The matrix porosity, which is composed of voids ≥ 50 μm, was measured for the irradiated rods and averaged 26%. The macroporosity of the unirradiated rod was 19%. Both values are within the range of macroporosities observed for fuel rods from capsule F-30. An example of a radial cross section showing the macroporosity in the matrix is shown in Fig. 4-22.

The results of the metallographic examination of the four irradiated fuel rods are presented in Tables 4-23 and 4-24. The irradiation performance of the fissile and fertile TRISO coated particles was satisfactory. The microstructures of the particle types before and after irradiation are shown in Fig. 4-23. The microstructures had not changed significantly after being exposed to a fast neutron fluence of ~1 x 10^{25} n/m^2 $(E > 29\ fJ)_{HTGR}$ and a time-averaged temperature of ~700°C. Approximately 1500 fissile and 925 fertile particles were examined in the four rods.

The OPyC coating failure was 0.5% and 1.1% for the $(Th,U)C_2$ and ThC_2 particles, the SiC coating failure was 0.7% and 0.5%, and the total coating failure was 0.3% ($0.1 \leq F\% \leq 0.5$; 95% confidence) and 0.2% ($0.0 \leq F\% \leq 0.7$; 95% confidence). The coating failures were apparently as-manufactured failures which occurred during coating or fuel rod fabrication. The following evidence supports this conclusion:

1. The appearance of the failed particles. Two examples of failed particles are shown in Fig. 4-24. Particle (a) has the appearance of having been crushed, and part of the coating is missing in particle (b). In both cases, as-manufactured failure, rather than in-pile failure, is indicated.

2. The kernels of most particles with total coating failure were at least partially leached. This indicates as-manufactured failure, since the as-manufactured fuel rods were leached with HCl.

3. The defective SiC coating fractions measured prior to irradiation using a burn-leach technique are the same as those measured for the four irradiated rods: 0.7% for $(Th,U)C_2$ particles and 0.5% for ThC_2 particles.

The chemical behavior of the TRISO particles was acceptable. No attack of the SiC coating was observed, and kernel migration was not seen. A small amount of a dense phase was observed in the buffer coating of some TRISO $(Th,U)C_2$ particles. All the particles with this dense phase had a low-density, porous IPyC coating. The dense phase is attributed to fuel dispersion in as-manufactured fissile A particles (Refs. 21 and 22). The fuel dispersion was apparently caused by chlorine in the buffer coating. The chlorine had diffused through a permeable IPyC coating during the SiC coating operation. Fuel dispersion was observed in one out of 131 particles in the unirradiated rod. The fuel dispersion in an unirradiated and an irradiated particle is shown in Fig. 4-25. The fuel dispersion did not detrimentally affect the irradiation performance of the particles.

4.3.5.2. Comparison of Calculated and Measured Fuel Failure. The metallographic examination of four irradiated fuel rods from fuel element 1-0743 revealed total coating failures of 0.3% and 0.2% for the $(Th,U)C_2$ and ThC_2 particles, respectively. However, based on the evidence discussed in Section 4.3.5.1, it was concluded that these were as-manufactured failures and that no in-pile failure occurred.

Fuel failure predictions for fuel element 1-0743 were obtained from SURVEY-PERFOR. In-pile failure due to manufacturing defects was predicted to be 0.32% for $(Th,U)C_2$ particles and 0.07% for ThC_2 particles. No in-pile failure due to fission product-SiC interactions, kernel migration, or the pressure vessel failure mechanism was predicted for either particle. In view of the observation of no in-pile failure, the model for failure due to manufacturing defects appears to be conservative.

TABLE 4-1
FSV FUEL ELEMENT 1-0743 AXIAL DIMENSIONS
(inches)[a]

Corner No.	Meas.	L Dim.[a]	M Dim.[b]	N Dim.[b]	P Dim.[b]	R Dim.[b]	S Dim.[b]
1	Pre I	9.0015	9.003	9.002	2.251	27.007	31.2345
	Robot	8.975	8.979	8.981	2.270	26.935	31.150
	PIE	8.964	8.976	8.985	2.2575	26.925	31.167
	Robot-Pre I	-0.027	-0.024	-0.021	+0.019	-0.072	-0.084
	PIE-Pre I	-0.038	-0.027	-0.017	+0.0065	-0.082	-0.068
2	Pre I	9.0015	9.002	9.003	2.2515	27.0065	31.233
	Robot	8.980	8.970	8.979	2.2610	26.929	31.147
	PIE	8.987	8.979	8.980	2.2575	26.946	31.165
	Robot-Pre I	-0.022	-0.032	-0.024	+0.010	-0.078	-0.086
	PIE-Pre I	-0.015	-0.023	-0.023	+0.006	-0.061	-0.068
3	Pre I	9.001	9.002	9.0015	2.2485	27.0045	31.233
	Robot	8.987	8.984	8.973	2.273	26.944	31.159
	PIE	8.989	8.984	8.982	2.2525	26.955	31.180
	Robot-Pre I	-0.014	-0.018	-0.029	+0.025	-0.061	-0.074
	PIE-Pre I	-0.012	-0.018	-0.020	+0.004	-0.050	-0.053
4	Pre I	9.0025	9.0005	9.0025	2.2515	27.0055	31.232
	Robot	8.996	8.990	8.993	2.260	26.979	31.182
	PIE	8.991	8.996	8.986	2.2565	26.973	31.195
	Robot-Pre I	-0.007	-0.011	-0.010	+0.009	-0.027	-0.050
	PIE-Pre I	-0.012	-0.005	-0.017	+0.005	-0.033	-0.037
5	Pre I	9.002	9.001	9.0025	2.253	27.0055	31.2315
	Robot	8.993	8.990	8.994	2.261	26.977	31.182
	PIE	8.993	8.994	8.991	2.2525	26.978	31.196
	Robot-Pre I	-0.009	-0.011	-0.009	+0.008	-0.029	-0.050
	PIE-Pre I	-0.009	-0.007	-0.012	-0.0005	-0.028	-0.036
6	Pre I	9.0015	9.0025	9.0025	2.2505	27.0065	31.233
	Robot	8.992	8.975	8.980	2.278	26.947	31.164
	PIE	8.977	8.986	8.988	2.2525	26.951	31.180
	Robot-Pre I	-0.010	-0.028	-0.023	+0.028	-0.060	-0.069
	PIE-Pre I	-0.025	-0.017	-0.015	+0.002	-0.056	-0.053
Robot	Mean	8.9872	8.9813	8.9833	2.2672	26.9518	31.1640
	Std Dev.	0.0082	0.0081	0.0084	0.0076	0.0213	0.0152
PIE	Mean	8.9835	8.9858	8.9853	2.2548	26.9547	31.1805
	Std Dev.	0.0111	0.0080	0.0040	0.0026	0.0192	0.0132
Pre I	Mean	9.0017	9.0018	9.0023	2.2510	27.0059	31.2328
	Std Dev.	0.0005	0.0009	0.0005	0.0015	0.0006	0.0010
PIE-Pre I	Mean	-0.0185	-0.0162	-0.0173	+0.0038	-0.0517	-0.0525
	Std Dev.	0.0110	0.0087	0.0038	0.0027	0.0197	0.0141
$\frac{\text{PIE-Pre I}}{\text{Pre I}}$ (% strain)		-0.21	-0.18	-0.19	+0.17	-0.19	-0.17

(a) 1 in. = 25.4 mm.

(b) See Fig. 2-5.

TABLE 4-2
FSV FUEL ELEMENT 1-0743 TRANSVERSE DIMENSIONAL
CHANGE - MINIMUM DISTANCE BETWEEN COOLANT HOLES
(inches)[a]

Holes 312 to 13		312 to 270	270 to 219	219 to 106	106 to 55	55 to 13	312 to 13			Mean	Std Dev.
Top of block	Pre I	1.594	1.597	3.818	1.595	1.601	12.695			1.5968	0.0031
	Robot	1.593	1.593	3.814	1.593	1.594	12.688			1.5933	0.0005
	PIE	1.5913	1.5978	3.8132	1.5942	1.5945	12.6813			1.5945	0.0027
	Robot-Pre I	-0.001	-0.004	-0.004	-0.002	-0.007	-0.007			-0.0033	0.0026
	PIE-Pre I	-0.0027	+0.0008	-0.0048	-0.0008	-0.0065	-0.0137			-0.0023	0.0031
Bottom of block	Pre I	1.598	1.594	3.816	1.601	1.598	12.700			1.5978	0.0029
	PIE	1.5918	1.5970	3.8189	1.6018	1.5955	12.6978			1.5965	0.0041
	PIE-Pre I	-0.0062	+0.0030	+0.0029	+0.0008	-0.0025	-0.0022			-0.0012	0.0040
Holes 319 to 6		**319 to 295**	**295 to 267**	**267 to 235**	**235 to 90**	**90 to 58**	**58 to 30**	**30 to 6**	**319 to 6**	**Mean**	**Std Dev.**
Top of block	Pre I	0.655	0.655	0.657	4.505	0.658	0.660	0.658	12.191	0.6572	0.0019
	Robot	0.646	0.665	0.639	4.514	0.657	0.648	0.658	12.181	0.6522	0.0095
	PIE	0.6548	0.6603	0.6572	4.4982	0.6599	0.6547	0.6583	12.1788	0.6575	0.0024
	Robot-Pre I	-0.009	+0.010	-0.018	+0.007	-0.001	-0.012	0	-0.010	-0.0050	0.0100
	PIE-Pre I	-0.0002	+0.0053	+0.0002	-0.0068	+0.0019	-0.0058	+0.0003	-0.0122	+0.0003	0.0036
Bottom of block	Pre I	0.653	0.654	0.655	4.508	0.656	0.657	0.662	12.196	0.6565	0.0029
	PIE	0.6564	0.6612	0.6558	4.5089	0.6564	0.6505	0.6638	12.1924	0.6574	0.0046
	PIE-Pre I	+0.0014	+0.0072	+0.0008	+0.0009	+0.0004	-0.0065	+0.0018	-0.0036	+0.0009	0.0044
Holes 303 to 22		**303 to 264**	**264 to 216**	**216 to 109**	**109 to 61**	**61 to 22**	**303 to 22**			**Mean**	**Std Dev.**
Top of block	Pre I	1.596	1.597	3.823	1.598	1.596	12.696			1.5968	0.0010
	Robot	1.589	1.590	3.819	1.585	1.586	12.669			1.5875	0.0024
	PIE	1.5946	1.5942	3.8144	1.5932	1.5936	12.6806			1.5939	0.0006
	Robot-Pre I	-0.007	-0.007	-0.004	-0.013	-0.010	-0.027			-0.0093	0.0029
	PIE-Pre I	-0.0014	-0.0028	-0.0086	-0.0048	-0.0024	-0.0154			-0.0029	0.0014
Bottom of block	Pre I	1.598	1.598	3.823	1.596	1.601	12.705			1.5983	0.0027
	PIE	1.5975	1.5989	3.8236	1.5978	1.5934	12.7045			1.5969	0.0024
	PIE-Pre I	-0.0005	+0.0009	+0.0006	+0.0018	-0.0076	-0.0005			-0.0014	0.0043
Holes 170 to 155		**170 to 167**	**167 to 164**	**164 to 161**	**161 to 158**	**158 to 155**	**170 to 155**			**Mean**	**Std Dev.**
Top of block	Pre I	1.594	1.596	3.819	1.595	1.594	12.690			1.5948	0.0010
	Robot	1.585	1.589	3.826	1.593	1.590	12.684			1.5893	0.0033
	PIE	1.5931	1.5911	3.8166	1.5931	1.5930	12.6781			1.5926	0.0010
	Robot-Pre I	-0.009	-0.007	+0.007	-0.002	-0.004	-0.006			-0.0055	0.0031
	PIE-Pre I	-0.0009	-0.0049	-0.0024	-0.0019	-0.0010	-0.0119			-0.0022	0.0019
Bottom of block	Pre I	1.594	1.596	3.817	1.597	1.596	12.692			1.5938	0.0013
	PIE	1.5935	1.5961	3.8168	1.5964	1.5947	12.6895			1.5952	0.0013
	PIE-Pre I	-0.0005	-0.0001	-0.0002	-0.0006	-0.0013	-0.0025			-0.0006	0.0006
Holes		**13 to 22**	**22 to 170**	**170 to 312**	**312 to 303**	**303 to 155**	**155 to 13**			**Mean**	**Std Dev.**
Top of block	Pre I	6.037	6.036	6.034	6.036	6.035	6.038			6.0360	0.0014
	Robot	6.028	6.026	6.025	6.024	6.027	6.025			6.0258	0.0015
	PIE	6.0326	6.0221	6.0243	6.0283	6.0276	6.0313			6.0277	0.0040
	Robot-Pre I	-0.009	-0.010	-0.009	-0.012	-0.008	-0.013			-0.0102	0.0019
	PIE-Pre I	-0.0044	-0.0139	-0.0097	-0.0077	-0.0074	-0.0067			-0.0083	0.0032
Bottom of block	Pre I	6.036	6.037	6.035	6.035	6.038	6.037			6.0364	0.0012
	PIE	6.0416	6.0405	6.0328	6.0338	6.0345	6.0423			6.0376	0.0043
	PIE-Pre I	+0.0056	+0.0035	-0.0022	-0.0012	-0.0035	+0.0053			+0.0013	0.0040

[a] 1 in. = 25.4 mm.

TABLE 4-3
FSV FUEL ELEMENT 1-0743
SQUARENESS DATUM PLANES
(inches)[a]

Face	Meas.	Maximum Displacement from Squareness at Vertical Incremental Distance up Length of Block[b]								
		1	2	3	4	5	6	7	8	9
A	Pre I	-0.0005	-0.00	-0.002	-0.002	-0.001	0.000	-0.002	-0.0015	-0.0001
	Robot	+0.0049	+0.0058	+0.0076	+0.0085	+0.0084	+0.0073	+0.0051	+0.0030	-0.0001
	PIE	+0.0021	+0.0037	+0.0049	+0.0056	+0.0048	+0.0045	+0.0035	+0.0020	-0.0001
	Robot-Pre I	+0.0054	+0.0068	+0.0096	+0.0105	+0.0094	+0.0073	+0.0071	+0.0045	0
	PIE-Pre I	+0.0026	+0.0047	+0.0069	+0.0076	+0.0058	+0.0045	+0.0055	+0.0035	0
B	Pre I	+0.001	+0.0005	0.000	+0.001	-0.0005	0.000	-0.001	-0.001	-0.001
	Robot	+0.0070	+0.0110	+0.0120	+0.0130	+0.0120	+0.0100	+0.0070	+0.0030	-0.001
	PIE	+0.0015	+0.0030	+0.0046	+0.0061	+0.0076	+0.0086	+0.0063	+0.0030	-0.0010
	Robot-Pre I	+0.0060	+0.0105	+0.0120	+0.0120	+0.0125	+0.0100	+0.0080	+0.0040	0
	PIE-Pre I	+0.0005	+0.0025	+0.0046	+0.0051	+0.0081	+0.0086	+0.0073	+0.0040	0
C	Pre I	+0.0005	+0.001	+0.001	+0.001	+0.001	+0.0015	+0.001	+0.0005	+0.0015
	Robot	+0.0043	-0.0076	+0.0088	+0.0101	+0.0104	+0.0087	+0.0068	+0.0052	+0.0015
	PIE	+0.0027	+0.0045	+0.0057	+0.0065	+0.0068	+0.0063	+0.0050	+0.0039	+0.0015
	Robot-Pre I	+0.0038	+0.0066	+0.0078	+0.0091	+0.0096	+0.0072	+0.0058	+0.0047	0
	PIE-Pre I	+0.0022	+0.0035	+0.0047	+0.0055	+0.0058	+0.0048	+0.0040	+0.0034	0
D	Pre I	+0.0005	+0.0005	+0.001	+0.001	+0.001	+0.0001	+0.0015	+0.002	+0.0025
	Robot	-0.0004	-0.0008	+0.0008	+0.0014	+0.0021	+0.0007	+0.0013	+0.0009	+0.0025
	PIE	-0.0010	-0.0020	-0.0023	[illegible]	-0.0023	-0.0012	-0.0011	+0.0004	[illegible]
	Robot-Pre I	-0.0009	-0.0013	-0.0002	[illegible]	+0.0011	+0.0006	[illegible]	-0.0011	[illegible]
	PIE-Pre I	-0.0015	-0.0025	-0.0033	-0.0034	-0.0033	-0.0013	-0.0026	-0.0024	0
E	Pre I	0.000	+0.0005	0.000	+0.0005	+0.001	+0.001	+0.001	+0.0015	+0.002
	Robot	-0.0021	-0.0022	-0.0043	-0.0054	-0.0046	-0.0047	-0.0038	-0.0009	+0.0020
	PIE	-0.0042	-0.0056	-0.0081	-0.0089	-0.0087	-0.0078	-0.0054	-0.0016	+0.0020
	Robot-Pre I	-0.0021	-0.0027	-0.0043	-0.0059	-0.0056	-0.0057	-0.0048	-0.0024	0
	PIE-Pre I	-0.0042	-0.0061	-0.0081	-0.0094	-0.0097	-0.0088	-0.0064	-0.0031	0
F	Pre I	0.000	+0.0005	+0.0005	0.000	0.000	0.000	+0.0005	+0.0005	+0.0005
	Robot	-0.0014	-0.0028	-0.0032	-0.0026	-0.0029	-0.0043	-0.0037	-0.0041	+0.0005
	PIE	-0.0020	-0.0036	-0.0047	-0.0050	-0.0051	-0.0041	-0.0035	-0.0018	+0.0005
	Robot-Pre I	-0.0014	-0.0033	-0.0037	-0.0026	-0.0029	-0.0043	-0.0042	-0.0046	0
	PIE-Pre I	-0.0020	-0.0041	-0.0052	-0.0050	-0.0051	-0.0041	-0.0040	-0.0023	0
Robot	Mean	+0.0021	+0.0031	+0.0036	+0.0042	+0.0042	+0.0030	+0.0021	+0.0012	+0.0009
	Std. Dev.	0.0038	0.0058	0.0068	0.0074	0.0071	0.0066	0.0050	0.0033	0.0013
PIE	Mean	-0.0002	0	0	+0.0003	+0.0005	+0.0011	+0.0008	+0.0010	+0.0009
	Std. Dev.	0.0027	0.0043	0.0058	0.0066	0.0068	0.0064	0.0048	0.0024	0.0013

[a] 1 in. = 25.4 mm.

[b] See detail T in Fig. 2-5 for interpretation of + and - values.

TABLE 4-4
FSV FUEL ELEMENT 1-0743
COOLANT HOLE DIAMETERS
(inches)[a]

Hole No.	Meas.	Hole Diameter (J)[b] Top	Bottom
13	Pre I	0.625	0.625
	Robot	0.625	ND[c]
	PIE	0.6228	0.6234
	Robot-Pre I	0	ND
	PIE-Pre I	-0.0022	-0.0016
22	Pre I	0.625	0.625
	Robot	0.626	ND
	PIE	0.6224	0.6234
	Robot-Pre I	+0.001	ND
	PIE-Pre I	-0.0026	-0.0016
155	Pre I	0.625	0.624
	Robot	0.623	ND
	PIE	0.6227	0.6227
	Robot-Pre I	-0.002	ND
	PIE-Pre I	-0.0023	-0.0013
170	Pre I	0.625	0.624
	Robot	0.624	ND
	PIE	0.6229	0.6225
	Robot-Pre I	-0.001	ND
	PIE-Pre I	-0.0021	-0.0015
303	Pre I	0.625	0.624
	Robot	0.623	ND
	PIE	0.6224	0.6225
	Robot-Pre I	-0.002	ND
	PIE-Pre I	-0.0026	-0.0015
312	Pre I	0.625	0.624
	Robot	0.624	ND
	PIE	0.6227	0.6232
	Robot-Pre I	-0.001	ND
	PIE-Pre I	-0.0023	-0.0008
Robot	Mean	0.6242	ND
	Std Dev.	0.0012	ND
PIE	Mean	0.6227	0.6230
	Std Dev.	0.0002	0.0004
Pre I	Mean	0.6250	0.6243
	Std Dev.	0	0.0006
PIE-Pre I	Mean	-0.0024	-0.0014
	Std Dev.	0.0002	0.0003
$\frac{\text{PIE-Pre I}}{\text{Pre}}$	(% strain)	-0.38	-0.22

[a] 1 in. = 25.4 mm.

[b] See Fig. 2.5.

[c] Not determined.

TABLE 4-5
FSV FUEL ELEMENT 1-0743
BOW OF SIX SIDE FACES[a]
(inches)[b]

Position	Face A		Face B		Face C		Face D		Face E		Face F	
	Robot	PIE	Robot	PIE	Robot	PIE	Robot	PIE	Robot	PIE	Robot	PIE
6[c]	+0.0040	+0.0036	+0.0047	+0.0047	+0.0044	+0.0021	-0.0016	-0.0019	-0.0026	-0.0034	-0.0004	+0.0018
7	+0.0049	+0.0023	+0.0064	+0.0046	+0.0042	+0.0021	-0.0017	-0.0018	-0.0006	-0.0031	-0.0003	-0.0020
8	+0.0050	+0.0023	+0.0074	+0.0019	+0.0042	+0.0028	-0.0008	-0.0014	-0.0024	-0.0047	-0.0012	-0.0021
9	+0.0049	+0.0026	+0.0055	+0.0043	+0.0044	[illegible]	-0.0007	-0.0016	-0.0025	-0.0035	-0.0002	-0.0021
10	+0.0031	+0.0019	+0.0066	+0.0047	+0.0053	[illegible]	+0.0015	-0.0009	-0.0024	-0.0034	-0.0013	-0.0021
11	+0.0052	+0.0034	+0.0112	+0.0081	+0.0076	+0.0053	0	-0.0017	-0.0048	-0.0063	-0.0016	-0.0039
12	+0.0068	+0.0044	+0.0100	+0.0077	+0.0058	+0.0052	+0.0006	-0.0027	-0.0040	-0.0057	-0.0014	-0.0040
13	+0.0060	+0.0041	+0.0118	+0.0039	+0.0074	+0.0045	-0.0016	-0.0027	-0.0028	-0.0066	-0.0024	-0.0040
14	+0.0058	+0.0037	+0.0108	+0.0074	+0.0074	+0.0044	-0.0014	-0.0033	-0.0042	-0.0059	-0.0006	-0.0033
15	+0.0070	+0.0056	+0.0094	+0.0079	+0.0068	+0.0037	-0.0022	-0.0031	-0.0032	-0.0066	+0.0002	-0.0030
16	+0.0090	+0.0066	+0.0121	+0.0097	+0.0092	+0.0054	-0.0028	-0.0040	-0.0058	-0.0088	+0.0008	-0.0040
17	+0.0087	+0.0048	+0.0132	+0.0093	+0.0106	+0.0055	-0.0021	-0.0044	-0.0048	-0.0084	-0.0009	-0.0044
18	+0.0080	+0.0055	+0.0132	+0.0058	+0.0086	+0.0058	-0.0004	-0.0034	-0.0052	-0.0096	-0.0026	-0.0052
19	+0.0087	+0.0053	+0.0125	+0.0098	+0.0092	+0.0063	-0.0001	-0.0032	-0.0055	-0.0084	-0.0016	-0.0051
20	+0.0077	+0.0046	+0.0128	+0.0100	+0.0089	+0.0065	+0.0005	-0.0023	-0.0062	-0.0087	-0.0019	-0.0052
21	+0.0084	+0.0054	+0.0144	+0.0110	+0.0092	+0.0073	0	-0.0027	-0.0066	-0.0099	-0.0032	-0.0058
22	+0.0086	+0.0060	+0.0150	+0.0111	+0.0106	+0.0068	+0.0002	-0.0035	-0.0070	-0.0100	-0.0018	-0.0058
23	+0.0090	+0.0064	+0.0146	+0.0078	+0.0098	+0.0066	-0.0002	-0.0038	-0.0066	-0.0109	-0.0018	-0.0058
24	+0.0096	+0.0058	+0.0136	+0.0106	+0.0108	+0.0061	-0.0008	-0.0049	-0.0064	-0.0098	-0.0002	-0.0052
25	+0.0100	+0.0069	+0.0138	+0.0109	+0.0096	+0.0062	-0.0014	-0.0047	-0.0064	-0.0101	+0.0004	-0.0045
26	+0.0100	+0.0070	+0.0145	+0.0114	+0.0110	+0.0064	-0.0020	-0.0047	-0.0070	-0.0107	-0.0010	-0.0042
27	+0.0095	+0.0059	+0.0150	+0.0109	+0.0110	+0.0067	-0.0015	-0.0015	-0.0060	-0.0103	-0.0015	-0.0053
28	+0.0090	+0.0058	+0.0140	+0.0097	+0.0100	+0.0069	0	-0.0042	-0.0060	-0.0113	-0.0020	-0.0060
29	+0.0095	+0.0060	+0.0135	+0.0109	+0.0110	+0.0070	+0.0005	-0.0039	-0.0065	-0.0105	-0.0020	-0.0060
30	+0.0085	+0.0054	+0.0140	+0.0113	+0.0095	+0.0074	+0.0015	-0.0028	-0.0070	-0.0104	-0.0035	-0.0064
31	+0.0086	+0.0053	+0.0136	+0.0106	+0.0088	+0.0068	+0.0010	-0.0026	-0.0064	-0.0097	-0.0028	-0.0059
32	+0.0074	+0.0057	+0.0130	+0.0101	+0.0094	+0.0065	-0.0002	-0.0036	-0.0060	-0.0099	-0.0032	-0.0056
33	+0.0080	+0.0057	+0.0124	+0.0111	+0.0082	+0.0064	-0.0018	-0.0035	-0.0064	-0.0108	+0.0032	-0.0052
34	+0.0084	+0.0056	+0.0124	+0.0104	+0.0092	+0.0063	-0.0012	-0.0049	-0.0066	-0.0098	-0.0008	-0.0046
35	+0.0090	+0.0066	+0.0122	+0.0104	+0.0104	+0.0059	-0.0016	-0.0042	-0.0066	-0.0097	+0.0046	-0.0039
36	+0.0070	+0.0056	+0.0089	+0.0088	+0.0088	+0.0050	-0.0022	-0.0041	-0.0062	-0.0084	-0.0008	-0.0028
37	+0.0073	+0.0051	+0.0098	+0.0083	+0.0074	+0.0052	-0.0019	-0.0041	-0.0062	-0.0083	-0.0021	-0.0042
38	+0.0060	+0.0049	+0.0098	+0.0092	+0.0064	+0.0052	-0.0016	-0.0037	-0.0038	-0.0089	-0.0024	-0.0048
39	+0.0073	+0.0050	+0.0105	+0.0081	+0.0068	+0.0055	-0.0009	-0.0032	-0.0065	-0.0081	-0.0024	-0.0036
40	+0.0057	+0.0046	+0.0102	+0.0089	+0.0061	+0.0059	-0.0005	-0.0021	-0.0058	-0.0080	-0.0031	-0.0033
41	+0.0038	+0.0032	+0.0068	+0.0058	+0.0044	+0.0041	0	-0.0012	-0.0032	-0.0052	-0.0034	-0.0036
42	+0.0032	+0.0036	+0.0070	+0.0054	+0.0052	+0.0036	-0.0006	-0.0022	-0.0050	-0.0053	-0.0016	-0.0020
43	+0.0040	+0.0036	+0.0062	+0.0063	+0.0046	+0.0040	-0.0024	-0.0026	-0.0032	-0.0056	-0.0026	-0.0033
44	+0.0052	+0.0037	+0.0072	+0.0053	+0.0046	+0.0039	-0.0016	-0.0031	-0.0048	-0.0055	-0.0014	-0.0027
45	+0.0040	+0.0040	+0.0056	+0.0060	+0.0052	+0.0035	-0.0008	-0.0025	-0.0058	-0.0061	-0.0002	-0.0019
46	+0.0020	+0.0018	+0.0013	+0.0025	+0.0016	+0.0014	-0.0014	-0.0006	-0.0032	-0.0025	-0.0006	[illegible]
47	+0.0021	+0.0017	+0.0026	+0.0023	+0.0008	+0.0018	-0.0013	-0.0010	-0.0014	-0.0020	+0.0007	+0.0007
48	+0.0010	+0.0017	+0.0026	+0.0028	+0.0008	+0.0017	-0.0012	-0.0008	-0.0006	-0.0025	+0.0022	-0.0012
49	+0.0011	+0.0018	+0.0025	+0.0021	+0.0016	+0.0018	-0.0003	-0.0006	-0.0025	-0.0019	-0.0008	[illegible]
50	+0.0019	+0.0017	+0.0024	-0.0021	-0.0003	+0.0017	+0.0005	0	-0.0016	-0.0014	-0.0017	-0.0015
Mean[d]	+0.0064	+0.0045	+0.0099	+0.0075	+0.0070	+0.0049	-0.0008	-0.0029	-0.0048	-0.0073	-0.0013	-0.0038
Std. Dev.	0.0026	0.0016	0.0040	0.0033	0.0031	0.0018	0.0010	0.0013	0.0019	0.0029	0.0013	0.0018

[a]See detail 3 in Fig. 2-5 for interpretation of + and − values.

[b]1 in. = 25.4 mm.

[c]Positions 1-5 and 51-55 have zero values.

[d]Excluding 1-5 and 51-55.

TABLE 4-[illegible]
FSV FUEL ELEMENT 1-0743
DISPLACEMENT FROM VERTICAL OF SIX SIDE FACES[a]
(inches)[b]

Position	Face A		Face B		Face C		Face D		Face E		Face F	
	Robot	PIE	Robot	PIE	Robot	PIE	Robot	PIE	Robot	PIE	Robot	PIE
6[c]	+0.002	+0.0038	+0.003	+0.0023	+0.003	+0.0008	0	+0.0002	+0.001	+0.0003	+0.001	+0.0001
7	+0.003	+0.0015	[illegible]	+0.0023	+0.003	+0.0008	0	+0.0004	+0.003	+0.0004	+0.001	+0.0001
8	+0.003	+0.0014	[illegible]	0	+0.003	+0.0015	+0.001	+0.0008	+0.001	+0.0013	0	0
9	+0.003	+0.0018	[illegible]	+0.0021	+0.003	+0.0019	+0.001	+0.0005	+0.001	0	+0.001	+0.0001
10	+0.001	+0.0009	+0.003	+0.0023	+0.004	+0.0020	+0.003	+0.0011	+0.001	+0.0001	0	0
11	+0.001	+0.0013	+0.004	+0.0033	+0.003	+0.0029	+0.003	+0.0022	+0.002	+0.0007	+0.001	+0.0002
12	+0.003	+0.0027	+0.003	+0.0032	+0.003	+0.0029	+0.004	+0.0015	+0.003	+0.0013	0	+0.0003
13	+0.002	+0.0023	+0.005	0	+0.005	+0.0020	+0.002	+0.0016	+0.004	+0.0002	0	+0.0003
14	+0.002	+0.0021	+0.004	+0.0028	+0.005	+0.0017	+0.002	+0.0010	+0.003	+0.0012	+0.002	+0.0009
15	+0.003	+0.0044	+0.002	+0.0032	+0.004	+0.0011	+0.001	+0.0011	+0.004	+0.0008	+0.003	+0.0009
16	+0.003	+0.0048	+0.001	+0.0026	+0.005	+0.0015	+0.002	+0.0022	+0.005	+0.0023	+0.005	+0.0018
17	+0.003	+0.0024	+0.003	+0.0025	+0.001	+0.0011	+0.003	+0.0021	+0.006	+0.0022	+0.003	+0.0019
18	+0.002	+0.0028	+0.003	0	+0.005	+0.0020	+0.005	+0.0031	+0.005	+0.0006	+0.001	+0.0012
19	+0.003	+0.0028	+0.002	+0.0031	+0.005	+0.0028	+0.005	+0.0031	+0.005	+0.0020	+0.002	+0.0014
20	+0.001	+0.0017	+0.002	+0.0028	+0.005	+0.0029	+0.005	+0.0036	+0.004	+0.0018	+0.002	+0.0010
21	0	+0.0016	0	+0.0014	+0.004	+0.0025	+0.006	+0.0037	+0.007	+0.0041	+0.002	+0.0025
22	+0.001	+0.0026	+0.001	+0.0022	+0.005	+0.0022	+0.007	+0.0049	+0.007	+0.0039	+0.003	+0.0030
23	[illegible]	+0.0028	+0.001	0	+0.005	+0.0016	+0.007	+0.0048	+0.007	+0.0027	+0.003	+0.0028
24	+0.002	+0.0026	0	+0.0015	+0.006	+0.0008	+0.006	+0.0037	+0.008	+0.0044	+0.005	+0.0032
25	+0.002	+0.0045	-0.001	+0.0014	+0.004	+0.0010	+0.005	+0.0036	+0.008	+0.0047	+0.006	+0.0033
26	0	+0.0039	-0.004	-0.0005	+0.004	-0.0002	+0.006	+0.0077	+0.011	+0.0078	+0.006	+0.0033
27	0	+0.0018	-0.002	-0.0005	+0.003	0	+0.007	+0.0058	+0.012	+0.0074	+0.005	+0.0052
28	-0.001	+0.0013	-0.003	0	+0.004	+0.0006	+0.009	+0.0066	+0.011	+0.0057	+0.004	+0.0047
29	0	+0.0018	-0.004	-0.0003	+0.004	+0.0012	+0.009	+0.0066	+0.011	+0.0069	+0.004	+0.0048
30	-0.002	+0.0006	-0.004	-0.0007	+0.003	+0.0014	+0.009	+0.0070	+0.010	+0.0071	+0.003	+0.0040
31	-0.004	-0.0004	-0.008	-0.0038	+0.001	-0.0004	+0.010	+0.0091	+0.014	+0.0112	+0.005	+0.0065
32	-0.004	+0.0007	-0.008	-0.0033	+0.001	-0.0004	+0.010	+0.0090	+0.015	+0.0110	+0.004	+0.0073
33	-0.004	+0.0003	-0.008	-0.0005	+0.001	-0.0011	+0.009	+0.0095	+0.014	+0.0095	+0.004	+0.0076
34	-0.003	+0.0007	-0.008	-0.0033	+0.002	-0.0017	+0.009	+0.0080	+0.015	+0.0114	+0.007	+0.0079
35	-0.003	+0.0029	-0.010	-0.0038	+0.002	-0.0020	+0.008	+0.0083	+0.015	+0.0124	+0.013	+0.0077
36	-0.001	+0.0013	-0.017	-0.0078	-0.001	-0.0042	+0.009	+0.0105	+0.019	+0.0174	+0.009	+0.0108
37	-0.008	-0.0008	-0.014	+0.0077	-0.001	-0.0041	+0.010	+0.0110	+0.019	+0.0165	+0.007	+0.0104
38	-0.008	-0.0014	-0.014	-0.0044	-0.002	-0.0038	+0.011	+0.0114	+0.018	+0.0148	+0.006	+0.0102
39	-0.006	-0.0009	-0.014	-0.0075	-0.003	-0.0026	+0.011	+0.0113	+0.018	+0.0127	+0.006	+0.0113
40	-0.009	-0.0021	-0.015	-0.0079	-0.003	-0.0025	+0.010	+0.0116	+0.018	+0.0164	+0.006	+0.0092
41	-0.013	-0.0044	-0.022	-0.0134	-0.006	-0.0055	+0.012	+0.0144	+0.024	+0.0227	+0.007	+0.0130
42	-0.012	-0.0031	-0.021	-0.0124	-0.006	-0.0056	+0.013	+0.0146	+0.023	+0.0225	+0.008	+0.0152
43	-0.012	-0.0036	-0.021	-0.0092	-0.005	-0.0060	+0.012	+0.0141	+0.024	+0.0215	+0.007	+0.0138
44	-0.010	-0.0028	-0.020	-0.0129	-0.005	-0.0067	+0.012	+0.0141	+0.024	+0.0228	+0.009	+0.0140
45	-0.012	-0.0009	[illegible]	-0.0130	-0.006	-0.0070	+0.012	+0.0141	+0.023	+0.0234	+0.011	+0.0136
46	-0.016	-0.0037	-0.031	-0.0188	-0.011	-0.0104	+0.013	+0.0181	+0.031	+0.0307	+0.012	+0.0172
47	-0.015	-0.0056	-0.028	-0.0182	-0.010	-0.0102	+0.014	+0.0184	+0.031	+0.0299	+0.011	+0.0181
48	-0.017	-0.0064	-0.028	-0.0147	-0.010	-0.0096	+0.015	+0.0186	+0.030	+0.0280	+0.013	+0.0181
49	-0.016	-0.0058	-0.029	-0.0180	-0.011	-0.0088	+0.015	+0.0182	+0.029	+0.0294	+0.010	+0.0155
50	-0.017	-0.0069	-0.030	-0.0195	-0.012	-0.0091	+0.014	+0.0176	+0.029	+0.0300	+0.010	+0.0171
51	-0.021	-0.0095	-0.036	-0.0240	-0.013	-0.0120	+0.015	+0.0195	+0.034	+0.0349	+0.013	+0.0207
52	-0.019	-0.0084	-0.035	-0.0223	-0.014	-0.0115	+0.017	+0.0210	+0.035	+0.0346	+0.012	+0.0215
53	-0.020	-0.0090	-0.034	-0.0194	-0.012	-0.0125	+0.018	+0.0216	+0.034	+0.0339	+0.012	+0.0214
54	-0.019	-0.0081	-0.034	-0.0228	-0.012	-0.0133	+0.017	+0.0215	+0.036	+0.0354	+0.013	+0.0209
55	-0.020	-0.0081	-0.037	-0.0237	-0.014	-0.0131	+0.016	+0.0208	+0.036	+0.0369	+0.014	+0.0194
Mean[d]	-0.0050	-0.0005	-0.0104	-0.0055	+0.0008	-0.0025	+0.0084	+0.0090	+0.0150	+0.0121	+0.0058	+0.0080
Std. Dev.	0.0080	0.0039	0.0136	0.0088	0.0065	0.0051	0.0050	0.0068	0.0111	0.0121	0.0042	0.0071

[a] See detail 7 in Fig. 3-1 for interpretation of + and - values.

[b] 1 in. = 25.4 mm.

[c] Positions 1-5 have zero values.

[d] Excluding 1-5.

TABLE 4-7
FSV FUEL ELEMENT 1-0743
DISTANCES ACROSS FLATS
(inches)[a]

Face[b]	Meas.	1 - 2	3 - 4	5 - 6	Mean	Std Dev.
A - D	Pre I			14.1772[c]		
	CC[d]			14.1730[d]		
	Robot	14.147	14.150	14.149		
		14.148	14.156	14.155	14.1525	0.0044
	PIE	14.151	14.151	14.154		
		14.157	14.156		14.1538	0.0028
	PIE-CC			-0.0190		
B - E	Pre I			14.1756[c]		
	CC[d]			14.1714[d]		
	Robot	14.153	14.150	14.152		
		14.150	14.150	14.150	14.1508	0.0013
	PIE	14.154	14.154	14.154		
		14.154	14.153		14.1538	0.0005
	PIE-CC			-0.0174		
C - F	Pre I			14.1769[c]		
	CC[d]			14.1714[d]		
	Robot	14.150	14.151	14.154	14.1532	0.0025
		14.157	14.154	14.153		
	PIE	14.159	14.157	14.154		
		14.151	14.152		14.1546	0.0034
	PIE-CC			-0.0187		
Robot	Mean	14.1525	14.1518	14.1522		
	Std Dev.	0.0043	0.0026	0.0023		
PIE	Mean	14.1543	14.1538	14.1540		
	Std Dev.	0.0032	0.0023	0		
CC[b]	Mean	ND[e]	ND	14.1724		
	Std Dev.			0.0008		
PIE-Pre I	Mean	ND	ND	-0.0184		
	Std Dev.			0.0009		
$\frac{\text{PIE-Pre I}}{\text{Pre I}}$ (% strain)				-0.13%		

[a] 1 in. = 25.4 mm.

[b] See Fig. 2-5.

[c] Cordax.

[d] Cordax corrected (CC).

[e] Not determined.

TABLE 4-8
FSV FUEL ELEMENT 1-0743 LENGTH
(inches)[a]

Meas.	Location[b]	Pre Char	Robot	PIE	Corners Only	PIE - Robot
1	C-324	31.2345	31.150	31.170	31.169	+0.020
2	321-322	ND[c]	31.154	31.169		+0.015
3	S-319	ND	31.147	31.168		+0.021
4	316-317	ND	31.148	31.168		+0.020
5	C-314	31.2330	31.147	31.167	31.165	+0.020
6	275-289	ND	31.147	31.170		+0.023
7	293-294	ND	31.155	31.171		+0.016
8	296-297	ND	31.154	31.173		+0.019
9	288-301	ND	31.163	31.173		+0.010
10	S-259	ND	31.163	31.175		+0.012
11	257-272	ND	31.1[illegible]4	31.176		+0.012
12	237-254	ND	31.[illegible]62	31.178		+0.0[illegible]6
13	251-252	ND	31.160	ND		ND
14	233-249	ND	31.156	31.178		+0.022
15	246-262	ND	31.153	31.175		+0.022
16	S-244	ND	31.155	31.173		+0.018
17	190-209	ND	31.156	31.178		+0.022
18	192-211	ND	31.162	31.179		+0.017
19	195-214	ND	31.162	31.181		+0.019
20	203-221	ND	31.166	31.181		+0.015
21	206-224	ND	31.168	31.180		+0.012
22	208-226	ND	31.166	31.179		+0.013
23	C-171	31.2330	31.164	31.182	31.180	+0.018
24	165-166	ND	31.163	31.182		+0.019
25	HH-163	ND	31.169	ND		ND
26	HH-200	ND	31.161	ND		ND
27	HH-198	ND	31.164	ND		ND
28	HH-127	ND	31.166	ND		ND
29	HH-125	ND	31.167	ND		ND
30	HH-162	ND	31.162	ND		ND
31	159-160	ND	31.165	31.184		+0.019
32	C-154	31.2330	31.159	31.182	31.180	+0.021
33	99-117	ND	31.173	31.185		+0.012
34	101-119	ND	31.174	31.189		+0.015
35	104-122	ND	31.171	ND		ND
36	111-130	ND	31.167	ND		ND
37	114-133	ND	31.173	31.189		+0.016
38	116-135	ND	31.169	31.186		+0.017
39	S-81	ND	31.174	31.190		+0.016
40	63-79	ND	31.173	31.192		+0.019
41	76-92	ND	31.171	ND		ND
42	73-74	ND	31.172	ND		ND
43	71-88	ND	31.178	ND		ND
44	53-68	ND	31.179	31.193		+0.014
45	S-66	ND	31.175	31.190		+0.015
46	24-37	ND	31.183	31.192		+0.009
47	28-29	ND	31.178	31.196		+0.018
48	31-32	ND	31.180	31.197		+0.017
49	36-50	ND	31.177	31.193		+0.016
50	C-11	31.2315	31.182	31.197	31.196	+0.014
51	8-9	ND	31.180	31.196		+0.016
52	S-6	ND	31.182	31.191		+0.009
53	3-4	ND	31.185	31.196		+0.011
54	C-1	31.2320	31.182	31.1[illegible]7	31.195	+0.013
Mean			31.1662	31.1824		+0.0165
Std. Dev.			0.0103	0.0095		+0.0037

(a) 1 in. = 25.4 mm.

(b) C = corner of element; S = side of element; HH = handling hole. For example, C-324 = between corner and hole number 324.

(c) ND = not determined.

TABLE 4-9
FSV FUEL ELEMENT 1-0743
DISTANCES BETWEEN CENTERLINES OF COOLANT HOLES
(inches)[a]

Hole to Hole	Pre I Top	Pre I Bottom	Robot Top	PIE Top	PIE Bottom	PIE - Pre I	% Strain
259 - 222	ND[b]	ND	2.5601	2.556	2.566		
222 - 181	ND	ND	2.5657	2.561	2.576		
181 - 144	ND	ND	2.5570	2.563	2.561		
144 - 103	ND	ND	2.5636	2.562	2.556		
103 - 66	ND	ND	2.5602	2.556	2.563		
259 - 66	ND	ND	12.8051	12.797	12.821		
312 - 270	ND	ND	2.2185	2.214	2.215		
270 - 219	ND	ND	2.2181	2.220	2.220		
219 - 106	ND	ND	4.4394	4.436	4.442		
106 - 55	ND	ND	2.2181	2.217	2.225		
55 - 13	ND	ND	2.2201	2.217	2.219		
312 - 13	13.3200	13.3245	13.3149	13.304	13.321	+0.0160 (top)	-0.12
						-0.0035 (bot)	-0.03
319 - 295	ND	ND	1.2710	1.277	1.282		
295 - 267	ND	ND	1.2900	1.283	1.284		
267 - 235	ND	ND	1.2640	1.279	1.279		
235 - 199	ND	ND	1.2930	1.279	1.298		
199 - 126	ND	ND	2.5722	2.562	2.547		
126 - 90	ND	ND	1.2750	1.280	1.287		
90 - 58	ND	ND	1.2830	1.283	1.280		
58 - 30	ND	ND	1.2740	1.277	1.274		
30 - 6	ND	ND	1.2840	1.281	1.287		
319 - 6	ND	ND	12.8063	12.801	12.818		
303 - 264	ND	ND	2.2130	2.217	2.220		
264 - 216	ND	ND	2.2147	2.217	2.222		
216 - 109	ND	ND	4.4437	4.437	4.447		
109 - 61	ND	ND	2.2113	2.216	2.221		
61 - 22	ND	ND	2.2130	2.216	2.217		
303 - 22	ND	ND	13.2947	13.303	13.327		
244 - 213	ND	ND	2.5561	2.558	2.562		
213 - 180	ND	ND	2.5762	2.561	2.567		
180 - 145	ND	ND	2.5570	2.564	2.560		
145 - 112	ND	ND	2.5534	2.558	2.570		
112 - 81	ND	ND	2.5555	2.558	2.568		
224 - 81	ND	ND	12.7975	12.800	12.827		
170 - 167	ND	ND	2.2110	2.216	2.216		
167 - 164	ND	ND	2.2150	2.214	2.219		
164 - 161	ND	ND	4.4510	4.439	4.440		
161 - 158	ND	ND	2.2180	2.216	2.220		
158 - 155	ND	ND	2.2151	2.216	2.218		
170 - 155	ND	ND	13.3091	13.301	13.312		
13 - 22	6.6620	6.6610	6.6545	6.655	6.665	-0.0070 (top)	-0.11
						+0.0040 (bot)	+0.06
22 - 170	6.6610	6.6615	6.6520	6.645	6.663	-0.0160 (top)	-0.24
						+0.0015 (bot)	+0.02
170 - 312	6.6590	6.6590	6.6490	6.647	6.656	-0.0120 (top)	-0.18
						-0.0030 (bot)	-0.05
312 - 305	6.6610	6.6590	6.6496	6.651	6.657	-0.010 (top)	-0.15
						-0.002 (bot)	-0.03
303 - 133	6.6600	6.6620	6.6516	6.650	6.657	-0.010 (top)	-0.15
						-0.005 (bot)	-0.08
133 - 13	6.6630	6.6615	6.6490	6.654	6.665	-0.009 (top)	-0.14
						+0.0035 (bot)	+0.05
Mean			4.2731	4.2720		Top, bottom	-0.16,
Std. Dev.			3.8059	3.8047			+0.01

(a) 1 in. = 25.4 mm.

(b) ND = not determined.

TABLE 4-10
FSV FUEL ELEMENT 1-0743
COOLANT HOLE DIAMETERS
(inches)[a]

Hole	Pre I Top	Pre I Bottom	Robot Top	PIE Top	PIE Bottom
6	ND[b]	ND	0.625	0.6227	0.6237
13	0.625	0.625	0.625	0.6228	0.6234
22	0.625	0.625	0.626	0.6224	0.6234
30	ND	ND	0.624	0.6227	0.6232
55	ND	ND	0.623	0.6225	0.6235
58	ND	ND	0.625	0.6228	0.6235
61	ND	ND	0.625	0.6224	0.6236
66	ND	ND	0.624	0.6234	0.6232
81	ND	ND	0.624	0.6227	0.6234
90	ND	ND	0.624	0.6231	0.6236
103	ND	ND	0.624	0.6232	0.6237
106	ND	ND	0.624	0.6228	0.6232
109	ND	ND	0.624	0.6228	0.6232
112	ND	ND	0.625	0.6222	0.6235
126	ND	ND	0.499	0.4975	0.4978
144	ND	ND	0.500	0.4974	0.4982
145	ND	ND	0.499	0.4976	0.4981
155	0.625	0.624	0.623	0.6227	0.6227
158	ND	ND	0.623	0.6230	0.6233
161	ND	ND	0.623	0.6229	0.6236
164	ND	ND	0.624	0.6224	0.6232
167	ND	ND	0.624	0.6229	0.6229
170	0.625	0.624	0.624	0.6229	0.6225
180	ND	ND	0.500	0.4970	0.4976
181	ND	ND	0.499	0.4976	0.4980
199	ND	ND	0.499	0.4973	0.4979
213	ND	ND	0.623	0.6232	0.6235
216	ND	ND	0.624	0.6226	0.6234
219	ND	ND	0.624	0.6228	0.6231
222	ND	ND	0.624	0.6226	0.6229
235	ND	ND	0.624	0.6228	0.6231
244	ND	ND	0.624	0.6225	0.6222
259	ND	ND	0.624	0.6232	0.6227
264	ND	ND	0.623	0.6228	0.6231
267	ND	ND	0.622	0.6218	0.6232
270	ND	ND	0.623	0.6222	0.6230
295	ND	ND	0.625	0.6227	0.6228
303	0.625	0.624	0.623	0.6224	0.6225
312	0.625	0.624	0.624	0.6227	0.6232
319	ND	ND	0.622	0.6222	0.6256
Mean[c]	0.625	0.6243	0.6242	0.6227	0.6230
Std. Dev.	0	0.0006	0.0012	0.0002	0.0004
Mean[d]			0.6239	0.6227	0.0233
Std. Dev.			0.0009	0.0003	0.0001

(a) 1 in. = 25.4 mm.

(b) ND = not determined.

(c) n = 6.

(d) n = 34.

TABLE 4-11
ACCURACY OF METROLOGY ROBOT MEASUREMENTS

Type of Measurement	Robot vs PIE[a]			Robot vs QC[b]		
	Number of Comparisons	Accuracy, 1σ (in.)[c]	Bias $\pm 1\sigma$[d] (in.)[c]	Number of Comparisons	Accuracy, 1σ (in.)[c]	Bias[e,f] (in.)[c]
Fuel element length	42	±0.004	0.011 ± 0.001	324	±0.005	0.007
Distance between fiducial holes	18	±0.007	0.000 ± 0.002	90	±0.003	0.000
Distance between coolant holes	30	±0.007	0.002 ± 0.001	--	ND[g]	ND
Distance across flats	15	±0.003	0.000 ± 0.001	102	±0.003	0.000
Coolant hole diameters	40	±0.001	-0.001 ± 0.000	--	ND	ND
Side face bow	270	±0.001	0.000 ± 0.000	--	ND	ND

[a] Comparison of robot and hot cell measurements for surveillance element 1-0743.

[b] Comparison of robot and QC measurements for calibration element 8-0182.

[c] 1 in. = 25.4 mm.

[d] Bias = PIE-Robot.

[e] Bias = QC-Robot.

[f] Uncertainty on bias is less than ±0.0005.

[g] ND = not determined.

TABLE 4-12
CALCULATED AND MEASURED IRRADIATION-INDUCED STRAINS AND BOW FOR FSV FUEL ELEMENT 1-0743

Parameter	Measured		Calculated[b]
	Metrology Robot	Hot Cell[a]	
Element average axial strain (%)	-0.182 ± 0.014	-0.170	-0.158
Axial strain Distribution (%)			
Corner 1	-0.239	-0.220	-0.145
Corner 2	-0.244	-0.218	-0.148
Corner 3	-0.205	-0.170	-0.160
Corner 4	-0.129	-0.118	-0.169
Corner 5	-0.127	-0.114	-0.166
Corner 6	-0.189	-0.170	-0.153
Element average[c] radial strain (%)	-0.103 ± 0.042	-0.130	-0.075
Bow (mm)	0.30	0.28	0.05

[a] No error estimates made.

[b] Obtained from SURVEY/STRESS calculations based on irradiation conditions from SURVEY analysis of FSV cycle 1 (36-time-interval SURVEY based on results from detailed GAUGE analysis of FSV cycle 1).

[c] Actually, the average radial strain at the top of the element.

TABLE 4-13
PLENUM DEPTH, FUEL STACK LENGTH, AND PUSH-OUT FORCE
MEASUREMENTS FOR FSV FUEL ELEMENT 1-0743

	Plenum Depth (in.)[a]			Stack Length (in.)[a]			Push-Out Force (lb)[a]	
Hole	Pre I	PIE	PIE-Pre I	Pre I	PIE	PIE-Pre I	Initial	Sustaining
12	1.630	1.7290	+0.0990	29.140	29.0216	-0.1184	0	0
47	2.453	2.5619	+0.1089	27.177	27.1108	-0.0662	0	4
157	1.649	1.7772	+0.1282	29.121	(b)	(b)	2.5[b]	1
189	1.645	1.7534	+0.1084	29.125	29.0206	-0.1044	0	2
278	1.654	1.7647	+0.1107	29.116	29.0129	-0.1031	1	1
285	1.661	1.7965	+0.1355	29.109	28.9455	-0.1635	0	3
Avg.	1.782	1.8971	+0.1151	28.798	28.6223	-0.1111	0.58	1.83
Std. Dev.	0.329	0.3265	+0.0138	0.7942	0.8455	0.0351	1.02	1.47
86	--	--	--	--	--	--	1.5	1
121	--	--	--	--	--	--	1	1
160	--	--	--	--	--	--	18	5
194	--	--	--	--	--	--	2	1
231	--	--	--	--	--	--	22	1
Avg.	--	--	--	--	--	--	8.90	1.80
Std. Dev.	--	--	--	--	--	--	10.24	1.79

[a] 1 in. = 25.4 mm; 1 lb = 4.448 N.

[b] All 15 rods broken in stack during unloading.

TABLE 4-14
BROKEN FUEL PARTICLES OBSERVED ON SURFACES OF
SEVENTEEN FUEL RODS FROM FSV FUEL ELEMENT 1-0743

Rod ID	No. of Broken Particles
12-2	16
12-7	9
12-13	12
47-2	14
47-7	16
47-8	9
47-14	8
189-2	21
189-7	10
189-14	15
278-2	9
278-8	21
278-13	17
285-2	9
285-7	9
285-8	11
285-13	11
Total	217
Mean	13

TABLE 4-15
MEASURED STRAINS FOR FUEL RODS
IRRADIATED IN FSV FUEL ELEMENT 1-0743

Fuel Stack ID[a]	Time and Fuel Stack Averaged Temperature (°C)	Stack Averaged Fast Fluence (10^{25} n/m^2) ($E > 29$ fJ)$_{HTGR}$	Stack Averaged Fuel Rod Strain			
			Radial		Axial	
			Strain (%)	±1σ (%)	Strain (%)	±1σ (%)
12	645	0.84	-0.31	0.05	-0.47	0.06
47	645	0.83	-0.34	0.02	-0.44	0.03
189	675	1.00	-0.34	0.02	-0.47	0.03
278	690	1.10	-0.43	0.02	-0.50	0.04
285	695	1.10	-0.39	0.05	-0.59	0.03

[a] These fuel stacks contained only fuel rods that had been dimensionally characterized prior to irradiation. Fuel stack 157 also contained precharacterized fuel rods, but all were broken during unloading from the element.

TABLE 4-16

DIMENSIONAL AND STRAIN DATA FOR FUEL RODS IRRADIATED IN FUEL STACK 12 OF FSV FUEL ELEMENT 1-0743

ROD NO.	PRE-IRRADIATION(A) MEASUREMENTS (IN) DIAM 1	DIAM 2	DIAM 3	LENGTH	POST-IRRADIATION MEASUREMENTS (IN) DIAM 1	DIAM 2	DIAM 3	LENGTH	RADIAL STRAIN (%) DIAM 1	DIAM 2	DIAM 3	AVG DIAM	AXIAL STRAIN (%)	ANISOTROPY (AX - RAD)
1	.4880	.4884	.4885	1.9490	.4722	.4879	.4848	1.9376	.861	-.102	-.757	.000	-.585	-.585
2	.4885	.4887	.4885	1.9410	.4873	.4872	.4862	1.9325	-.246	-.307	-.471	-.341	-.438	-.097
3	.4897	.4901	.4897	1.9380	.4868	.4866	.4859	1.9401	-.592	-.714	-.776	-.694	.108	.802
4	.4886	.4886	.4885	1.9510	.4866	.4875	.4868	1.9325	-.409	-.225	-.348	-.327	-.948	-.621
5	.4898	.4900	.4897	1.9410	.4882	.4879	.4872	1.9291	-.327	-.429	-.511	-.422	-.613	-.191
6	.4881	.4887	.4886	1.9390	.4872	.4871	.4859	1.9263	-.184	[illegible]	-.553	-.355	-.655	-.300
7	.4889	.4895	.4890	1.9610	.4868	.4877	.4867	1.9524	-.430	-.368	-.470	-.423	-.439	-.016
8	.4884	.4886	.4885	1.9390	.4894	.4878	.4852	1.9316	.205	-.164	-.676	-.212	-.382	-.170
9	.4885	.4900	.4894	1.9430	.4877	.4885	.4871	1.9329	-.164	-.306	-.470	-.313	-.520	-.207
10	.4889	.4896	.4896	1.9410	.4865	.4874	.4867	1.9311	-.491	-.449	-.592	-.511	-.510	.001
11	.4896	.4897	.4897	1.9390	.4870	.4885	.4870	1.9311	-.531	-.245	-.551	-.442	-.407	.035
12	.4883	.4882	.488[illegible]	1.9360	.4872	.4872	.4868	1.9266	-.225	-.205	-.287	-.239	-.486	-.247
13	.4885	.4881	.4888	1.9440	.4891	.4874	.4867	1.9366	.123	-.143	-.430	-.150	-.381	-.231
14	.4882	.4887	.4891	1.9410	.4910	.4885	.4871	1.9347	.574	-.041	-.409	.041	-.325	-.366
AVG	.4887	.4891	.4890	1.9431	.4881	.4877	.4864	1.9339	-.131	-.288	-.521	-.313	-.470	-.157
S.D.												.195	.228	.338

(A) PRE-IRRADIATION AIR GAUGE MEASUREMENTS WERE INCREASED BY 0.0014 INCH TO MAKE MEASUREMENTS COMPATIBLE WITH THE POST-IRRADIATION MICROMETER TYPE MEASUREMENTS (REF. 17)

1 IN. = 25.4 MM

TABLE 4-17

DIMENSIONAL AND STRAIN DATA FOR FUEL RODS IRRADIATED IN FUEL STACK 47 OF FSV FUEL ELEMENT 1-0743

ROD NO.	PRE-IRRADIATION(A) MEASUREMENTS (IN) DIAM 1	DIAM 2	DIAM 3	LENGTH	POST-IRRADIATION MEASUREMENTS (IN) DIAM 1	DIAM 2	DIAM 3	LENGTH	RADIAL STRAIN (%) DIAM 1	DIAM 2	DIAM 3	AVG DIAM	AXIAL STRAIN (%)	ANISOTROPY (AX - RAD)
1	.4893	.4902	.4899	1.9370	.4877	.4880	.4875	1.9310	-.327	-.449	-.490	-.422	-.310	.112
2	.4884	.4879	.4887	1.9380	.4867	.4869	.4866	1.9278	-.348	-.205	-.430	-.328	-.526	-.199
3	.4886	.4890	.4889	1.9390	.4879	.4868	.4866	1.9279	-.143	-.450	-.470	-.355	-.572	-.218
4	.4890	.4897	.4898	1.9410	.4880	.4877	.4862	1.9297	-.204	-.498	-.735	-.449	-.582	-.133
5	.4881	.4896	.4897	1.9430	.4887	.4875	.4866	1.9341	.123	-.429	-.633	-.313	-.458	-.145
6	.4891	.4891	.4890	1.9420	.4867	.4883	.4867	1.9331	-.491	-.164	-.470	-.375	-.458	-.083
7	.4881	.4886	.4888	1.9420	.4867	.4876	.4858	1.9314	-.287	-.205	-.614	-.368	-.546	-.177
8	.4889	.4897	.4895	1.9390	.4880	.4885	.4866	1.9319	-.184	-.245	-.592	-.341	-.366	-.026
9	.4881	.4887	.4887	1.9420	.4877	.4865	.4866	1.9340	-.082	-.450	-.430	-.321	-.412	-.091
10	.4889	.4891	.4894	1.9400	.4871	.4873	.4866	1.9349	-.368	-.368	-.572	-.436	-.263	.173
11	.4882	.4885	.4887	1.9380	.4875	.4877	.4871	1.9299	-.143	-.164	-.327	-.212	-.418	-.206
12	.4891	.4896	.4896	1.9570	.4887	.4880	.4868	1.9462	-.082	-.327	-.572	-.327	-.552	-.225
13	.4886	.4888	.4887	1.9400	.4871	.4873	.4875	1.9330	-.307	-.307	-.246	-.286	-.361	-.074
14	.4884	.4894	.4896	1.9390	.4881	.4875	4882	1.9339	-.061	-.388	-.286	-.245	-.263	-.018
AVG	.4886	.4891	.4892	1.9412	.4876	.4875	.4868	1.9328	-.208	-.326	-.491	-.341	-.435	-.094
S.D.												.068	.112	.122

(A) PRE-IRRADIATION AIR GAUGE MEASUREMENTS WERE INCREASED BY 0.0014 INCH TO MAKE MEASUREMENTS COMPATIBLE WITH THE POST-IRRADIATION MICROMETER TYPE MEASUREMENTS (REF. 17)

1 IN. = 25.4 MM

TABLE 4-18

DIMENSIONAL AND STRAIN DATA FOR FUEL RODS IRRADIATED IN FUEL STACK 189 OF FSV FUEL ELEMENT 1-0743

ROD NO.	PRE-IRRADIATION (A) MEASUREMENTS (IN) DIAM 1	DIAM 2	DIAM 3	LENGTH	POST-IRRADIATION MEASUREMENTS (IN) DIAM 1	DIAM 2	DIAM 3	LENGTH	RADIAL STRAIN (%) DIAM 1	DIAM 2	DIAM 3	AVG DIAM	AXIAL STRAIN (%)	ANISOTROPY (AX - RAD)
	* * * ROD 1 IS BROKEN * * *													
2	.4885	.4885	.4886	1.9410	.4869	.4868	.4858	1.9324	-.328	-.348	-.573	-.416	443	-.027
3	.4886	.4893	.4893	1.9380	.4882	.4872	.4863	1.9289	-.082	-.429	-.613	-.375	-.470	-.095
4	.4888	.4895	.4890	1.9470	.4867	.4872	.4863	1.9367	-.430	-.470	-.552	-.484	-.529	-.045
5	.4885	.4899	.4890	1.9470	.4870	.4882	.4863	1.9298	-.307	-.347	-.552	-.402	-.883	-.481
6	.4883	.4889	.4889	1.9420	.4878	.4873	.4863	1.9328	-.102	-.327	-.511	-.314	-.474	-.160
7	.4881	.4884	.4883	1.9420	.4880	.4878	.4863	1.9348	-.020	-.123	-.410	-.184	-.371	-.186
8	.4893	.4891	.4895	1.9390	.4872	.4877	.4863	1.9305	-.429	-.286	-.654	-.456	-.438	.018
9	.4883	.4899	.4894	1.9400	.4884	.4879	.4872	1.9309	.020	-.408	-.450	-.279	-.469	-.190
10	.4883	.4884	.4883	1.9490	.4881	.4872	.4863	1.9409	-.041	-.246	-.410	-.232	-.416	-.184
11	.4884	.4888	.4889	1.9390	.4863	.4874	.4863	1.9306	-.430	-.286	-.532	-.416	-.433	-.017
12	.4884	.4891	.4899	1.9380	.4882	.4878	.4871	1.9297	-.041	-.266	-.572	-.293	-.428	-.136
13	.4887	.4888	.4887	1.9460	.4888	.4868	.4858	1.9384	.020	-.409	-.593	-.327	-.391	-.063
14	.4881	.4884	.4882	1.9460	.4875	.4865	.4868	1.9384	-.123	-.389	-.287	-.266	-.391	-.124
15	.4886	.4897	.4899	1.9410	.4873	.4879	.4878	1.9335	-.266	-.368	-.429	-.354	-.386	-.032
AVG	.4885	.4891	.4890	1.9425	.4876	.4874	.4865	1.9334	-.183	-.336	-.510	-.343	-.466	-.123
S.D.												.087	.128	.124

(A) PRE-IRRADIATION AIR GAUGE MEASUREMENTS WERE INCREASED BY 0.0014 INCH TO MAKE MEASUREMENTS COMPATIBLE WITH THE POST-IRRADIATION MICROMETER TYPE MEASUREMENTS (REF. 17)

1 IN. = 25.4 MM

TABLE 4-19

DIMENSIONAL AND STRAIN DATA FOR FUEL RODS IRRADIATED IN FUEL STACK 278 OF FSV FUEL ELEMENT 1-0743

ROD NO.	PRE-IRRADIATION (A) MEASUREMENTS (IN) DIAM 1	DIAM 2	DIAM 3	LENGTH	POST-IRRADIATION MEASUREMENTS (IN) DIAM 1	DIAM 2	DIAM 3	LENGTH	RADIAL STRAIN (%) DIAM 1	DIAM 2	DIAM 3	AVG DIAM	AXIAL STRAIN (%)	ANISOTROPY (AX - RAD)
1	.4895	.4899	.4894	1.9390	.4877	.4873	.4864	1.9288	-.368	-.531	-.613	-.504	-.526	-.022
2	.4889	.4899	.4896	1.9400	.4871	.4875	.4869	1.9284	-.368	-.490	-.551	-.470	-.598	-.128
3	.4889	.4897	.4898	1.9430	.4873	.4874	.4864	1.9315	-.327	-.470	-.694	-.497	-.592	-.095
4	.4888	.4896	.4895	1.9410	.4876	.4873	.4867	1.9306	-.245	-.470	-.572	-.429	-.536	-.107
5	.4885	.4884	.4886	1.9400	.4889	.4865	.4858	1.9288	.082	-.389	-.573	-.293	-.577	-.284
6	.4897	.4896	.4896	1.9430	.4871	.4873	.4867	1.9320	-.531	-.470	-.592	-.531	-.566	-.035
7	.4881	.4892	.4887	1.9410	.4862	.4867	.4855	1.9290	-.389	-.511	-.655	-.518	-.618	-.100
8	.4888	.4888	.4891	1.9460	.4877	.4865	.4856	1.9327	-.225	-.471	-.716	-.470	-.683	-.213
9	.4888	.4888	.4884	1.9440	.4876	.4867	.4852	1.9360	-.245	-.430	-.655	-.443	-.412	.032
10	.4880	.4885	.4884	1.9430	.4876	.4869	.4862	1.9311	-.082	-.328	-.450	-.287	-.612	-.326
11	.4885	.4896	.4900	1.9390	.4869	.4878	.4875	1.9302	-.328	-.368	-.510	-.402	-.454	-.052
12	.4886	.4884	.4884	1.9470	.4871	.4870	.4865	1.9435	-.307	-.287	-.389	-.328	-.180	.148
13	.4897	.4895	.4898	1.9400	.4867	.4879	.4869	1.9322	-.613	-.327	-.592	-.511	-.402	.108
14	.4884	.4888	.4885	1.9360	.4871	.4869	.4865	1.9321	-.266	-.389	-.409	-.355	-.201	.153
AVG	.4888	.4892	.4891	1.9416	.4873	.4871	.4863	1.9319	-.301	-.423	-.569	-.431	-.497	-.066
S.D.												.085	.152	.147

(A) PRE-IRRADIATION AIR GAUGE MEASUREMENTS WERE INCREASED BY 0.0014 INCH TO MAKE MEASUREMENTS COMPATIBLE WITH THE POST-IRRADIATION MICROMETER TYPE MEASUREMENTS (REF. 17)

1 IN. = 25.4 MM

TABLE 4-20

DIMENSIONAL AND STRAIN DATA FOR FUEL RODS IRRADIATED IN FUEL STACK 285 OF FSV FUEL ELEMENT 1-0743

ROD NO.	PRE-IRRADIATION(A) MEASUREMENTS (IN) DIAM 1	DIAM 2	DIAM 3	LENGTH	POST-IRRADIATION MEASUREMENTS (IN) DIAM 1	DIAM 2	DIAM 3	LENGTH	RADIAL STRAIN (%) DIAM 1	DIAM 2	DIAM 3	AVG DIAM	AXIAL STRAIN (%)	ANISOTROPY (AX - RAD)
1	.4891	.4898	.4898	1.9380	.4873	.4870	.4863	1.9248	-.368	-.572	-.715	-.551	-.681	-.130
2	.4892	.4886	.4887	1.9410	.4872	.4864	.4863	1.9278	-.205	-.450	-.491	-.382	-.680	-.298
3	.4886	.4889	.4888	1.9400	.4894	.4882	.4866	1.9294	.164	-.143	-.450	-.143	-.546	-.403
4	.4896	.4896	.4898	1.9400	.4892	.4874	.4864	1.9283	-.082	-.449	-.694	-.408	-.603	-.195
5	.4886	.4895	.4897	1.9410	.4861	.4874	.4871	1.9295	-.512	-.429	-.531	-.491	-.592	-.102
6	.4884	.4886	.4885	1.9410	.4849	.4860	.4858	1.9293	-.717	-.532	-.553	-.600	-.603	-.002
7	.4879	.4884	.4888	1.9370	.4867	.4864	.4865	1.9273	-.246	-.409	-.471	-.375	-.501	-.125
8	.4894	.4898	.4900	1.9430	.4877	.4877	.4856	1.9298	-.347	-.429	-.898	-.558	-.679	-.121
9	.4884	.4893	.4891	1.9400	.4864	.4879	.4882	1.9269	-.409	-.286	-.184	-.293	-.675	-.382
10	.4883	.4884	.4885	1.9410	.4905	.4877	.4871	1.9263	.451	-.143	-.287	.007	-.757	-.764
11	.4893	.4895	.4900	1.9420	.4901	.4884	.4868	1.9288	.164	-.225	-.653	-.238	-.680	-.442
12	.4887	.4898	.4896	1.9420	.4864	.4866	.4866	1.9349	-.471	-.653	-.613	-.579	-.366	.213
13	.4882	.4884	.4886	1.9420	.4857	.4865	.4864	1.9339	-.512	-.389	-.450	-.450	-.417	.033
	* * * ROD 14 IS BROKEN * * *													
15	.4879	.4889	.4897	1.9420	.4860	.4871	.4873	1.9336	-.389	-.368	-.490	-.416	-.433	-.017
AVG	.4886	.4891	.4893	1.9407	.4874	.4872	.4866	1.9293	-.249	-.391	-.534	-.391	-.587	-.195
S.D.												.175	.119	.246

(A) PRE-IRRADIATION AIR GAUGE MEASUREMENTS WERE INCREASED BY 0.0014 INCH TO MAKE MEASUREMENTS COMPATIBLE WITH THE POST-IRRADIATION MICROMETER TYPE MEASUREMENTS (REF. 17)

1 IN. = 25.4 MM

TABLE 4-21
COMPRESSION TESTING OF FUEL RODS FROM
FSV FUEL ELEMENT 1-0743
FAILURE LOAD AT RUPTURE

Unirradiated Rods		Irradiated Rods	
Fuel Rod ID	Force (lb)[a]	Fuel Rod ID	Force (lb)[a]
1	113	70-1	125
2	95	70-2	155
3	100	70-3	139
4	110	70-4	136
5	95	70-5	118
6	114	70-6	121
7	102	70-7	123
8	103	70-8	151
9	124	70-9	127
10	102	70-10	100
		70-11	122
		70-12	102
		70-13	125
		70-14	124
		70-15	110
Mean	105.8		121.8
Standard deviation	9.3		13.3
Standard deviation/$\sqrt{n}$	2.9		3.7

[a] 1 lb = 4.448 N

TABLE 4-22
FISSION GAS RELEASE MEASUREMENTS FOR FUEL RODS IRRADIATED IN FSV FUEL ELEMENT 1-0743

Fuel Rod ID	Time-Averaged Maximum Fuel Temp. (°C)[a]	Fast[a] Fluence (10^{25} n/m2) ($E > 29$ fJ)$_{HTGR}$	Fission Gas Release[b]		Burnup[a] (% FIMA)	
			Preirrad.	Postirrad.	Fissile	Fertile
12-2	690	0.8		1.1×10^{-4}	6.1	0.3
12-7	660	0.8			6.2	
12-13	625	0.8			6.2	
47-2	685	0.8			6.1	
47-7	660	0.8			6.2	
47-14	625	0.8			6.2	
189-7	695	1.0			6.2	
285-2	750	1.1			6.1	
285-7	720	1.1			6.2	
285-14	680	1.1			6.2	
47-8	655	0.8			6.2	
278-8	745	1.0	1.3×10^{-4}(c)	9.3×10^{-5}	6.2	
285-8	710	1.1			6.2	
189-2	720	1.0		9.2×10^{-5}	6.1	
189-14	655	1.0		5.5×10^{-5}	6.2	
278-12	745	1.0		8.2×10^{-5}	6.2	
278-13	670	1.1		8.8×10^{-5}	6.2	
Average	690	0.9	1.3×10^{-4}	1.0×10^{-4}	6.2	0.3

[a] From SURVEY analysis based on detailed (335 time intervals) GAUGE analysis of cycle 1 and axial power and flux profiles from FEVER.

[b] R/B of Kr-85m at 1000°C.

[c] Measured on group of five rods including rods 47-8, 278-8, and 285-8. Rod 157-8, one of the five rods, was broken during disassembly and could not be measured for fission gas release.

TABLE 4-23
FISSILE PARTICLE RESULTS OF METALLOGRAPHIC EXAMINATION OF FUEL RODS IRRADIATED IN FSV FUEL ELEMENT 1-0743

Fuel Rod ID	Irradiation Conditions			Fissile Particles						
	Maximum Time-Averaged Temp. (°C)	Fluence $\times 10^{25}$ n/m^2 ($E > 29$ fJ)$_{HTGR}$	Burnup (% FIMA)	Number of Particles Examined	Failure (%)					IPyC Debonding (%)
					Buffer	IPyC	SiC	OPyC	Total Coating	
189-2	720	1.0	6.1	316	0	0	0	0	0	11.1
189-14	655	1.0	6.2	337	0	1.8	1.5	0.6	0.6	17.5
278-2	745	1.0	6.1	333	0	0.3	1.2	1.2	0.3	14.4
278-8	705	1.1	6.2	521	0	0.[illegible]	0.4	0.2	0.2	11.1
Average 95% confidence	705	1.0	6.2	1507 (total)	0	0.5 $0.3 \leq F \leq 0.9$	0.7 $0.4 \leq F \leq 1.2$	0.5 $0.2 \leq F \leq 0.8$	0.3 $0.1 \leq F \leq 0.5$	15.0

TABLE 4-24
FERTILE ANALYSIS RESULTS OF METALLOGRAPHIC EXAMINATION OF FUEL RODS IRRADIATED IN FSV FUEL ELEMENT 1-0743

Fuel Rod ID	Irradiation Conditions: Maximum Time-Averaged Temp. (°C)	Irradiation Conditions: Fluence $\times 10^{25}$ n/m^2 $(E > 29\ fJ)_{HTGR}$	Irradiation Conditions: Burnup (% FIMA)	Fertile Particles: Number of Particles Examined	Fertile Particles: Failure (%): Buffer	Fertile Particles: Failure (%): IPyC	Fertile Particles: Failure (%): SiC	Fertile Particles: Failure (%): OPyC	Fertile Particles: Failure (%): Total Coating	IPyC Debonding (%)	Matrix Macro-porosity (%)
189-2	720	1.0	0.3	266	ND[a]	ND	0.8	1.5	0.4	ND	36.4
189-14	655	1.0	0.3	186	2.7	0.5	0	0	0	9.1	21.6
278-2	745	1.0	0.3	267	1.9	2.6	1.1	2.2	0.4	6.0	ND
278-8	705	1.1	0.3	204	ND	ND	0	0	0	ND	20.5
Average 95% confidence	705	1.0	0.3	923 (total)	2.2 ND	1.7 ND	0.5 $0.2 \leq F \leq 1.2$	1.1 $0.6 \leq F \leq 1.8$	0.2 $0.0 \leq F \leq 0.7$	7.3	26.2

[a] ND = not determined.

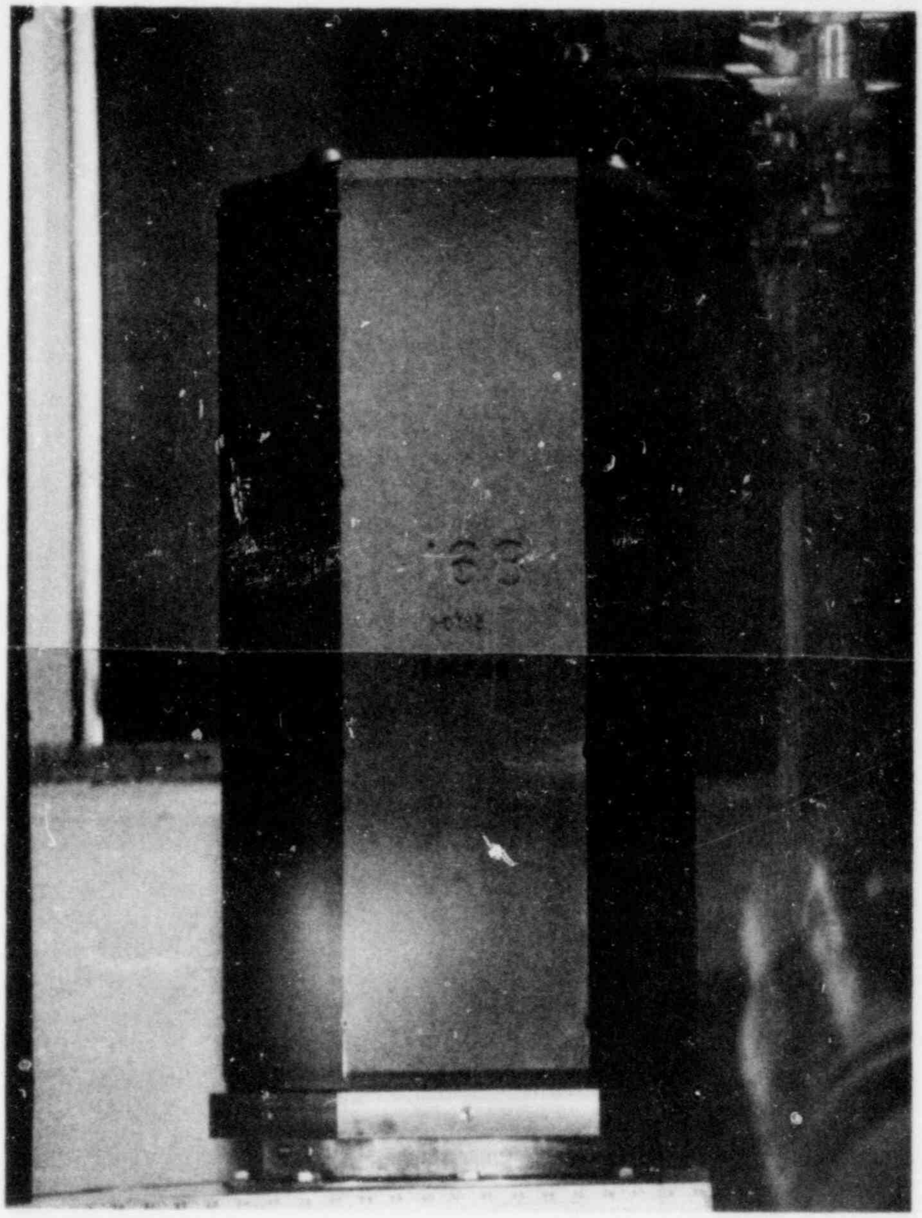

Fig. 4-1. FSV fuel element 1-0743, side face A: vertical and horizontal scrapes observed in vicinity of serial number

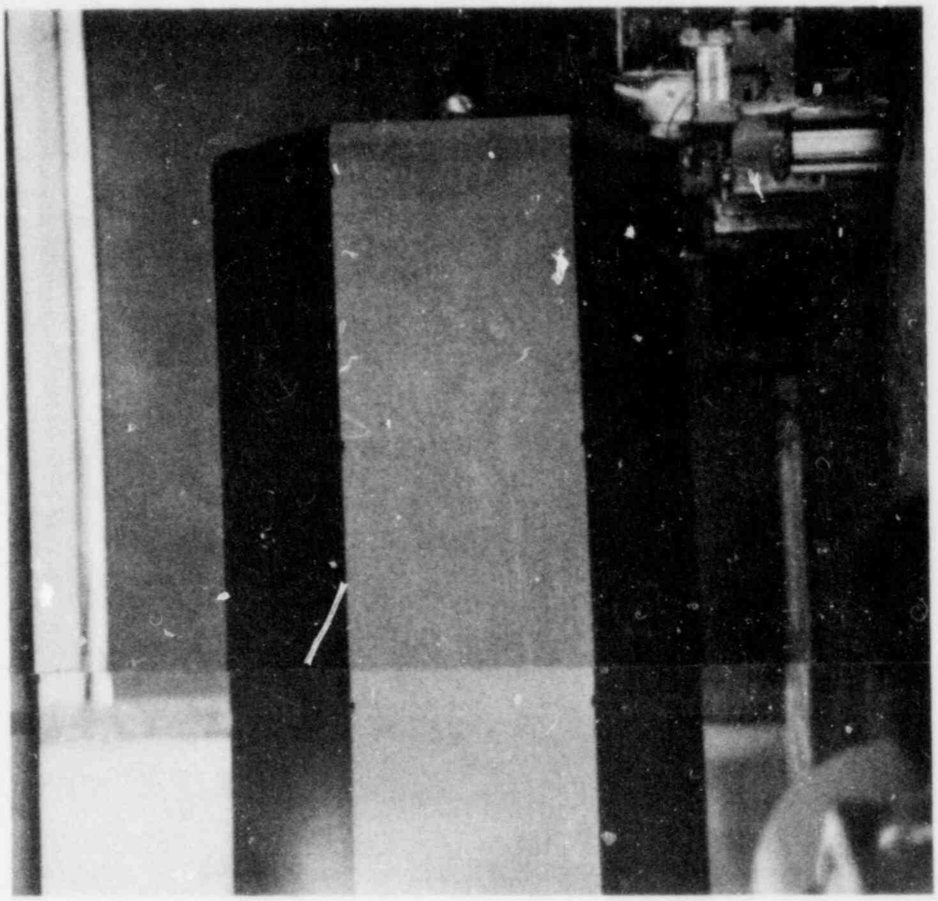

Fig. 4-2. FSV fuel element 1-0743, side face B: long scratch observed starting near top center and extending down face

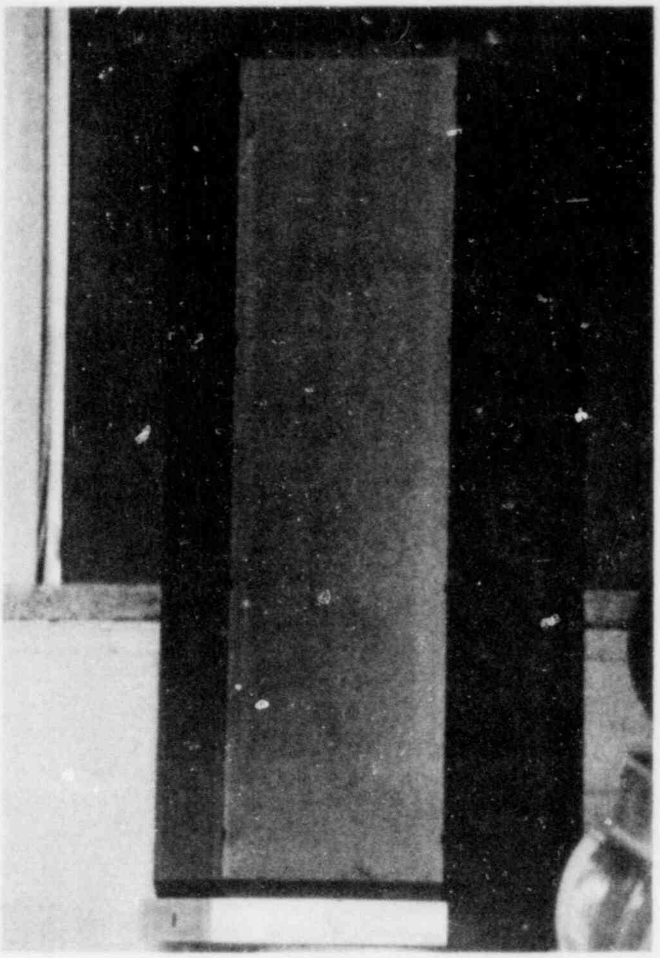

Fig. 4-3. FSV fuel element 1-0743, side face C: rub marks observed down both sides of element

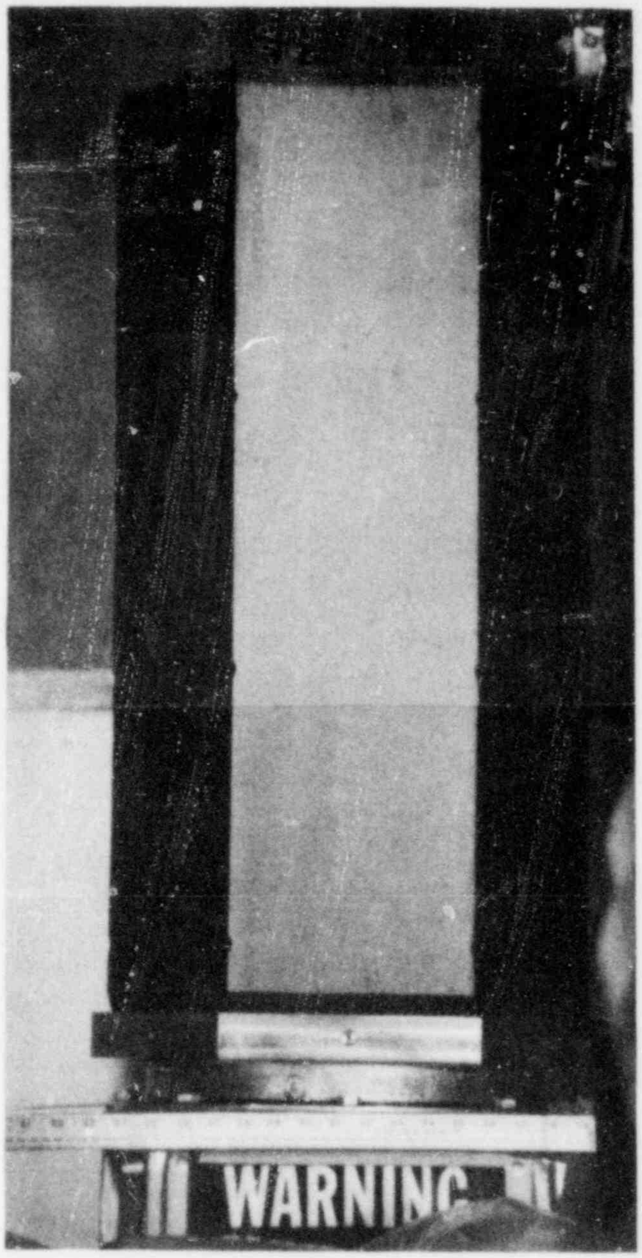

Fig. 4-4. FSV fuel element 1-0743, side face D: rub marks and scrapes observed on surface of element

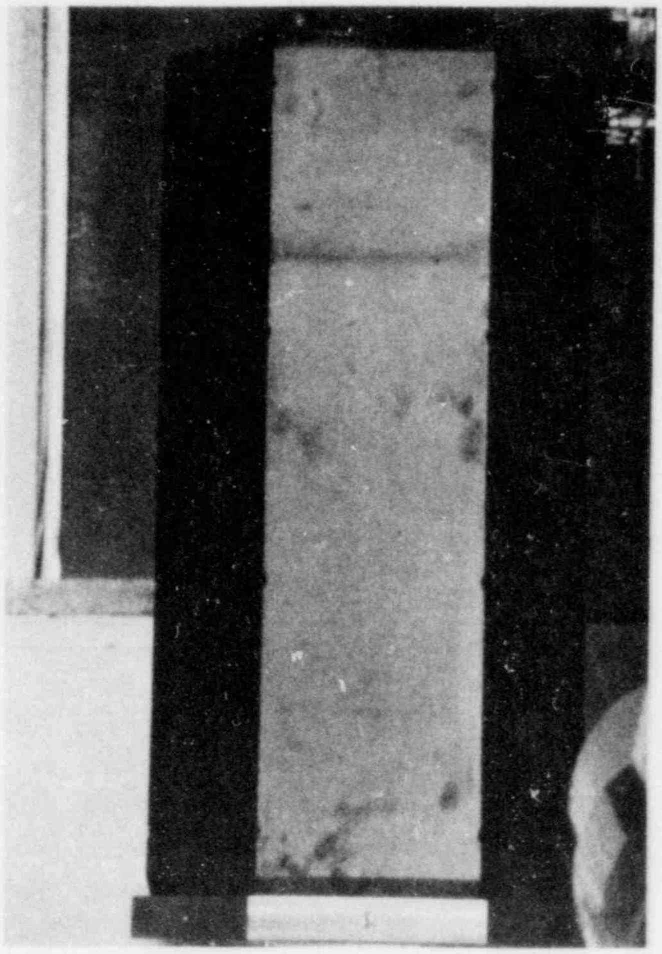

Fig. 4-5. FSV fuel element 1-0743, side face E: numerous dark smudges (most likely soot deposits) observed on surface of element

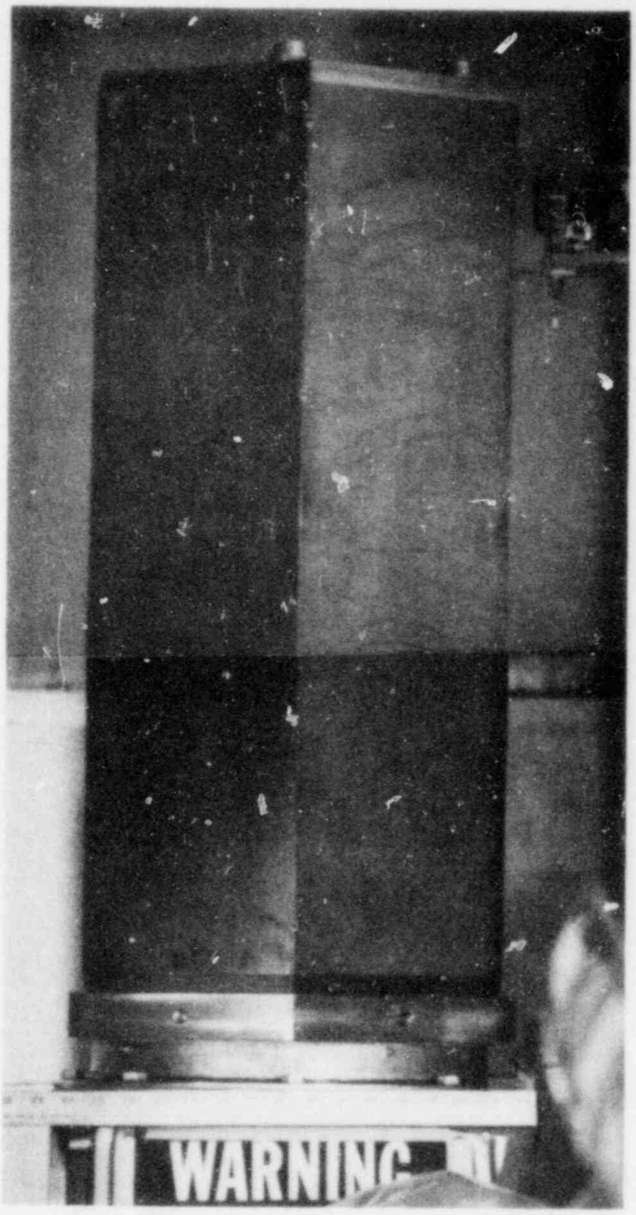

Fig. 4-6. FSV fuel element 1-0743, side faces E (on left) and F (on right); numerous horizontal markings (most likely scrapes) observed on face F

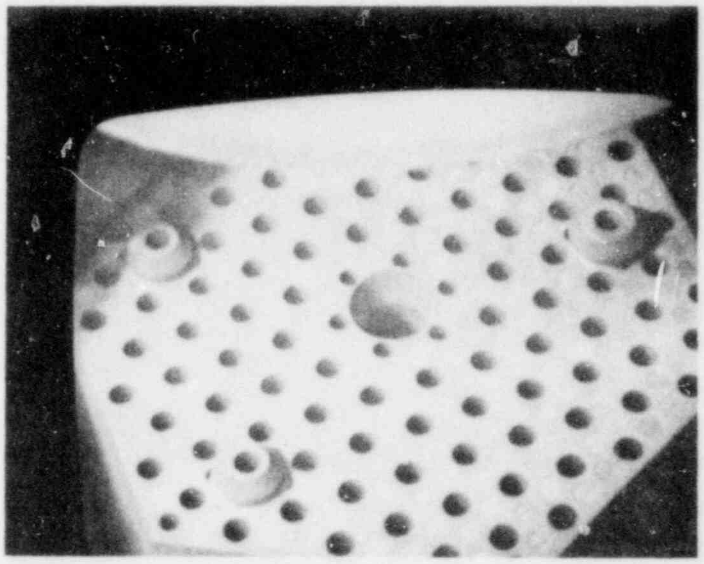

Fig. 4-7. FSV fuel element 1-0743, top surface: fuel handling machine extension sleeve is at top of photograph

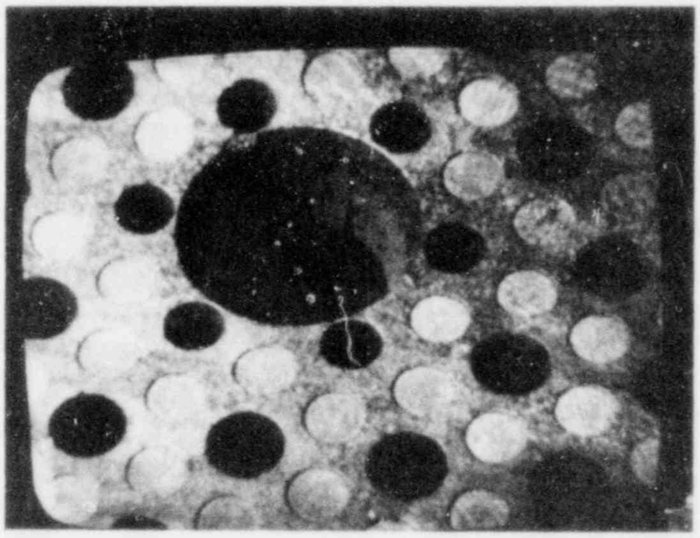

Fig. 4-8. FSV fuel element 1-0743, close-up of fuel handling hole: small chip observed at edge of hole

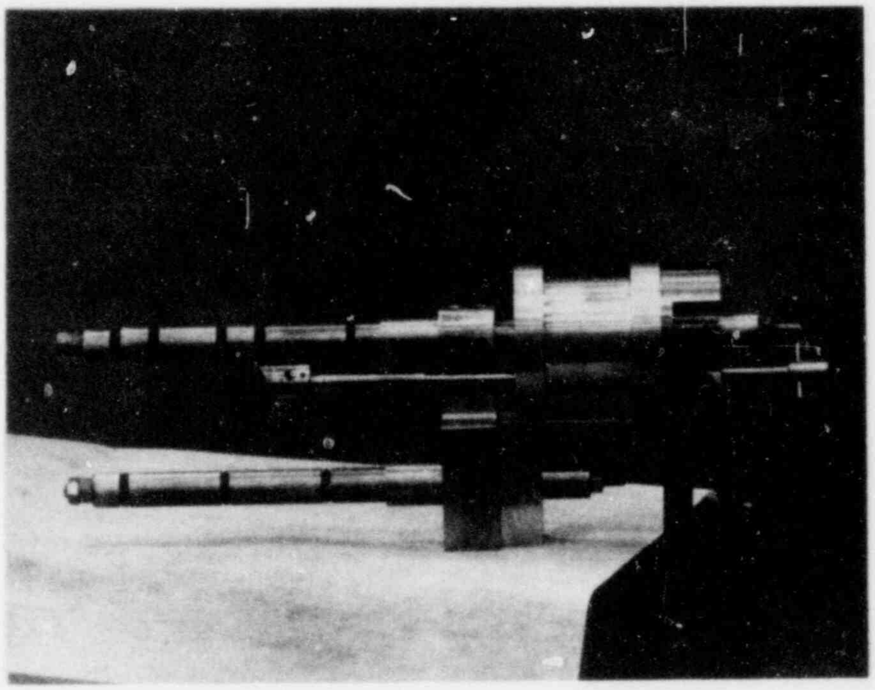

Fig. 4-9. Coring tool

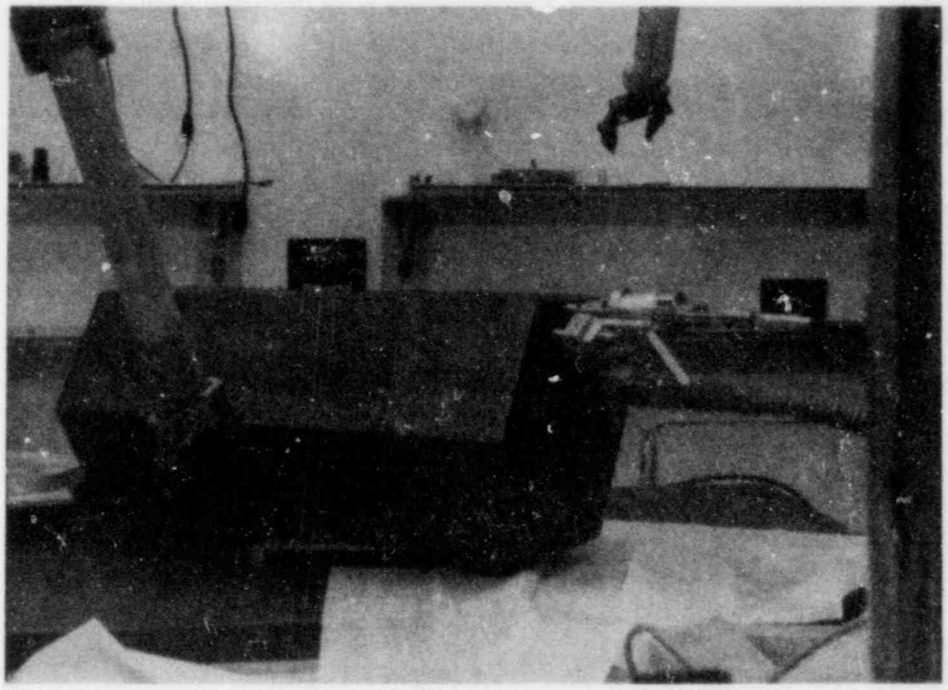

Fig. 4-10. Coring tool in operation

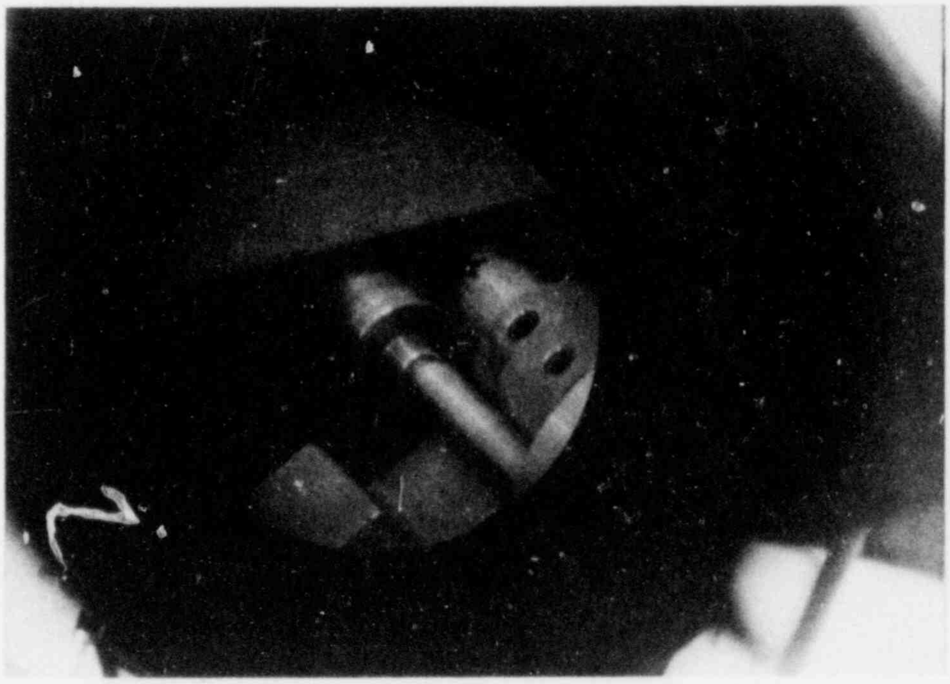

Fig. 4-11. Close-up of coring tool in operation

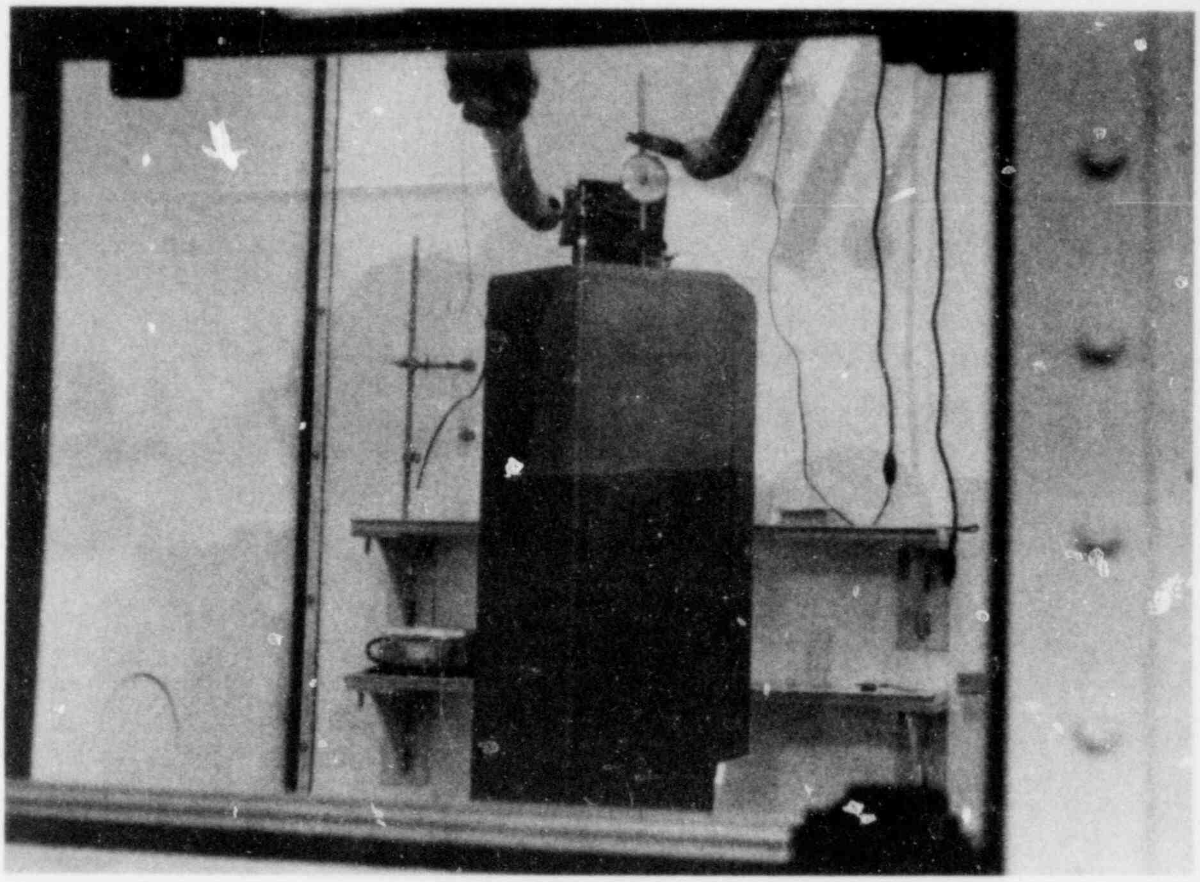

Fig. 4-12. Plenum depth measurement at top surface of fuel element

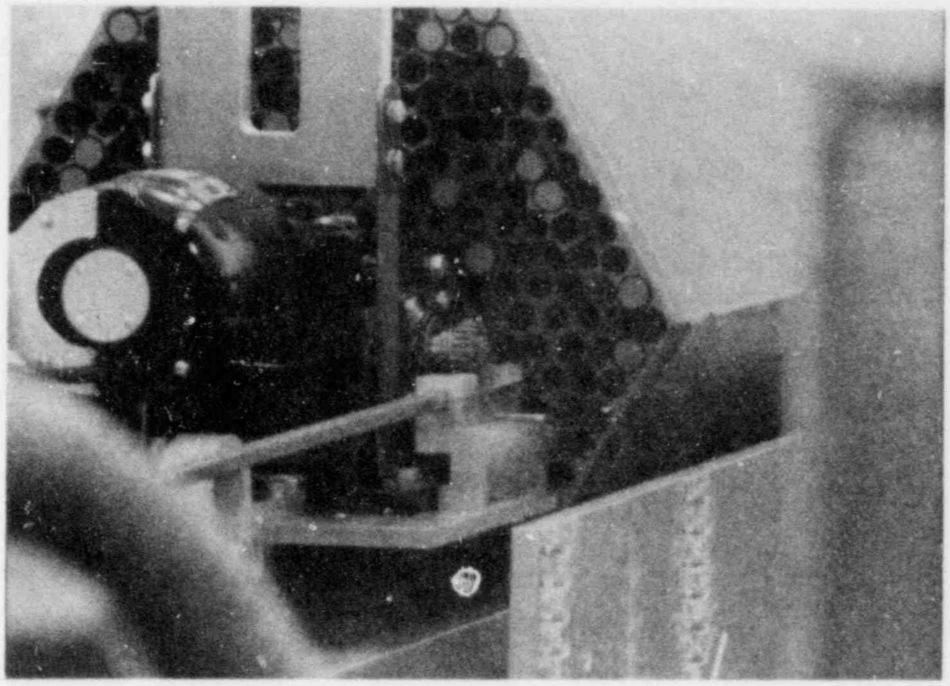

Fig. 4-13. Push-out drive in operation

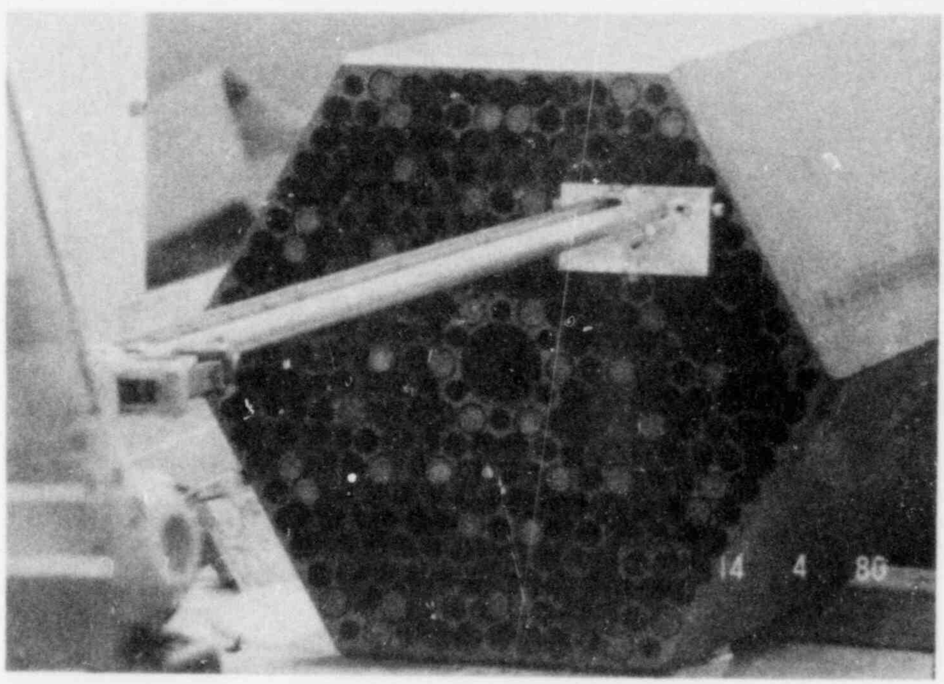

Fig. 4-14. Dual-tube receiving trough for fuel rod stacks

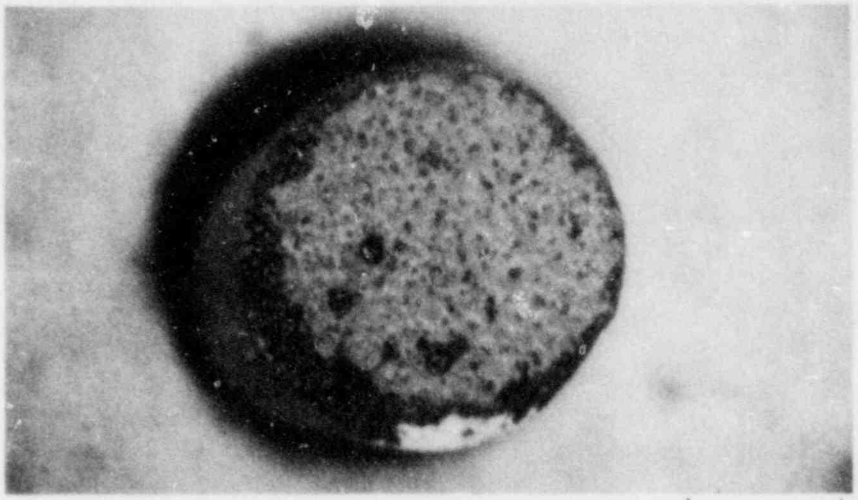

(a) 5000 μm

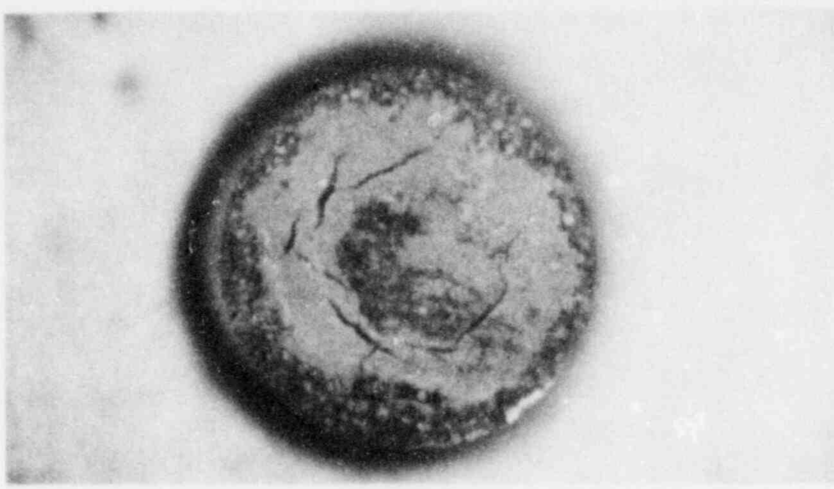

(b) 5000 μm

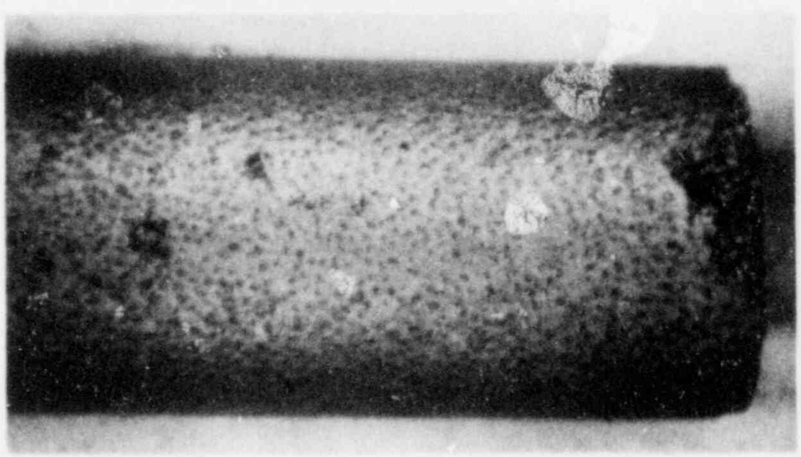

(c) 5000 μm

Fig. 4-15. Fuel rods irradiated in FSV fuel element 1-0743. Chipping and end cap cracking observed at ends of rods: (a) rod 12-2, end of rod is chipped (S8020-1); (b) rod 278-13: cracks in matrix end cap (S8020-34); rod 47-14: chipping at end of rod, failed fuel particles observed (S8020-77).

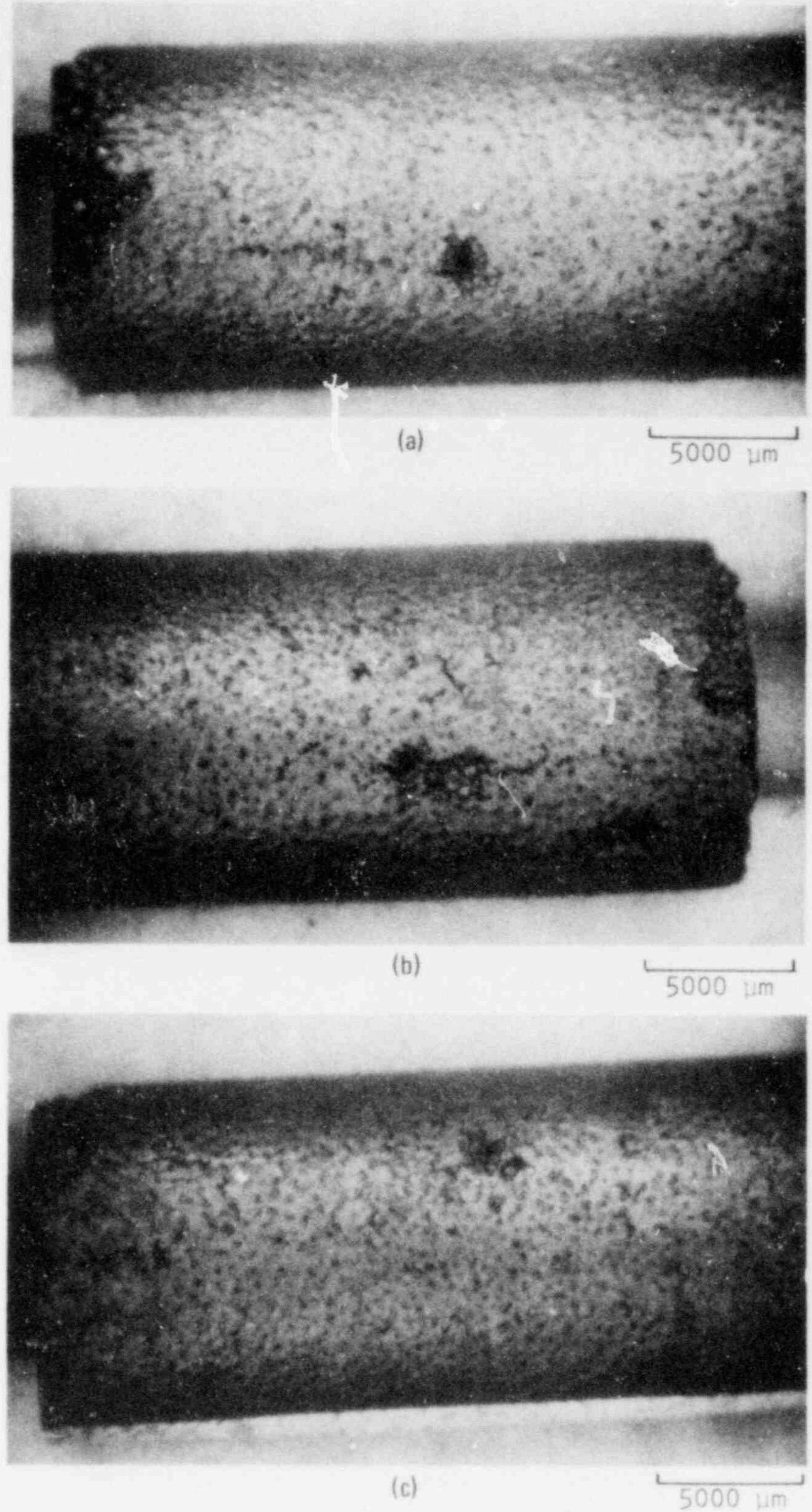

Fig. 4-16. Fuel rods irradiated in FSV fuel element 1-0743. Debonding observed on surfaces of rods: (a) rod 278-2 (S8020-20); (b) rod 278-8 (S8020-27); (c) rod 189-7 (S8020-56); striation resulting from interaction of loose particles or graphite debris (from coring operation) with fuel rod during removal from element also observed.

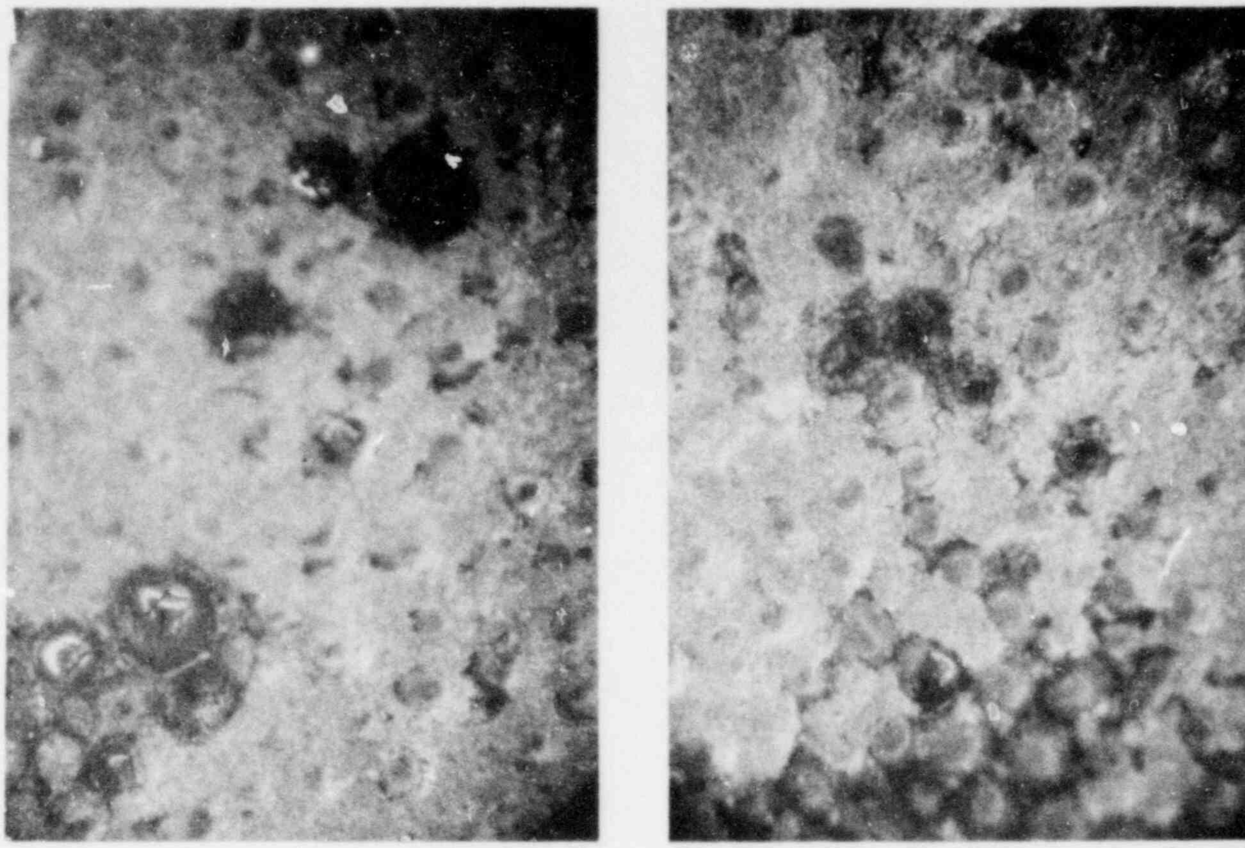

(a) 500 µm

(b) 500 µm

Fig. 4-17. Fuel rods irradiated in FSV fuel element 1-0743. Broken particles observed on end surfaces of fuel rods: (a) rod 12-2 (S8020-8); (b) rod 12-7 (S8020-11).

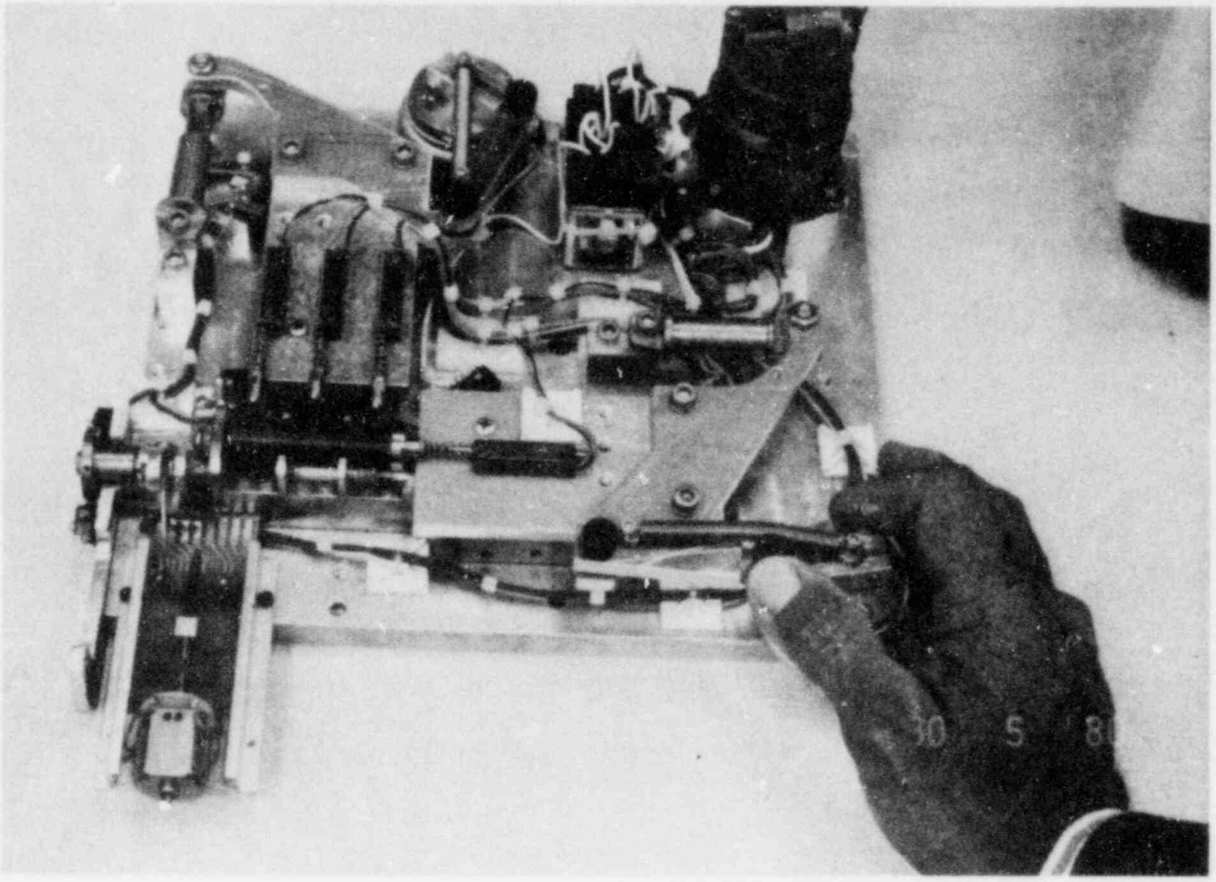

Fig. 4-18. Automated fuel rod dimensioning device used for metrology of fuel rods irradiated in FSV fuel element 1-0743

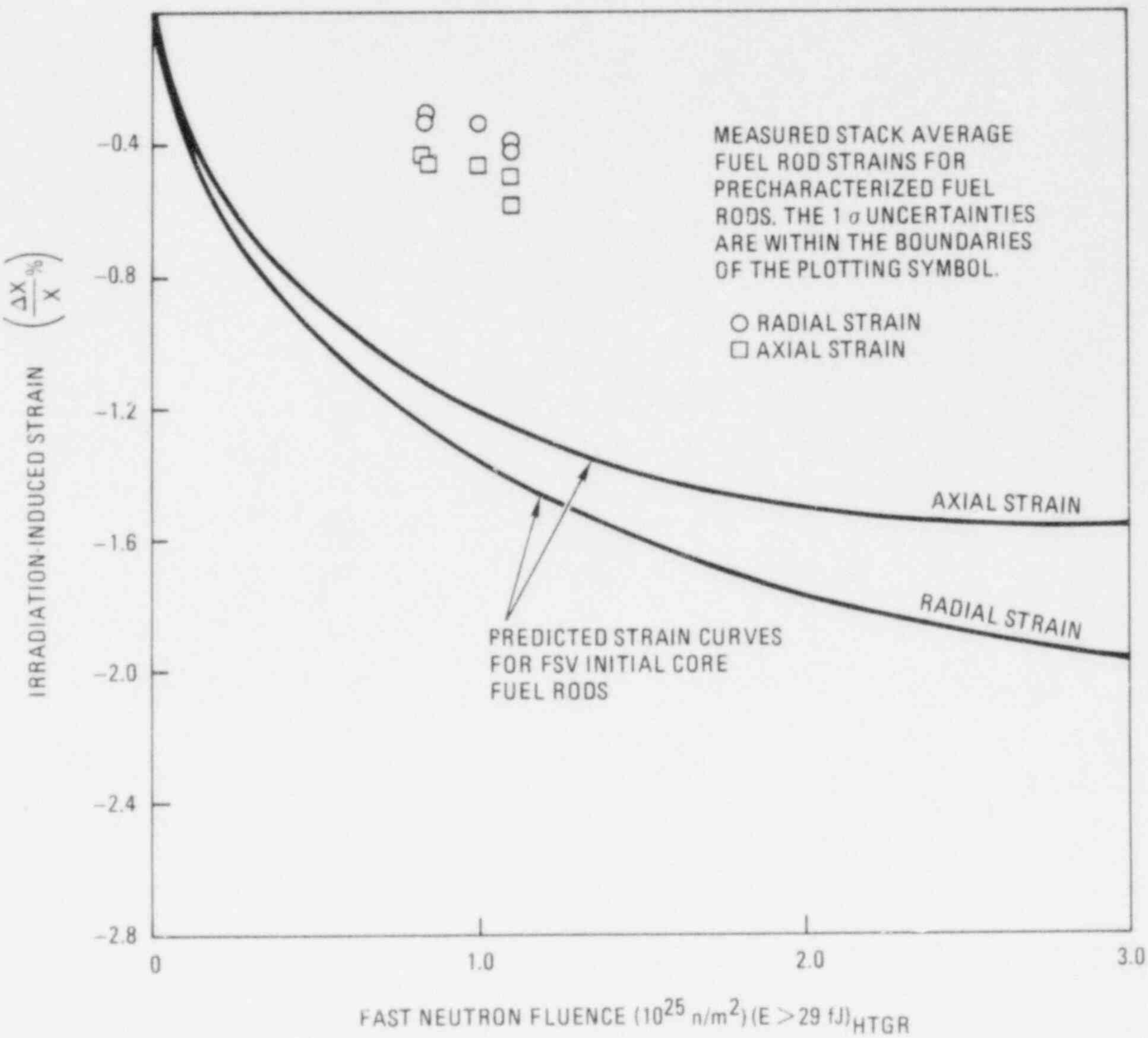

Fig. 4-19. Comparison of calculated and measured strain for fuel rods irradiated in FSV fuel element 1-0743

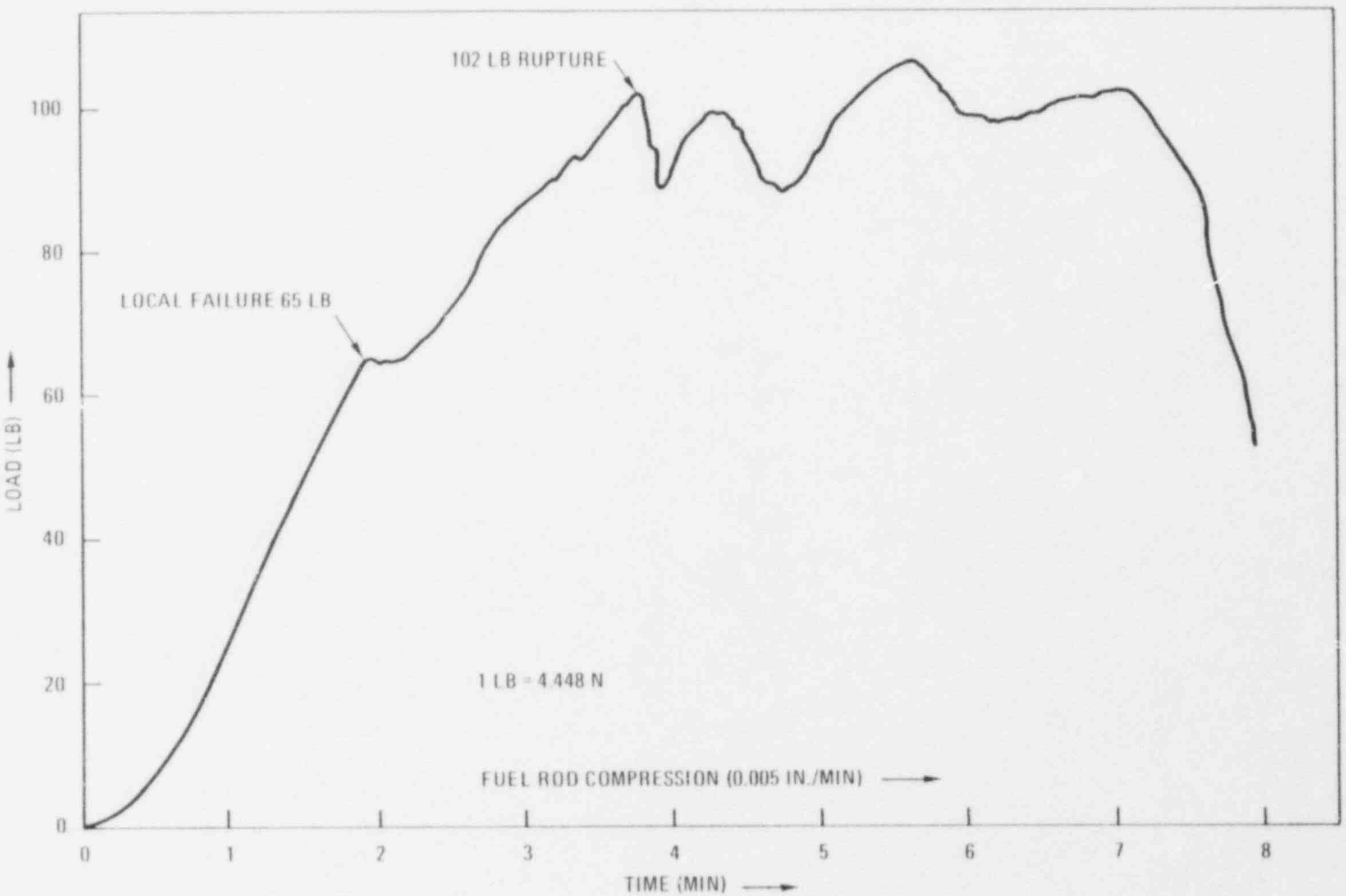

Fig. 4-20. Load distribution during strength testing of a typical irradiated fuel rod from FSV fuel element 1-0743

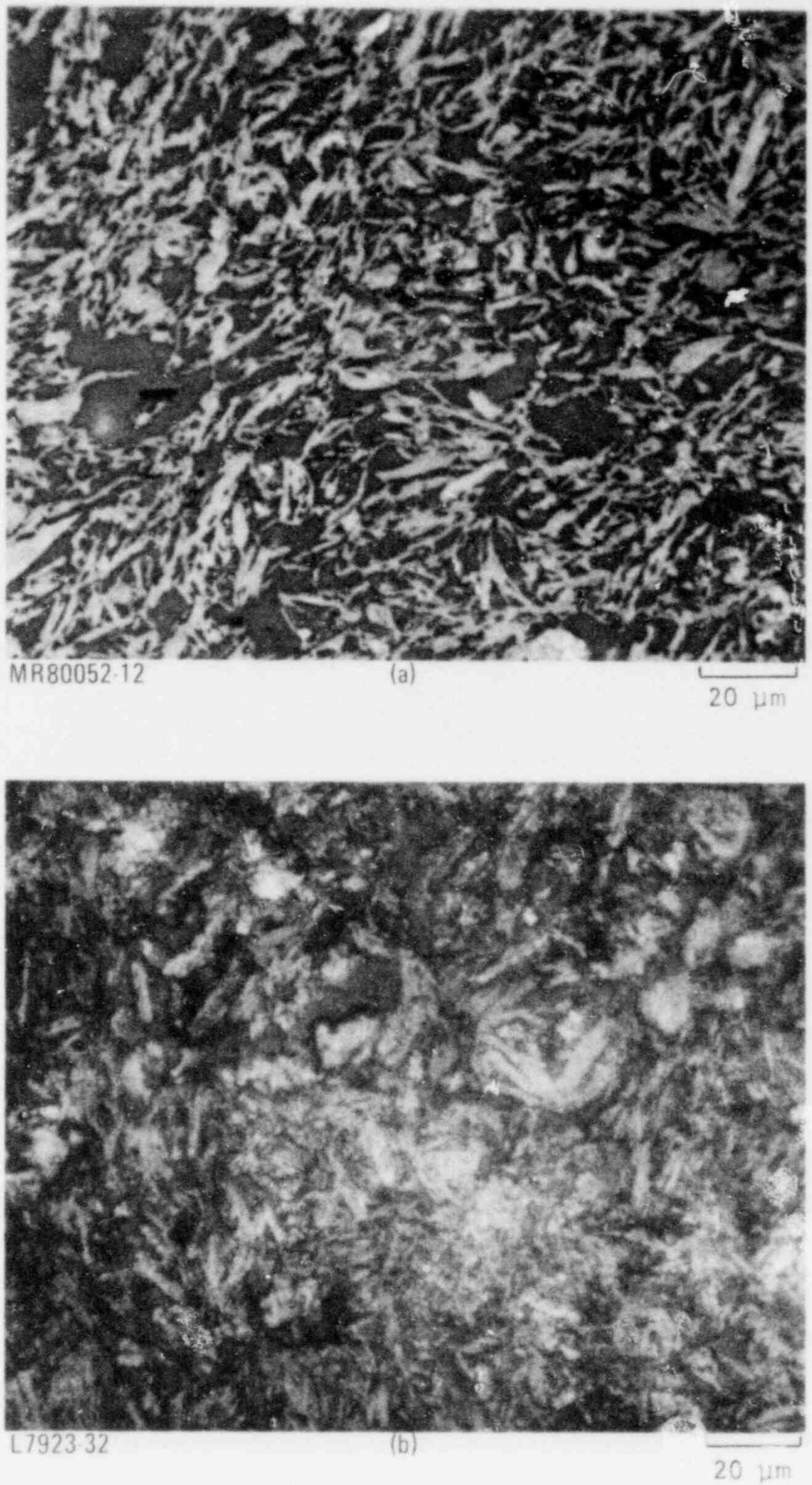

Fig. 4-21. Photomicrographs representative of matrix phase: (a) unirradiated; (b) irradiated in FSV fuel element 1-0[illegible]-3 at 720°C to a fluence of 1.0×10^{25} n/m^2 (E > 29 fJ)$_{HTGR}$. The matrix phase is difficult to distinguish in (b) because the polished section was etched.

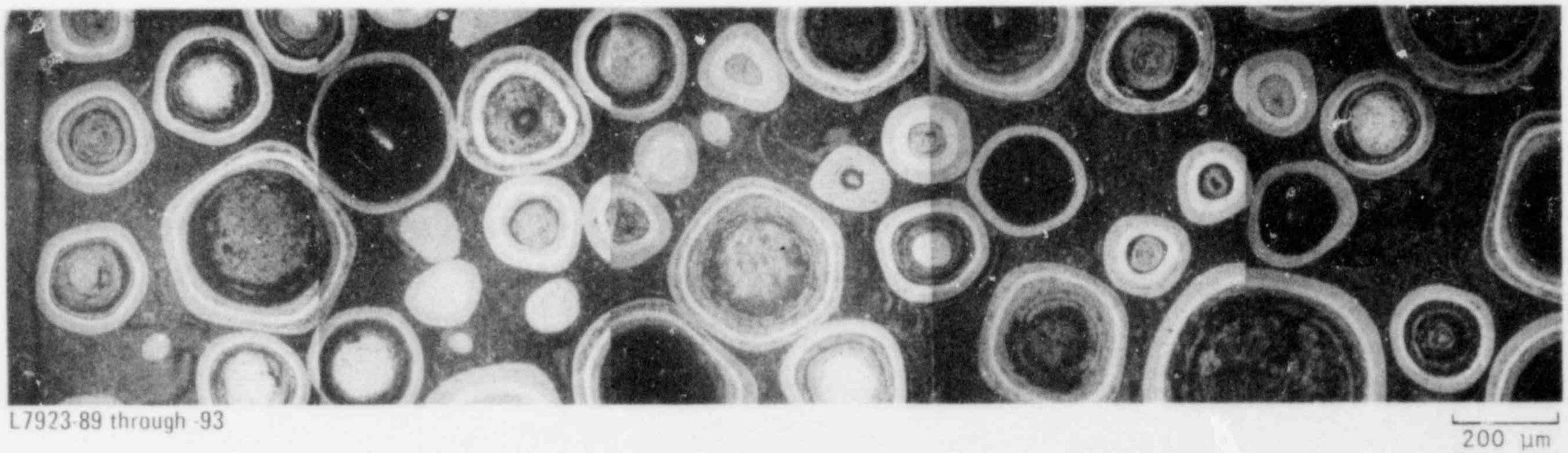

Fig. 4-22. Representative photomicrograph of composite of radial cross section of fuel rod irradiated in FSV fuel element 1-0743 at 705°C to a fluence of 1.1×10^{25} n/m^2 $(E > 29\ fJ)_{HTGR}$. The matrix phase is difficult to distinguish because the polished section was etched.

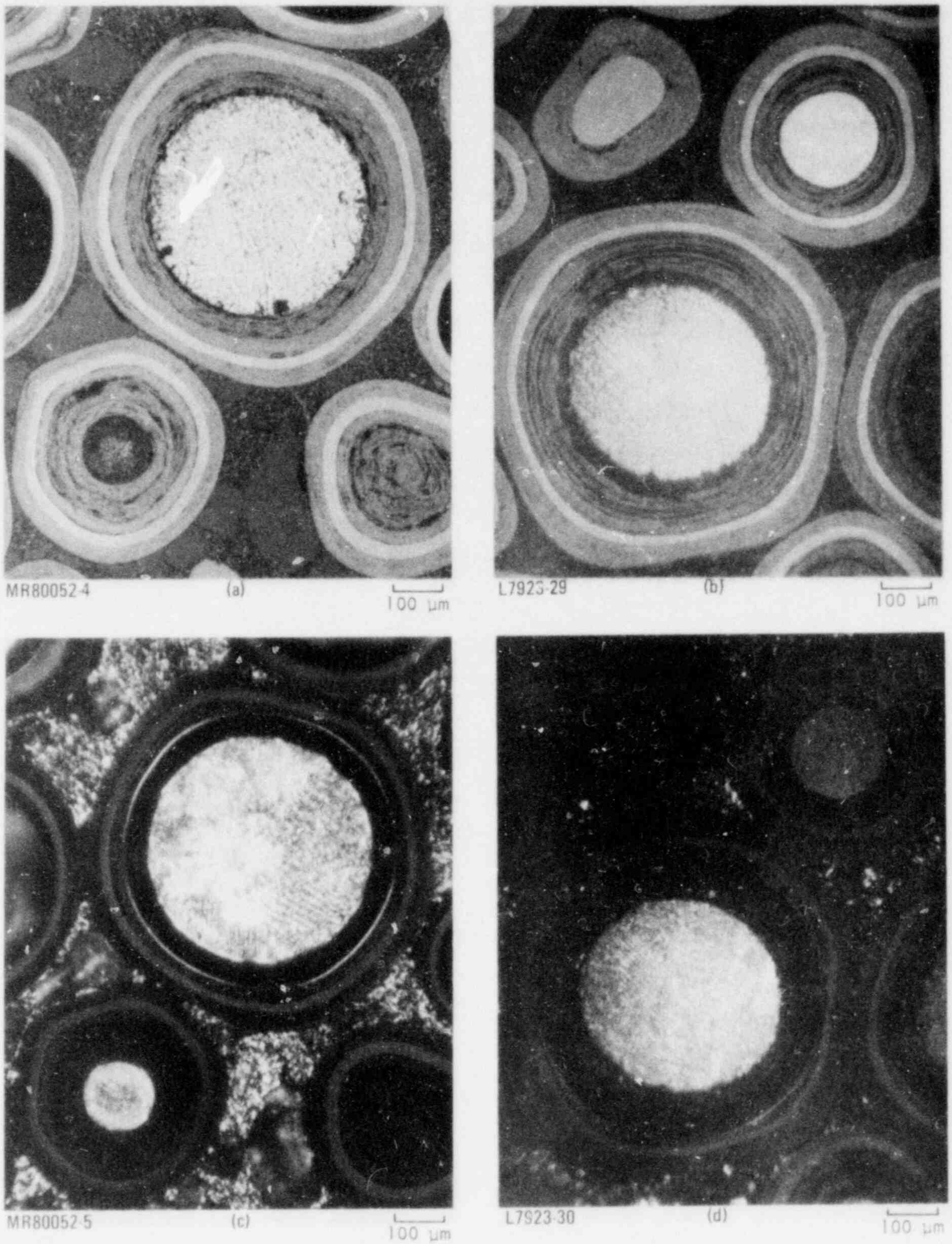

Fig. 4-23. Photomicrographs of fissile (small) and fertile (large) particles: (a) and (c) unirradiated; (b) and (d) irradiated in FSV fuel element 1-0743 to a fluence of 1.0×10^{25} n/m^2 $(E > 29\ fJ)_{HTGR}$ at a temperature of 720°C. (a) and (b) bright field illumination; (c) and (d) polarized light.

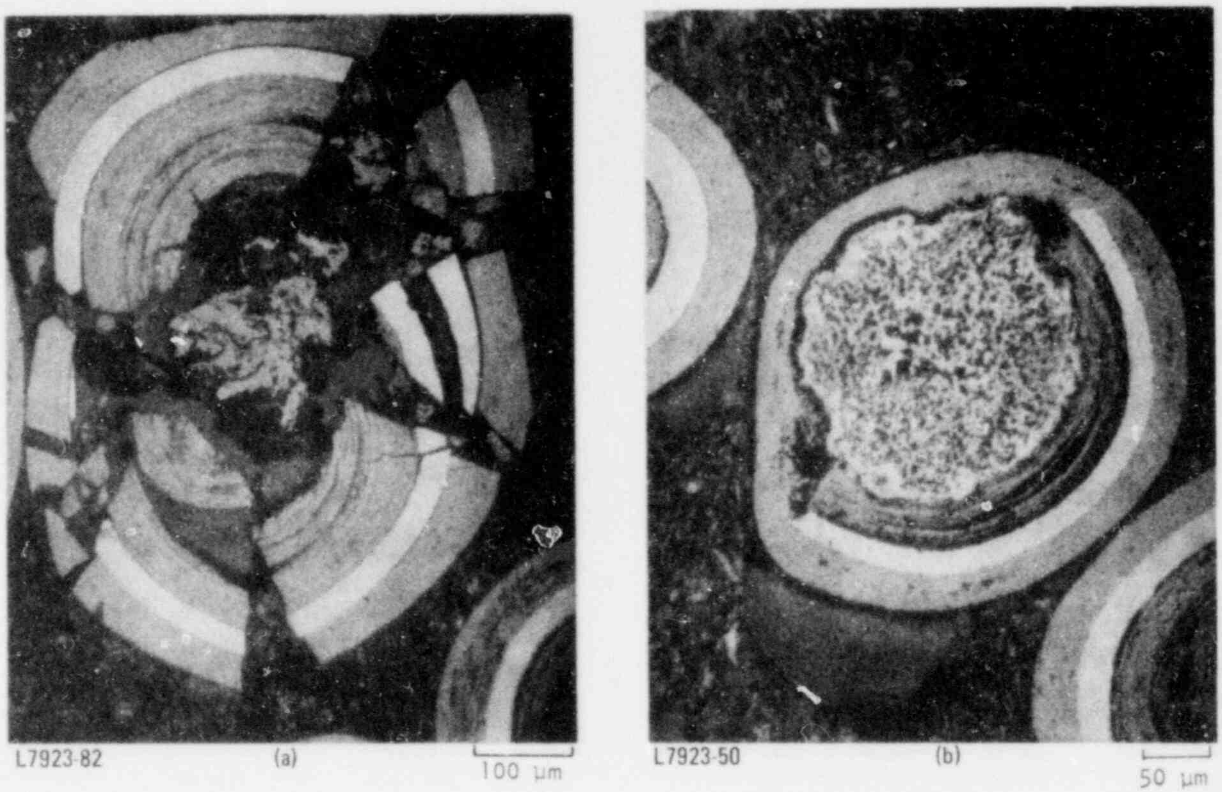

Fig. 4-24. Photomicrographs of examples of as-manufactured defective particles in irradiated fuel rods: (a) total coating failure, (b) SiC coating failure

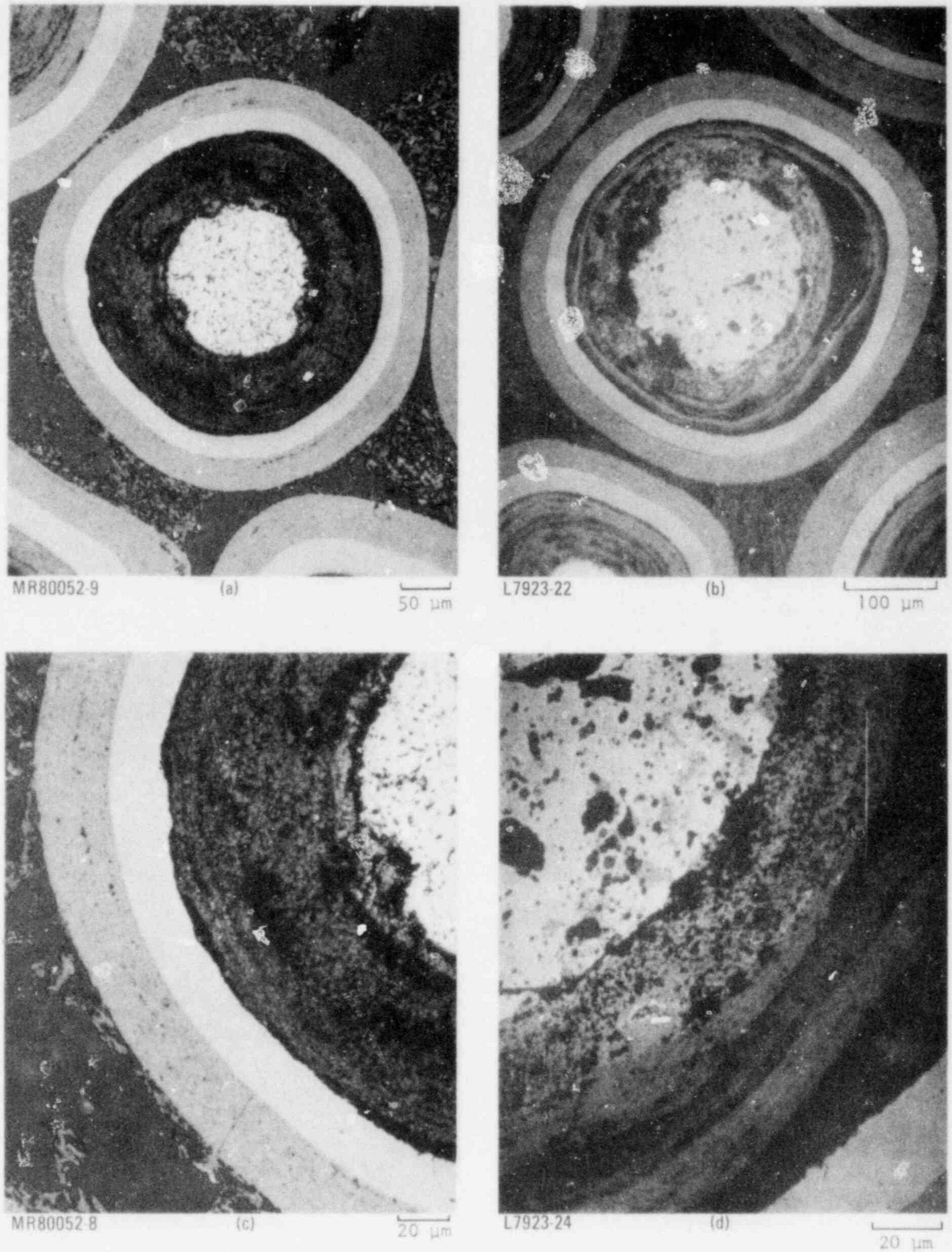

Fig. 4-25. Photomicrographs of TRISO $(Th,U)C_2$ particles apparently exhibiting slight fuel dispersion in buffer coating: (a) and (c) unirradiated; (b) and (d) irradiated in FSV fuel element 1-0743 at 720°C to a burnup of 6.1% FIMA. Note the low-density IPyC coating.

5. SUMMARY AND CONCLUSIONS

FSV fuel element 1-0743 was irradiated for 174 EFPD in core location 17.04.F.06, experiencing an average fast neutron exposure of about 0.95 x 10^{25} n/m^2 (E > 29 fJ)$_{HTGR}$, a time- and volume-averaged fuel temperature in the vicinity of 680°C, fissile and fertile fuel particle burnups of about 6.2% and 0.3% FIMA, respectively, and a total burnup of 12,210 MWd/tonne. The element was removed from the reactor during the first refueling in February 1979. After undergoing nondestructive examination in the hot service facility at FSV in July 1979, the element was shipped to the GA hot cell for extensive PIE.

The PIEs of fuel element 1-0743 at FSV and at GA were performed as part of the DOE-sponsored surveillance program for FSV. The purpose of these examinations was to verify the good performance of the fuel element and to acquire in-pile data for verification of core design methods. In addition, the examination of the element at GA was designed to verify the techniques developed for nondestructive examination of core components in the hot service facility at FSV. The results of the PIEs of fuel element 1-0743 are summarized below.

5.1. FUEL ELEMENT PERFORMANCE

The performance of the fuel element was excellent. Specific observations are as follows:

1. The graphite fuel body was in good condition. No cracks were observed on any of the surfaces. All observed blemishes were surface markings only and had not etched the graphite to a harmful extent.

2. The graphite fuel block was dimensionally stable. The average shrinkage in the block was only 1.3 mm in length and 0.5 mm across flats. The maximum observed bow was only 0.3 mm.

3. No evidence of mechanical interaction between the fuel rods and fuel body was found. A clearance of at least 37 mm was observed between the top fuel rod and the fuel hole plug in six fuel holes for which plenum depth measurements were made. Except in a few cases, very little force was required to push the fuel rods out of the block. Misalignment of the fuel rod receiving trough, and debris from the coring and removal of the fuel hole plugs and graphite containment are believed to be causes of the occasionally high push out forces.

4. Although minor cracking in the matrix end caps and some surface debonding were observed, the fuel rods were in good condition. No more than 21 broken fuel particles were observed on the surface of any rod. About 3% of the [illegible] ere broken, but the majority were broken during unloading, [illegible]. the evidence indicates that the remainder were broken prior to assembly of the element.

5. Irradiation-induced dimensional changes in the fuel rods were small and slightly anisotropic. The average radial and axial strains were -0.36% and -0.49%, respectively. The matrix porosity, which is composed of voids $\geq$50 μm, increased from 19% prior to irradiation to 26% after irradiation.

6. The fuel rod compressive strength increased by approximately 15% as a result of irradiation.

7. The results of fission gas release measurements and metallography indicate no in-pile fuel failure. Approximately 1500 fissile and 925 fertile particles were examined during metallography. For the $(Th,U)C_2$ and ThC_2 particles, respectively, the OPyC coating

failure was 0.5% and 1.1%, the SiC coating failure 0.7% and 0.5%, and the total coating failure 0.3% and 0.2%. However, the evidence indicates that the failed coatings were as-manufactured failures which occurred during coating or fuel rod fabrication.

8. The chemical behavior of the particles was acceptable. No chemical attack on SiC coatings was observed, and no kernel migration was seen. A small amount of a dense phase, attributed to fuel dispersion in as-manufactured particles, was observed in the buffer coating of some $(Th,U)C_2$ particles. The fuel dispersion did not detrimentally affect the performance of the particles.

5.2. VERIFICATION OF HTGR CORE DESIGN METHODS

HTGR design codes used to calculate irradiation and performance parameters for fuel element 1-0743 are summarized below:

GAUGE: column average power, neutron flux, and nuclide inventories. Radial power distributions, neutron fluences, and fuel burnup can be obtained from GAUGE output using the appropriate axial distributions obtained from another source. Two GAUGE analyses were performed for FSV cycle 1, a "detailed" GAUGE for which the power history was represented by 335 time intervals, and a "short" GAUGE for which the power history was represented by only 11 time intervals.

FEVER: axial power, neutron flux, and nuclide inventory distributions.

BUG-2: axial power, neutron flux, and nuclide inventory distributions for fuel elements influenced by control rods in neighboring elements.

GATT: axial and radial power distributions, neutron fluence, and fuel burnup.

SURVEY: temperatures and fuel performance. SURVEY also calculates neutron fluences and fuel burnup by bringing together GAUGE, FEVER, and BUG-2 results. SURVEY analysis for FSV cycle 1 is based on the "detailed" GAUGE.

SURVEY/STRESS: stresses, strains, and deformation for the graphite fuel body.

Verification of HTGR core design methods cannot be accomplished from comparisons of experimental observations and design code calculations for one element. Instead, many such comparisons for core components which have collectively experienced a wide range of irradiation conditions are required. One of the primary objectives of the FSV surveillance program is to provide the in-pile data required for these comparisons. The results of comparisons between measurements and design code calculations for fuel element 1-0743 should be reviewed with this in mind. The results are as follows:

1. Radial power distribution: The observed tilt in the time-averaged power distribution was 9% (relative to element average power), and the calculated tilts were 13% from SURVEY-detailed GAUGE and 4% from the short GAUGE. At EOL, the observed tilt was 8% and calculated tilts were 4% from SURVEY-detailed GAUGE, 3% from GATT, and 4% from the short GAUGE. The agreement between calculated and measured local to block average power factors was within 7.5% for all local points. This is well within the ±10% (1σ) uncertainty for GAUGE calculations.

2. Axial power distribution: At EOL, the agreement between calculated and measured local to block average power factors was within about 3% at all axial positions. The time-averaged distributions were also in good agreement except near the bottom of the block, where the axial power was underpredicted by about 10%. The reason for this discrepancy is that the FEVER model cannot account for the control rod in region 34, which was partially inserted during much of cycle 1. The effect of this control rod was to tilt the axial power toward the bottom of the element.

3. Neutron fluences: The agreement between measured and calculated fast fluences was within 6% for all comparisons. Calculated fluences were obtained from SURVEY-detailed GAUGE, GATT, and short GAUGE-GATT. The predicted thermal fluence (from short GAUGE-GATT) is 11.9% smaller than the thermal fluence determined from V-Co dosimeters and 39.9% greater than the fluence determined from pure V dosimeters. The fluence determined from the V dosimeters is believed to be in error.

4. Temperature: The calculated temperature for each temperature monitor was approximately 25°C greater than the measured temperature. In all cases, the calculated temperature was within the 95% confidence limits for the measured temperature.

5. Fuel burnup: The relative differences between measured and calculated composite burnups (indicative of total power generation) were 3.5% ± 2.0% (1σ) for SURVEY-detailed GAUGE, 9.9% ± 1.9% (1σ) for GATT, and 17.6% ± 1.7% (1σ) for FEVER. In all cases, calculated burnups were less than measured burnups. The fissile particle burnup was slightly better predicted than the fertile burnup.

6. Isotopic composition: The atom % concentrations of U-234, U-235, U-236, and U-238 in the UC_2 particles irradiated in the burnup monitors were measured and calculated. The relative differences in the measured and calculated atom % concentrations are 0.4% ± 0.2% (1σ) for U-234, 3.7% ± 0.0% for U-235, 18.9% ± 0.2% (1σ) for U-236, and 10.5% ± 0.1% (1σ) for U-238. The concentrations of U-234 and U-235 were overpredicted; the concentrations of U-236 and U-238 were underpredicted.

7. Fuel body strain (H-327 graphite): A comparison of measured and calculated strains and bow for all 49 segment 1 fuel elements examined at FSV is presented in Ref. 1.

8. Fuel rod strain: The radial strain was predicted to be approximately 1.3%, but strains of only about 0.4% were measured. Axial strains were also overpredicted by about a factor of 3. One possible explanation is that the model used to predict the strain was developed primarily from design data in the fast fluence range 4 to 10 x 10^{25} n/m^2 $(E > 29\ fJ)_{HTGR}$ and extrapolated to low fluence. This extrapolation may have introduced some error into the model.

9. Fuel performance: In-pile failure was calculated to be 0.32% for the $(Th,U)C_2$ fissile particles and 0.07% for the ThC_2 fertile particles. These failures were attributed to manufacturing defects. The conclusion from the fuel rod examination was that no in-pile failure occurred. The model for failure due to manufacturing defects therefore appears to be conservative.

5.3. VERIFICATION OF NONDESTRUCTIVE EXAMINATION TECHNIQUES

Techniques for performing visual, metrological, and gamma spectroscopic examinations of core components in the hot service facility at FSV using automated data acquisition systems were verified. The results are as follows:

1. A visual examination of the fuel block was performed in the hot cell. Nothing of significance was observed that had not been observed during the earlier examination at FSV using the metrology robot TV camera system.

2. In order to verify the results of the metrological examination performed at FSV using the metrology robot, the metrological examination was repeated at GA using conventional hot cell measuring techniques. A comparison of the results of these measurements with the results obtained with the metrology robot, and comparisons of robot measurements and QC measurements on a calibration fuel block established that the accuracy of the metrology robot is ±0.18 mm (0.007 in.) (1σ) or better for each type of robot measurement after corrections are applied for observed measurement biases.

3. The element average composite burnups determined from gamma scanning and from destructive measurements agreed to within 2.8% ± 2.1% (1σ).

4. The gamma scan robot currently being developed for gamma scanning core components at FSV was successfully employed (in a preliminary state of development) to examine fuel element 1-0743 in the hot cell at GA.

6. ACKNOWLEDGMENTS

The authors wish to acknowledge the following contributors to this report:

Preparation and Preirradiation Characterization of Element

W. W. Hudritsch, W. J. Scheffel, and O. M. Stansfield

Element Irradiation

Courtesy of Public Services of Colorado (PSC)

Nuclear, Thermal, and Strain Calculations

V. Malakhof, S. C. Bachelor, M. Y. Wan, and W. Shen

Data Reduction

F. McCord

Data Acquisition at Hot Cell

H. O. Johnson and staff, D. W. Hill, F. McCord, T. L. Smith, and W. E. Simpson

Analysis of Gamma Scan Data

R. C. Jensen (San Diego State University)

Burnup Analysis

T. B. Crockett, D. M. Fleishman, and M. A. Hiatt

Fission Gas Release Measurements

R. W. Tomlin

Analysis of SiC Temperature Monitors

P. W. Flynn and R. G. Hudson

Editing/Typing

J. E. Weaver and staff

7. REFERENCES

1. Miller, C. M., and J. J. Saurwein, "Non-destructive Examination of 51 Fuel and Reflector Elements from Fort St. Vrain Core Segment 1," DOE Report GA-A16000, General Atomic Company, to be published.
2. Wagner, M. R., "GAUGE, A Two-Dimensional Few Group Neutron Diffusion-Depletion Program for a Uniform Triangular Mesh," USAEC Report GA-8307, General Atomic Company, March 15, 1968.
3. Kraetsch, H., and M. R. Wagner, "GATT, A Three-Dimensional Few Group Neutron Diffusion Theory Program for a Hexagonal-z Mesh," USAEC Report GA-8547, General Atomic Company, January 1, 1969.
4. Todt, F. W., and L. J. Todt, "FEVER/M1, A One-Dimensional Depletion Program for Reactor Fuel Cycle Analysis," General Atomic Report GA-9780, October 22, 1969.
5. Dorsey, J. P., R. Froehlich, and F. Todt, "BUG-2/BUGTRI, Two-Dimensional Multigroup Burnup Codes for Rectangular and Hexagonal Geometry," USAEC Report GA-8272, General Atomic Company, August 22, 1969.
6. Georghiou, D. L., "SURVEY, A Computer Code for the Thermal and Fuel Performance Analysis of High-Temperature Gas-Cooled Reactors," General Atomic Company, unpublished data, November 1978.
7. Smith, P. D., "SURVEY/STRESS, A Model to Calculate Irradiation-Induced Stresses, Strains, and Deformations in an HTGR Fuel Block Using Viscoelastic Beam Theory," General Atomic Report GA-A13712, October 20, 1975.
8. Malakhof, V., "GATT, Analysis of FSV Cycle 1," General Atomic Company, unpublished data, August 1979.
9. Malakhof, V., "Analytical Results for FSV Surveillance Element 17.04.F.06," General Atomic Company, unpublished data, July 25, 1980.

10. Saurwein, J. J., and C. F. Wallroth, "Nuclear and Thermal Design Verification for the Peach Bottom High-Temperature Gas-Cooled Reactor," DOE Report GA-A14726, General Atomic Company, September 1979.
11. Boden, R. J., "Fuel Rod Homogeneity - FSV Segments 1, 7, and 8," General Atomic Company, unpublished data, April 22, 1980.
12. Mathews, D., and V. Malakhof, "FSV Dosimetry Cross Sections," General Atomic Company, unpublished data, September 15, 1980.
13. Palentine, J. E., "The Development of Silicon Carbide as a Routine Irradiation Temperature Monitor and Its Calibration in a Thermal Reactor," J. Nucl. Mater. 61, 243-253 (1976).
14. Peterson, J. F., "TAC2D, A General Purpose Two-Dimensional Heat Transfer Computer Code," USAEC Report GA-8868, General Atomic Company, September 6, 1969.
15. Miller, C. M., "Test Specification for Metrology of FSV Graphite Fuel Elements," General Atomic Company, unpublished data, June 10, 1980.
16. McCord, F., and T. L. Smith, "Test Procedure for Metrology of Irradiated FSV Fuel Rods using the Fuel Rod Measuring Device (MICROBOT)," General Atomic Company, unpublished data, April 30, 1980.
17. Jameson, L., "Bias for the Fort St. Vrain Preirradiation Fuel Rod Diameter Measurements," General Atomic Company, unpublished data, July 16, 1980.
18. Kovacs, W. J., and D. P. Harmon, "Irradiation-Induced Dimensional Changes in HTGR Fuel Rods," General Atomic Company, unpublished data, October 1979.
19. "Fuel Design Data Manual," Issue C, General Atomic Company, unpublished data.
20. Scott, C. B., and D. P. Harmon, "Postirradiation Examination of Capsule F-30," General Atomic Report GA-A13208, April 1, 1975.
21. Stansfield, O. M., "Thermally Induced Fuel Dispersion in Production Fuel Particles," General Atomic Company, unpublished data, October 14, 1971.
22. Stansfield, O. M., "Additional Discussion of Thermally Induced Fuel Dispersion in Production Fuel Particles," General Atomic Company, unpublished data, January 27, 1972.

APPENDIX A

DISCUSSION OF BURNUP ANALYSIS

by

T. B. Crockett

Three monitor packages removed from Stacks 12 and 278 of FSV-Surveillance Element No. 1 contained fissile particles which were analyzed in accordance with procedure ACD;RC-001, "Atom Percent Fission in Fissile and Fertile Fuel Particles." Since these monitor packages had not been designed to incorporate fertile particles, the fertile particles we did use for assay had to be selected from fuel rods. We separated the Th/U fissile and Th fertile particles based on Cs-134/Cs-137 end-of-life ratio. After selection of the Th fertile particles an abbreviated burnup analysis was performed rather than that specified in ACD:RC-001.

The fissile fuel particles were cleaned to remove external contamination, and after this cleaning operation each particle was measured for prominent fission products. Fission product ratios were calculated for each sample to reveal any abnormal fuel particles, i.e., either damaged or particles foreign to set being analyzed.

The ASTM radiochemical method was used in the analysis of the fissile fuel particles. This method uses fission product Cs-137 as burnup monitor. In addition to the fission product method, the fissile fuel particles were analyzed by a mass spectrometric uranium isotopic analysis method. This method measures burnup through changes in uranium isotopic composition and can be applied only to fuel particles that do not contain thorium or U-233 before irradiation; thus it is not applicable for fertile fuel particles.

Replicate analyses were preformed on the fissile particles passing the selection criteria. Initially, the particles were crushed and dissolved in perchloric acid mixture. These solutions containing fission products and uranium were separated by an anion exchange method. A portion of the U fraction from each of the samples was analyzed mass spectrometrically for both uranium concentration and uranium isotopic composition. Results from isotope dilution mass spectrometric analyses are compared with colorimetric results in Table 1; and the fissile fuel particle atom percent uranium isotopic composition results (both archive and irradiated) are in the attached report.

The mass spectrometric data from the LFE report was treated in accordance with ASTM procedure E244, "Atom Percent Fission in Uranium and Plutonium Fuel (Mass Spectrometric Method)." Burnup determined by this method is shown in the attached computer printout. Table 2 provides a comparison of mass spectrometric fissile burnup with that measured radiochemically.

Fertile burnup analysis by the abbreviated case basically took advantage of the fact that due to elapsed time since end of irradiation, no Pa-233 activity remained in these fertile particles. We then proceeded to irradiate (in TRIGA) these particles along with bare kernel ThO_2 standards and generated Pa-233 activity. By virtue of the µCi Pa-233/mgm Th in the bare kernels, we computed the Th weight in the FSV particles on the basis of their respective Pa-233 activities. We made an estimate of the end-of-life U in these particles by comparing fission product Ce 143 in the FSV fertile particles with that produced in some bare kernels enriched UO_2 particles. After consideration of the differences between U-233 and U-235 fission cross-sections and fission product yields plus estimating U-233 to be 85 - 90% of the final end-of-life U the overall error is roughly 20%. This has little effect upon the final FIMA values since the U represents only 1.3% of end-of-life heavy metal content. The fertile FIMA's shown in Table 3 were computed by the following equation:

$$F_3 = \frac{F}{Th^O} \times 100 = \frac{F}{Th^R + -U^R + F} \times 100 = \%\ \text{FIMA}$$

where:

F_3 = Heavy element atom percent fission from U-233 (Th-232).

F = Fissions per total sample = N'/Y.

N' = Atoms of Cs-137 (corrected for decay during and after irradiation).

Y = Fractional fission yields of Cs-137 (6.80%).

Th^O = Initial atoms of thorium.

U^R = Remaining atoms of uranium.

Th^R = Remaining atoms of thorium.

One last item worth noting is that the ASTM Method generates a flux value based on the isotopic composition change. I have underlined those values on the attached computer printout. The fission to capture value for U-235 (.2238) was obtained from the materials you originally provided.

cc: D. Hill D. Flieshman M. Hiatt

TABLE 1

SAMPLE MONITOR	IDENTITY PARTICLE	MASS SPEC* U μGM	CHEMISTRY* U μGM
21	4	10.93	10.69
21	5	8.40	8.40
22	3	9.53	9.57
22	4	10.12	9.81
81	4	9.08	9.37
81	5	10.11	9.52

* After chemical yield correction

TABLE 2

SAMPLE MONITOR	IDENTITY PARTICLE	RADIOCHEMISTRY FIMA	ASTM MASS SPEC FIMA
21	4	32.1	30.2
21	5	32.2	30.8
22	3	31.7	30.3
22	4	31.6	30.1
81	4	33.7	32.8
81	5	31.6	31.1

TABLE 3

FERTILE FIMA's

SAMPLE STACK	IDENTITY ROD	PARTICLE	FIMA %
12	4	1	.30
12	4	2	.31
12	4	8	.30
12	11	3	.31
12	11	4	.32
12	11	5	.33
279	3	2	.35
279	3	6	.33
279	3	8	.35

MASS SPECTROMETRIC ANALYSIS REPORT

REPORT TO
GENERAL ATOMIC COMPANY
P. O. BOX 81608
SAN DIEGO, CALIFORNIA 92138

ORDER NUMBER
BL-81-99 PR-740855

LFE ENVIRONMENTAL
ANALYSIS LABORATORIES DIVISION
2030 WRIGHT AVENUE
RICHMOND, CALIFORNIA 94804

AUGUST 18, 1980

PREPARED BY KATSUMI YAMAMOTO, SUPERVISOR
MASS SPECTROMETRY

APPROVED BY R. MELGARD
LABORATORY OPERATIONS MANAGER

GENERAL ATOMIC COMPANY
BL-81-99 PR-740835

URANIUM ANALYSIS

ATOM PERCENT

	Monitor	Part	234	235	236	238
B3	21	#4	0.300 ±0.004	79.93 ±0.03	10.80 ±0.03	8.475 ±0.021
B4	21	#5	0.795 ±0.003	79.87 ±0.04	10.79 ±0.04	8.548 ±0.022
B5	22	#3	0.795 ±0.007	79.92 ±0.05	10.80 ±0.04	8.48 ±0.04
B6	22	#4	0.792 ±0.007	79.97 ±0.04	10.788 ±0.025	8.46 ±0.03
B7	81	#4	0.797 ±0.005	79.29 ±0.05	11.10 ±0.04	±8.81 ±0.04
B8	81	#5	0.7979 ±0.0016	79.39 ±0.06	11.23 ±0.06	8.582 ±0.027

PARTS PER MILLION

	234	235	236	238	TOTAL
B3	0.00773 ±0.00009	0.775 ±0.008	0.1052 ±0.0011	0.0832 ±0.0009	0.971 ±0.010
B4	0.00586 ±0.00007	0.592 ±0.006	0.0803 ±0.0009	0.0641 ±0.0007	0.742 ±0.008
B5	0.00669 ±0.00009	0.675 ±0.007	0.0916 ±0.0011	0.0726 ±0.0009	0.846 ±0.009
B6	0.00708 ±0.00010	0.718 ±0.008	0.0973 ±0.0011	0.0769 ±0.0009	0.899 ±0.010
B7	0.00639 ±0.00008	0.638 ±0.007	0.0898 ±0.0010	0.0718 ±0.0009	0.806 ±0.009
B8	0.00712 ±0.00008	0.712 ±0.008	0.1012 ±0.0013	0.0779 ±0.0009	0.898 ±0.010

GENERAL ATOMIC COMPANY
BL-81-99 PR-740855

URANIUM ANALYSIS

		ATOM PERCENT			
	Archive	234	235	236	238
B9		0.6421 ±0.0015	93.202 ±0.006	0.2701 ±0.0014	5.886 ±0.005

		WEIGHT PERCENT			
		234	235	236	238
B9		0.6389 ±0.0015	93.133 ±0.006	0.2711 ±0.0014	5.957 ±0.005

GENERAL ATOMIC

GENERAL ATOMIC COMPANY
P. O. BOX 81608
SAN DIEGO, CALIFORNIA 92138